

Sodium Metal Anodes for Energy Storage

Zur Erlangung des akademischen Grades eines

DOKTORS DER NATURWISSENSCHAFTEN

(Dr. rer. nat.)

von der KIT-Fakultät für Chemie und Biowissenschaften

des Karlsruher Instituts für Technologie (KIT)

genehmigte

DISSERTATION

von

M.Sc. Philipp Schüdel

1. Referent: Prof. Dr. Stefano Passerini

2. Referent: Prof. Dr. Jens Tübke

Tag der mündlichen Prüfung: 13.12.2017

Für Ilona

Eidesstattliche Erklärung

Hiermit versichere ich, dass ich die vorliegende Arbeit ohne unzulässige Hilfe Dritter und ohne Benutzung anderer als der angegebenen Hilfsmittel angefertigt habe; die aus fremden Quellen direkt oder indirekt übernommenen Gedanken sind als solche kenntlich gemacht.

Karlsruhe, 02.11.2017

Philipp Schüdel

Acknowledgement

This doctoral thesis was composed at Fraunhofer Institute for Chemical Technology (ICT) and was supervised by Prof. Dr. Stefano Passerini of Karlsruhe Institute of Technology (KIT) and Helmholtz Institute Ulm (HIU).

I want to thank Prof. Dr. Passerini very much for taking me on as an external Ph.D. student as well as for the continuous support, the interesting discussions and the input he has provided me with.

I would also like to thank Prof. Dr. Jens Tübke as my second reviewer for agreeing to take part in evaluating this work, for providing a great work environment at Fraunhofer ICT and for helping me out whenever necessary. Furthermore, I would like to thank Prof. Dr. Karsten Pinkwart for also making my work at Fraunhofer ICT possible.

My gratitude goes to my local supervisor, Dr. Michael Holzapfel, who has provided me with invaluable input and insight into battery research while also being a good friend. I also thank Dr. Markus Hagen for giving me the possibility to work on some of his projects, for believing in my abilities and for his continuing friendship. Another colleague and friend, whose help I am especially thankful for, is Julian Becherer.

Furthermore, I want to thank Oliver Witzgall for the work he did for his bachelor's thesis, which it was my privilege to supervise; Hubert Weyrauch and Ramona Speck for SEM imaging, Eberhard Nold for XPS analysis, Christoph Vaalma for providing NaNCM cathodes, and Nataliya Roznyatovskaya and Jens Noack for their help with the Gamry potentiostat.

I thank all coworkers at Fraunhofer ICT, while special thanks go to the colleagues who not only supported me throughout my work but were also good friends: Dr. Nils Baumann, Thomas Buczkowski, Michael Schäffer, Benjamin Bechtle, Dr. Katharina Ahlbrecht, Patrick Fanz, Theodosios Famprikis and Dr. Tilman Jurzinsky.

Last but not least, I thank my family for their support and especially Ilona Schwarzensteiner, my partner in life who has done more for me than anyone could ever wish for.

Table of Contents

| | |
|--|-------------|
| Eidesstattliche Erklärung | III |
| Acknowledgement | IV |
| Table of Contents | VI |
| Index of Abbreviations and Symbols | VIII |
| 1 Introduction | 1 |
| 2 Fundamentals | 3 |
| 2.1 Electrochemical Energy Storage in Batteries..... | 3 |
| 2.1.1 Basics | 3 |
| 2.1.2 Properties..... | 5 |
| 2.1.3 Cost | 9 |
| 2.2 Anodes..... | 11 |
| 2.2.1 Carbonaceous Anodes..... | 11 |
| 2.2.2 Metal Anodes | 12 |
| 2.2.3 Solid-Electrolyte-Interphase (SEI) and Dendrites | 15 |
| 2.3 Cathodes..... | 18 |
| 2.3.1 Sodium Nickel Cobalt Manganese Oxide (NaNCM) Cathodes..... | 18 |
| 2.3.2 Sulfur Cathodes..... | 19 |
| 2.4 Liquid Nonaqueous Electrolytes | 23 |
| 2.4.1 Electrolyte Basics | 23 |
| 2.4.2 Electrolyte Solvents..... | 24 |
| 2.4.3 Conducting Salts..... | 25 |
| 2.4.4 Additives | 26 |
| 3 Experimental | 28 |
| 3.1 Materials and Chemicals..... | 28 |
| 3.1.1 Sodium Metal and Lithium Metal..... | 28 |
| 3.1.2 Solvents and Conducting Salts..... | 29 |
| 3.1.3 Electrolytes..... | 30 |
| 3.1.4 Separators | 31 |
| 3.1.5 Substrates..... | 31 |
| 3.1.6 NaNCM cathodes..... | 32 |
| 3.1.7 Sulfur Cathode Materials | 32 |
| 3.1.8 Test Cells | 33 |
| 3.2 Techniques..... | 35 |
| 3.2.1 Galvanostatic Cycling..... | 35 |

| | |
|--|------------|
| 3.2.2 Cyclic Voltammetry (CV) | 38 |
| 3.2.3 Electrochemical Impedance Spectroscopy (EIS) | 39 |
| 3.2.4 Scanning Electron Microscopy (SEM)..... | 39 |
| 3.2.5 X-Ray Photoelectron Spectroscopy (XPS)..... | 40 |
| 3.2.6 Sulfur Cathode Preparation | 41 |
| 4 Results and Discussion..... | 42 |
| 4.1 Electrolyte Screening..... | 42 |
| 4.1.1 Unsuitable Solvents..... | 43 |
| 4.1.2 Coulombic Efficiency | 44 |
| 4.1.3 Galvanostatic Cycling Profiles of Select Electrolytes | 48 |
| 4.1.4 Additional galvanostatic testing | 58 |
| 4.2 Electrolyte Stability | 61 |
| 4.2.1 Stability Comparison | 61 |
| 4.2.2 Cyclic Voltammetry Discussion..... | 64 |
| 4.3 Electrolyte Conductivity | 70 |
| 4.4 Sodium Deposition Comparison by SEM..... | 73 |
| 4.4.1 Sodium Deposition on Stainless Steel..... | 73 |
| 4.4.2 Sodium Deposition on Copper Foil..... | 85 |
| 4.5 SEI Examination by XPS | 88 |
| 4.5.1 Overview Survey Spectra | 89 |
| 4.5.2 Detail Element Spectra | 91 |
| 4.6 Sodium Metal/NaNCM Cells..... | 95 |
| 4.6.1 NaBF ₄ /tetraglyme and NaPF ₆ /PC..... | 95 |
| 4.6.2 NaBF ₄ / NaPF ₆ /tetraglyme..... | 99 |
| 4.7 Alkalimetal/Sulfur Cells..... | 101 |
| 4.7.1 Lithium Sulfur Cells..... | 101 |
| 4.7.2 Sodium Sulfur Cells..... | 105 |
| 5 Conclusion and Outlook | 113 |
| Bibliography | 117 |

Index of Abbreviations and Symbols

| Abbreviation | Chem. Formula | Meaning |
|--------------|--|--|
| | Li | Lithium |
| | Na | Sodium |
| | S | Sulfur |
| | S ₈ | Octatomic Sulfur |
| | LiCO ₃ | Lithium carbonate |
| | NiCl ₂ | Nickel chloride |
| | LiMO ₂ | Lithium transition-metal dioxide |
| | C | Carbon |
| | O | Oxygen |
| | F | Fluorine |
| | Na ₂ S _n | Sodium polysulfides |
| | Na ₂ S | Sodium sulfide |
| | LiNO ₃ | Lithium nitrate |
| | NaBF ₄ | Sodium tetrafluoroborate |
| | NaPF ₆ | Sodium hexafluorophosphate |
| | NaClO ₄ | Sodium perchlorate |
| PP | (C ₃ H ₆) _n | Polypropylene |
| NaNCM | Na _x Ni _a Co _b Mn _c O ₂ | Sodium-nickel-cobalt-manganese oxide |
| NaTFSI | | Sodium bis(trifluoromethane)sulfonimide |
| LiTFSI | | Lithium bis(trifluoromethane)sulfonimide |
| NaFSI | | Sodium bis(fuorosulfonyl)imide |
| NaTf | | Sodium trifluoromethanesulfonate |
| Diglyme | | Diethylene glycol dimethyl ether |
| Tetraglyme | | Tetraethylene glycol dimethyl ether |
| EC | | Ethylene carbonate |
| DEC | | Diethyl carbonate |

| Abbreviation | Chem. Formula | Meaning |
|---------------------|----------------------|-------------------------------|
| PC | | Propylene carbonate |
| FEC | | Fluoroethylene carbonate |
| 1,3-DIOX | | 1,3-Dioxolane |
| 1,2-DME | | 1,2-Dimethoxyethane |
| EV | | Electric vehicle |
| T | | Temperature |
| Li-S | | Lithium-sulfur |
| Li-ion | | Lithium ion |
| Na-ion | | Sodium ion |
| Na-S | | Sodium-sulfur |
| et al. | | et alii, "and others" |
| i.e. | | id est, "that is" |
| e.g. | | exempli grātiā, "for example" |
| CE | | Coulombic efficiency |
| C | | Specific capacity |
| RT | | Room temperature |
| SHE | | Standard hydrogen electrode |
| SC | | Short circuit |
| M | | Molar, mol l ⁻¹ |
| approx. | | Approximately |
| SEI | | Solid electrolyte interphase |
| HT | | High temperature |
| ch. | | Chapter |
| CS | | Conducting salt |
| WE | | Working electrode |
| x | | times (magnification) |
| OCV | | Open circuit voltage |
| fig. | | Figure |

| Abbreviation | Chem. Formula | Meaning |
|------------------------|----------------------|--|
| wt% | | Weight percent |
| vol% | | Volume percent |
| ICT | | Fraunhofer Institute for Chemical Technology |
| HIU | | Helmholtz Institute Ulm |
| XPS | | X-ray photoelectron spectroscopy |
| SEM | | Scanning electron microscopy |
| EIS | | Electrochemical impedance spectroscopy |
| CV | | Cyclic voltammetry, cyclic voltammogram |
| Q_{charge} | | Charge capacity |
| $Q_{\text{discharge}}$ | | Discharge capacity |
| Q_{loss} | | Capacity loss (Aurbach test) |
| Q_{hc} | | Charge capacity for high capacity cycle (Aurbach test) |
| Q_{end} | | Charge capacity for last charge step (Aurbach test) |
| Q_{lc} | | Discharge capacity for low capacity cycle (Aurbach test) |

1 Introduction

Even today, the demand for energy storage is immense. High-performance batteries that are cheap, safe and reliable are needed for electro-mobility, stationary energy storage, and consumer electronics such as smartphones, tools, and laptops. At the moment, lithium-ion (Li-ion) is the battery technology of choice, since it has no major drawbacks. For years, most of the battery research has been focused on this topic. However, Li-ion is reaching its physical limits in terms of energy density, and new electrochemical storage materials are being developed. Most of these “next generation” systems, such as lithium-sulfur (Li-S) and lithium-air, rely on lithium metal as the anode with the highest energy density potential. So far, making this material viable for commercial application has proven difficult. Furthermore, the cost of lithium has risen drastically over the last few years and is projected to continue to do so due to the political push for E-mobility and renewable energy generation and the resulting ever-increasing demand for energy storage. As an example, Li-S batteries have the potential to drastically reduce the cost per kWh of energy storage due to sulfur being comparatively cheap. Compared to Li-ion, the amount of required lithium would increase significantly, though, which might negate the cost savings.

For this reason, it is important to identify alternatives to lithium-based systems altogether. One such alternative is sodium-based energy storage. While sodium provides many similar characteristics to lithium, the major difference between the two lies in sodium’s much higher availability. This means that it is much cheaper and that manufacturers could cope much better with an increased demand in the future. For this reason, sodium-ion batteries have received a significant amount of attention over the last few years. While a lot of progress has been made in this area, some fear that the technology can not satisfy the increasing need for higher energy density, though, since it already compares unfavorably with Li-ion systems in this regard. Similar to Li-S, attempts have been made to develop room-temperature sodium-sulfur (RT-Na-S) batteries, which combine a sodium metal anode with a sulfur cathode. High-temperature solid electrolyte Na-S systems have been used for stationary energy storage for quite some time but RT-Na-S has proven difficult to realize mainly due to sodium metal anode. Similar to lithium metal, sodium metal provides high energy density but suffers from

low stability and even higher safety risks, due to its high reactivity. However, if such a system could be realized, it would have the potential to provide cheap stationary energy storage, for example for renewable energy power plants.

In this work, it was attempted to cycle sodium metal anodes with high efficiency. In order to do so, a wide variety of liquid electrolytes was screened. The efficiency of sodium metal plating and stripping out of these electrolytes onto different substrates was determined and some of the deposits were studied through scanning electron microscopy (SEM). The electrochemical stability and the conductivity of a smaller selection of electrolytes were determined. For the most promising candidate, the solid electrolyte interphase (SEI) was examined by X-ray photoelectron spectroscopy. Furthermore, full cells with sodium metal anodes and sodium nickel cobalt manganese oxide (NaNCM) cathodes were built using some of the electrolytes studied in this work. In order to create high-energy-density cells, sulfur cathodes were manufactured and tested with lithium metal anodes and a well-established electrolyte as well as with sodium metal anodes and two previously identified high-efficiency sodium electrolytes.

2 Fundamentals

2.1 Electrochemical Energy Storage in Batteries

2.1.1 Basics

A battery cell is an entity which can convert chemical energy stored within its active material into electrical energy through a redox-reaction. This entails a transfer of electrons from one active material to the other through a conducting circuit. In rechargeable systems or secondary batteries, the process can be reversed in order to recharge the system. In general, cells are composed of three main components:

- a) A cathode: a positive or oxidizing electrode which accepts electrons and is itself reduced during the discharge process.
- b) An anode: a negative or reducing electrode which releases electrons and is itself oxidized during the discharge process.
- c) An electrolyte: a medium which is ion-conductive and allows for a charge transfer between the electrodes. Electrolytes can be liquid, solid or gel-like. The most common electrolytes are liquid and are composed of a solvent and a conducting agent like a salt dissolved therein. Furthermore, it can contain additives which improve certain properties of the electrolyte.

In addition, most commonly used cells include a separator layer, which inhibits the direct contact between the electrodes and thus protects the cell from short circuits while allowing ion transfer.

While the term “battery” is often used colloquially when referring to electrochemical cells, it is actually defined as an array of cells. Depending on the intended capacity and voltage, these cells are connected in either parallel or serial configuration or a combination thereof. [1]

Lithium-ion Batteries

Lithium-ion (Li-ion) batteries are one of the most widely adopted types of electrochemical storage. While they are not studied in this research, they represent the state of the art of current battery research and exhibit an array of properties which any new battery system must try to match or improve upon. For this work, lithium-ion cells are explained briefly and are used as an example with which to compare the systems studied herein. Figure 1 shows a schematic of a Li-ion cell.

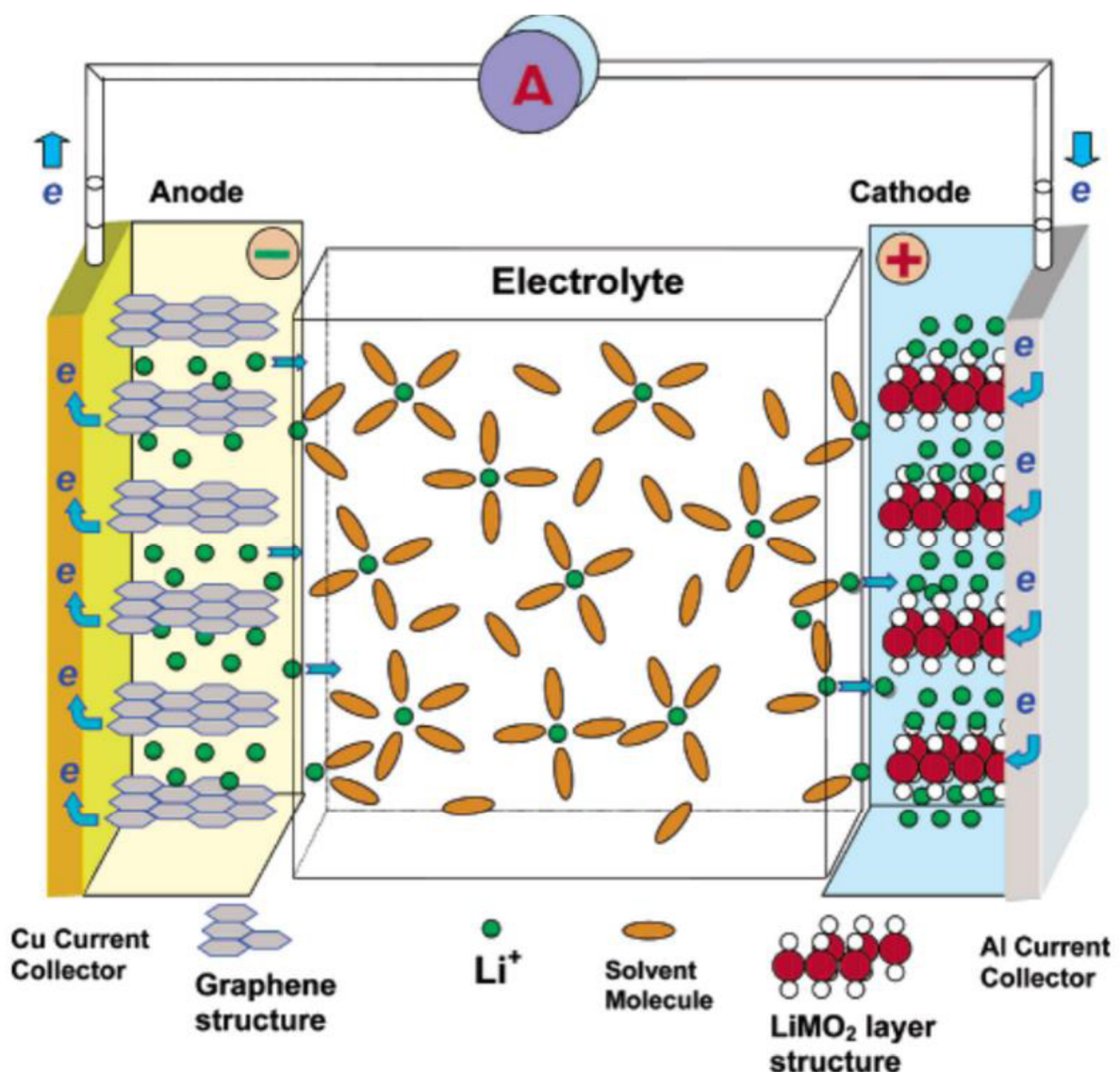


Figure 1: Schematic of a Li-ion battery during discharge. [2]

In most Li-ion systems, the anode mostly consists of graphite, which serves as an intercalation material for lithium. The electrolyte is a solution of a lithium salt in a suitable solvent, e.g. carbonate esters. There is a variety of cathode materials used for lithium-ion cathodes, most of which are transition-metal-oxide based intercalation electrodes. During the discharge process, lithium is oxidized at the anode and is transported through the electrolyte to the cathode where it is reduced and intercalated. At the same time, a flow of electrons occurs in the opposite direction through the external circuit. During charging, this process is reversed. [3]

2.1.2 Properties

Battery systems are defined by a set of properties through which they can be compared and evaluated. All of them are important and none should be neglected when new systems are studied and improved.

Energy Density

One of the most important characteristics of batteries is their energy density, i.e. the amount of energy that can be stored per unit of weight (gravimetric) or volume (volumetric) of the battery. [1] Here, an important distinction has to be made. In going from a battery cell, which contains only the most basic components, to a full battery module, made up of a multitude of individual cells, one has to add a considerable amount of electrochemically inactive weight in the form of casings, safety equipment, and management systems. Thus, it has to be specified what system a given energy density refers to. In this context, gravimetric energy density is one of the most important and most discussed parameters of any battery system.

The amount of storable energy per battery-volume, or volumetric energy density, is of equal importance since space is restricted in many battery applications such as cars and cell phones. Some of the next-generation systems of batteries, like lithium-sulfur, for example, improve upon Li-ion systems in terms of gravimetric energy density but struggle to reach the same volumetric energy density. [1]

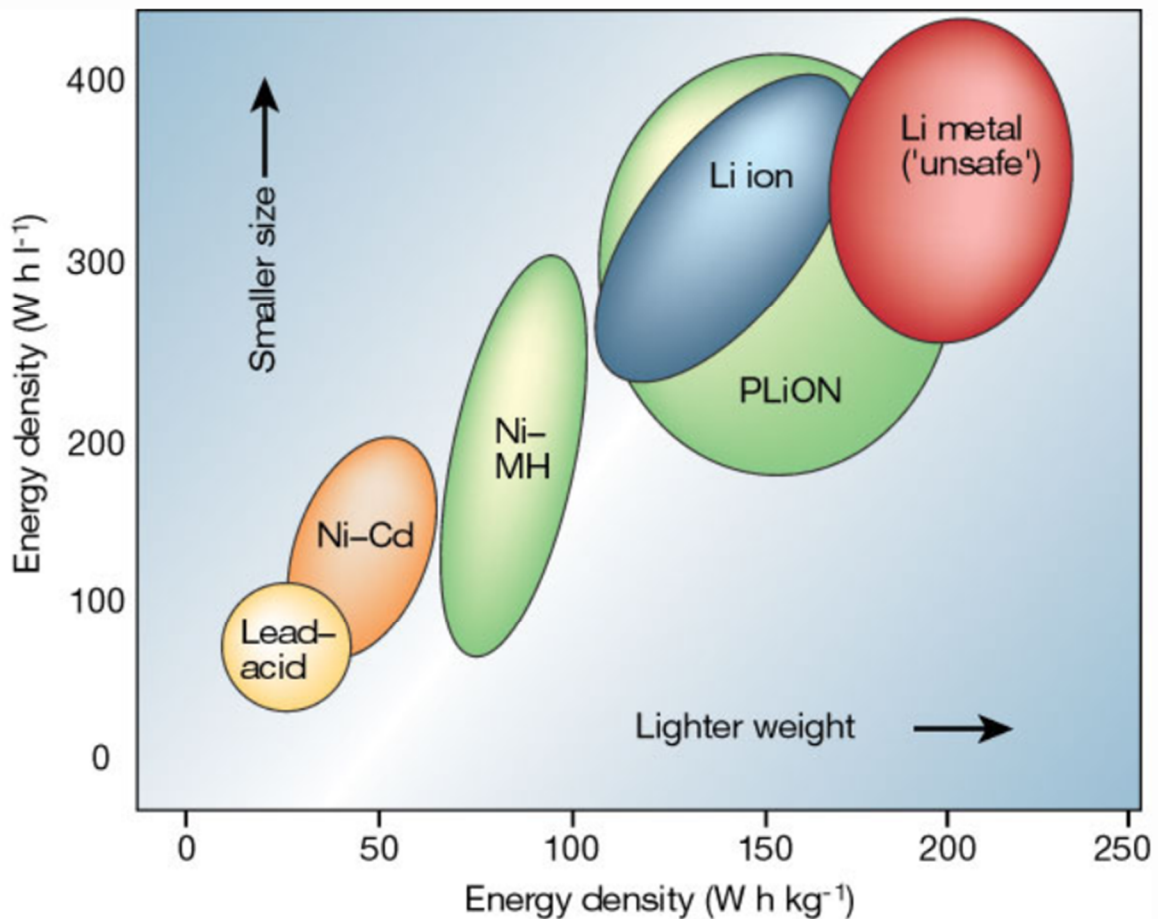


Figure 2: Comparison of different battery technologies in terms of volumetric (W h l^{-1}) and gravimetric (W h kg^{-1}) energy density. Here PLiON denotes polymer-Li-ion. [4]

Gravimetric Capacity (Specific Capacity)

A cell characteristic which is closely related to energy density is specific capacity. While this term may also refer to volumetric capacity it is most often used to give a measure of the amount of charge which can be stored in a given mass of material (gravimetric capacity). Theoretical values for the specific capacity of an active material are often given, although they may be far from what is actually attainable in a cell. Other measures like capacity per electrode mass can also be interesting and are important when considering real-world application of battery chemistries. In a cell, the mean gravimetric capacity is related to the gravimetric energy density by the average cell voltage in the following fashion:

$$\text{Energy Density} = \text{Specific Capacity} * \text{Voltage}$$

The specific capacity of an electrode can be determined through galvanostatic cycling, which is further elaborated on in ch. 3.2.1. [1]

Power Density

Similar to energy density, gravimetric and volumetric power density are among the most important characteristics of cells and batteries. They define how fast a given amount of energy can be stored in or released from an electrochemical storage entity, i.e. how fast a battery or cell can be charged and discharged. This becomes particularly important when dealing with high-energy batteries, as are used, for example, in automotive applications. Aside from fast-charging, high specific power and power density become very relevant for cars, if high performance is required. A particular battery system might provide an acceptable amount of range for an EV, while not being able to provide the required power at the same weight or the same volume. Another example of an application, where high power density is important, is starter batteries. Here, a high amount of power has to be achieved over a short amount of time. While power density is linked to internal cell resistance, it is heavily dependent upon measuring conditions. Thus, it is not a notion as characteristic of a technology as capacity, for example. [1]

Voltage

The voltage of an electrochemical cell is determined by the choice of active materials. The standard reduction potential of active materials vs. hydrogen is given in the galvanic series, which serves to compare the electrochemical behavior of metals. The potential difference in a galvanic cell is only measurable between two half-cells when equilibrium has been established at the phase boundary. The phase boundary is the interface between electrode and electrolyte. This is why the standard hydrogen electrode (SHE) has been established as a reference in order to be able to compare half-cell potentials. The SHE has a defined potential of 0 V as an electrode in a 1 M acidic solution at a temperature of 25 °C and 1013.25 mbar of pressure. The standard reductive potential of a redox pair is then defined as the potential difference between its half-cell and a SHE.

The potential of a cell where no current is flowing is referred to as the open circuit voltage (OCV). [5]

For commercial applications, it is desirable to combine materials with a high difference in standard potentials into a galvanic cell, since a higher potential difference results in a higher average voltage which in turn increases the energy density of the cell, as described above. Most commercially available batteries have operational voltages between 1 V and 4 V. [1]

Overpotential

When a current is applied to a secondary battery during either charging or discharging, the actual voltage between the electrodes is different from the OCV. In electrochemistry, these differences in voltage are referred to as overpotentials. They result from parasitic processes taking place in the cell such as chemical reactions between electrode and electrolyte. [1]

Coulombic Efficiency

The coulombic efficiency (CE) or faradaic efficiency is defined as the ratio between the charge- and discharge-capacities for one cycle of an electrochemical cell and is a measure of the reversibility of the underlying reactions. It is used to determine faradaic losses during cycling which occur during unwanted side reactions. These losses result in heat generation and/or chemical byproducts. One reaction that influences the CE is the solid-electrolyte interphase (SEI) generation which is further elaborated on in ch. 2.2.3. A high CE is needed in commercial cells in order to avoid loss of active materials. Current Li-ion cells consistently reach very high CEs of nearly 100%. [1] A half-cell's CE can be determined through galvanostatic cycling, for example (ch. 3.2.1).

Safety

Due to the high amount of stored chemical energy, batteries can pose a high risk. Since batteries contain both the oxidizer (cathode) and fuel (anode) in a sealed container, safety concerns are of utmost importance. If these two components start to react chemically, their whole chemical energy is converted directly into heat and gas because of the intimate contact. While there are many safety concerns for cells and batteries, short circuits (SCs) are among the most common causes of critical battery failure. SCs can occur, for example through an impact upon the cell which leads to a failure of the separator and a rapid discharge of the cell's energy. This can lead to gassing, fires, and even explosions. Alkali metals like lithium and sodium pose a particularly high risk because of their high reactivity. In contact with water, large amounts of hydrogen gas are generated which, again, can result in explosion or fire. [6] Furthermore, they are prone to dendrite formation which can lead to SCs and is further elaborated on in chs. 2.2.2 and 2.2.3. Another important aspect of battery safety is operation temperature. When batteries are subjected to temperatures beyond their acceptable range (-30 °C to +60 °C for most Li-ion batteries), critical failures can occur such as evaporation of electrolyte, SCs, thermal runaway and liquefaction of electrode materials (e.g. sodium metal). [1]

While the potential dangers of most battery systems are numerous, there is a range of measures that can be taken in order to deal with them. Modern battery management systems host a variety of solutions like pressure switches and other fail-safes, which allow for secure operation. Furthermore, safety can be built into the cell chemistry itself through the use of gel- and solid-electrolytes which can act as a protective layer between the electrodes. [1,7]

2.1.3 Cost

When considering new technologies and chemistries for battery applications, cost is probably the determining factor for viability on the market. In the past, many new battery systems have been developed but have fallen short of mass production due to a high cost of either the involved materials or of manufacturing. While these systems

might find an application in specialty fields such as military and aerospace, their cost prohibits them from finding their way into more mainstream areas of technology such as mobile phones and the automotive industry. It has to be noted that some of the costs of new battery systems can be offset by high volume production and the economies of scale but most of the time, this is not enough. In this regard, the manufacturing process is extremely relevant, since a battery manufacturer will be hesitant to change or replace existing and costly infrastructure in order to accommodate new processes. The most important aspect of battery cost though is the price of materials contained within them. Two factors mainly influence the cost of raw materials. On one hand, there is availability. For example, sodium is 440 times more common than lithium in the earth's crust. [8] This makes it easier to recover and results in a much lower price. On the other hand, there is demand. In recent years, there has been massive development all over the world in order to switch to renewable energies and to reduce the use of hydrocarbons for energy purposes. Because of this, demand for Li-ion batteries has risen dramatically which in turn drives up the demand for lithium carbonate (LiCO_3), the base material for lithium-related chemistries. It is possible that the expansion of lithium production necessary to cope with the rise in demand will not be accomplishable. This would result in a massive increase in price for lithium-based systems. [9] It is also one of the reasons why research into sodium-based batteries has increased dramatically over the last few years. If the price of LiCO_3 increases significantly, the viability of sodium-based batteries might be increased even when considering the significant disadvantage in energy density and operating voltage compared to lithium-ion technologies.

2.2 Anodes

In order to achieve high-performance batteries, the choice of anode is of crucial importance. The focus of this work is the study of sodium metal anodes as an alternative to the materials most commonly used in batteries today. Nevertheless, a short overview of some of these materials and their most important characteristics is given in this chapter.

2.2.1 Carbonaceous Anodes

For lithium-ion batteries, graphite anodes are the standard as well as the most common type of carbonaceous electrode. Indeed it was the invention of graphite anodes that made lithium-ion batteries viable by being orders of magnitude more stable than lithium-metal anodes. Graphite anodes belong to the group of intercalation electrodes where the active material is intercalated in between layers of the carrier material. Due to the fact that 6 graphite atoms are needed in order to accommodate one lithium ion, the theoretical capacity of graphite is only 372 mAh g⁻¹, much lower than that of lithium metal at 3860 mAh g⁻¹. On the other hand, graphite has a very low potential versus lithium metal, a very long plateau in its voltage profile, high stability over thousands of cycles as well as very low cost and high availability in its favor. [7]

Unfortunately, the use of graphite in sodium-based systems has been a lot less successful so far, due to the fact that sodium hardly forms staged intercalation compounds with graphite. [10] Furthermore, electrochemical insertion of sodium into graphite can be expected to occur below the sodium plating potential (≤ 0.1 V). Because of this, the reductive or charging process cannot be observed. For disordered carbons, however, insertion of sodium occurs at a higher voltage than in graphite. [11] In this subclass, hard carbons have emerged as the most suitable anode materials for sodium-ion batteries yet. These carbonaceous materials are synthesized at temperatures above 1000 °C and have been shown to exhibit specific capacities in excess of 300 mAh g⁻¹ with good stability. [12]

One disadvantage that is common to all carbonaceous materials is the formation process that batteries featuring this type of anode have to go through before being ready for use. This process involves slowly cycling the cell 2-3 times after production in order to deal with irreversible capacity losses as well as gas formation which occur during the first few cycles. These phenomena are mostly due to SEI-formation, which is discussed in ch. 2.2.3.

2.2.2 Metal Anodes

Lithium

Pure lithium metal is the first anode material to have been used in lithium-based batteries. To this day, a lot of research is focused on making this material viable for use in commercial cells due to its very high specific capacity of 3860 mAh g⁻¹ and its standard reduction potential of -3.04 V vs. hydrogen. Unfortunately, lithium metal also has a number of disadvantages that make it mostly unusable in commercial applications the most important of which is dendrite formation and its consequences which are further elaborated on in ch. 2.2.3. In general, it is important to note that due to its high reactivity, lithium creates problems in terms of battery safety as well as performance. So far, it has not been possible to create rechargeable lithium metal batteries that match the longevity of commercial Li-ion cells. However, improvements in this field have been made in the recent past and lithium metal anode cells are being commercialized in conjunction with polymer electrolytes. [13]

Another area where lithium metal anodes are being used is primary cells. For this type of cells, the drawbacks of dendrite formation, electrolyte degradation, and short circuits are irrelevant since no replating of lithium takes place. At the same time, these cells exhibit high energy densities while being comparatively costly.

Furthermore, lithium metal is one of the most promising anode materials when it comes to post-Li-ion technologies and the study thereof. These technologies are supposed to improve upon the current state of the art Li-ion batteries in a drastic manner mostly in terms of energy density and cost. Two of the most hopeful candidates for replacing Li-ion are lithium-air and lithium-sulfur (Li-S). Most iterations of these high-energy-density

systems combine a high capacity cathode like sulfur with a lithium metal anode. Unfortunately, these cells run into the same kind of problems as described before (safety issues, short cycle life). Indeed, it has been argued that the lithium metal anode is the most problematic part in these systems and there have been significant efforts to replace this high capacity anode altogether. [14,15]

Sodium

When compared to lithium metal, the use of sodium metal as an anode seems counterintuitive. At a theoretical specific capacity of 1166 mAh g^{-1} , sodium has less than a third of the capacity of lithium while sharing much of the same problems. Indeed, sodium metal is even more reactive than lithium metal and thus needs to be treated with much higher care. For example, while lithium metal foil can be handled in a dry room, the same is not possible with sodium metal, as it even reacts with oxygen from the air. The only suitable environment for handling unprotected sodium is a glovebox filled with inert gas such as argon. One of the most important issues arising from sodium's high reactivity is increased safety concerns. If, for example, a sodium metal anode were to be employed in a car battery, a crash of said car could lead to exposure of the metal to air and lead to a violent reaction. Another disadvantage of sodium is its standard reduction potential of -2.71 V vs. hydrogen. The lower standard potential means that if you replace lithium metal with sodium metal in a cell, the cell's operating potential and thus its energy density will be significantly reduced.

However, sodium metal has some redeeming qualities that might make it a viable anode material in the future one of which is cost. As mentioned earlier, sodium is a lot more common in the earth's crust than lithium which in turn increases its availability and drives down cost. Unfortunately, as there is a multitude of different grades available and since the market is always changing, it is not easy to get reliable numbers on resource prices for lithium- and sodium carbonate. One website listed the price of one metric ton of battery grade LiCO_3 as 144500 RMB or more than 21 737 US\$ at the time. [16] The same source did not list a price for sodium carbonate but an online trading website showed prices between 292 US\$ and 1160 US\$ per metric ton of 99.8% pure NaCO_3 . [17] These prices are certainly subject to change but they give a good indication of the enormous difference between the two materials. For a more direct comparison, at the

time of writing, on the website of Acros Organics, the price for 2.5 kg of LiCO_3 was approx. 6 times higher than the price of the same amount of NaCO_3 . As discussed in ch. 2.1.3, the price difference between these two materials is only going to increase with the rising demand for consumer electronics and EV's.

One could argue that the price of sodium metal as an anode material is still higher than that of most carbonaceous materials, especially graphite. It has to be taken into account though, that carbonaceous materials are not electrochemically active by themselves and need metallic cations in order to function as an anode. If the price for LiCO_3 increases further, carbonaceous anodes in conjunction with lithium ions become less and less viable. Furthermore, when compared to the theoretical specific capacity of graphite anodes in Li-ion systems at 372 mAh g^{-1} , sodium metal's theoretical capacity is more than 3 times greater. This means that in terms of cost per Ah, sodium metal is one of the best solutions currently available for battery anodes.

One other significant advantage that sodium metal has over lithium metal is the choice of current collector material. In Li-based systems, copper, a comparatively heavy and costly material, is normally used as the current collector. This is because aluminium, which is lighter and cheaper than copper, alloys with Li and thus cannot be used. For Na, this is not the case, which means that this is another area where costs and weight could be saved at the cell-level. [18]

It is interesting to note that while they have not been made viable for room temperature systems yet, Na metal anodes are already being employed in high-temperature (HT) batteries such as the Na-S accumulator. Being kept at temperatures between 300 and 350 °C, it combines a liquid Na anode with a liquid sulfur cathode and a Na-ion conducting ceramic solid-state electrolyte. At an operating voltage of 2.1 V, this system has a theoretical energy density of 790 Wh kg^{-1} . Because of the need for perpetual heating, actual energy densities are much lower than that, though. [5]

In order to provide an overview, the specific capacity of a range of anode materials along with their respective potentials vs. Li/Li^+ is shown in figure 3.

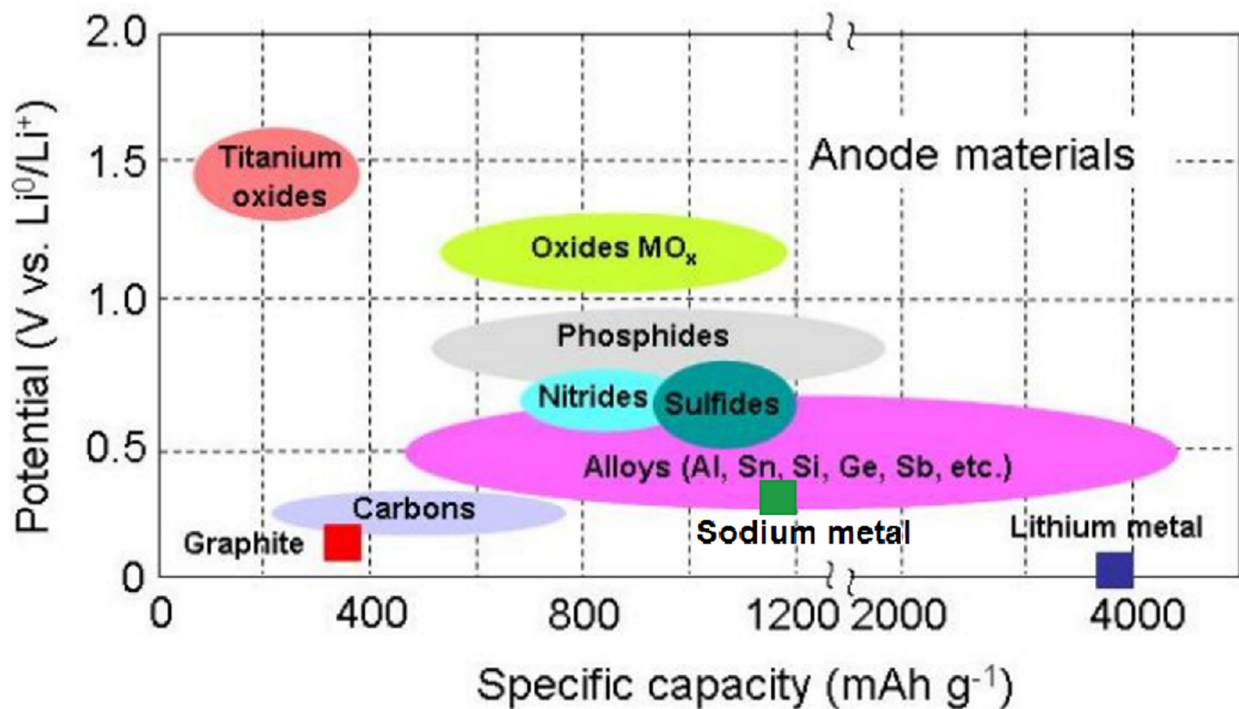


Figure 3: The potential vs. Li/Li^+ and the corresponding specific capacity of a selection of active anode materials. Reproduced and modified from Mauger et al. [19]

2.2.3 Solid-Electrolyte-Interphase (SEI) and Dendrites

For all battery electrodes, the interface between active electrode material and electrolyte plays an important role. Since most active materials are highly reactive, they are not thermodynamically stable in contact with electrolytes, especially liquid ones. Because of this, a reaction takes place when the two come into contact. An interface layer is created that contains the reaction products. This layer is called the solid electrolyte interphase or SEI. In some cases, the SEI may only form if a current is applied to the system. In other cases, the SEI forms instantaneously but changes as soon as a current is applied. If a system forms a stable SEI, it is created in the first cycle and persists afterward. This leads to an overpotential and diminishes the efficiency of the first cycle. It is also the reason why cells containing carbonaceous electrodes, such as graphite, normally need to go through formation before being ready for use. A good SEI must combine a number of properties. Firstly, it should be ion-conductive for whichever active species is used in the cell. For example, a Li-ion anode's SEI should be conductive

for lithium ions. Secondly, it should not be too thick for that would lead to impedances which would diminish the performance of the cell. Thirdly, in most cases, the SEI should protect the anode from direct contact with the electrolyte. That means that it should be impenetrable for molecules contained in the electrolyte in order to prevent further direct contact between electrolyte and electrode. If this is not the case, continuous degradation of both these components may occur and ultimately lead to a cell failure. Last but not least, the SEI should be stable. That is to say, it should be uniform, insoluble in the electrolyte, and resistant to damage from cycling. If this is not the case, cracks and deformations may form and the SEI may have to be rebuilt each cycle. This may lead to bad CEs, electrolyte and electrode degradation, and cell failure. [1,20] SEI components can be identified through Fourier-transform infrared spectroscopy (FTIR), Raman spectroscopy or X-ray photoelectron spectroscopy.

If the SEI is unstable, dendrite formation may occur on the electrode surface. While this topic is also important for carbonaceous electrodes, here it will only be discussed in the context of metal anodes. Dendrite formation refers to non-uniform deposits on the active surfaces of electrodes. For example, a dendrite might be a needle-like outgrowth perpendicular to the anode plane which has formed during electrochemical reduction. The reason for the occurrence of dendrites is usually a local fluctuation in current density which may be caused by a variance in SEI thickness. [20] These formations can grow to a length of a few μm and may even pierce a cell's separator. In this case, a short circuit (SC) may occur, as direct contact would be established between the two electrodes. This would, at the very least, impede the performance of the cell and in the worst case, lead to catastrophic failure. [1] In some cases, dendritic growth can form mossy layers on top of metallic anodes instead of individual needles. Here, the risk of SCs is decreased but other negative effects might occur, such as increased impedance, loss of active material, and electrolyte decomposition. In some cases, small dendrites form and bend or break off from the anode. These structures may become disconnected and thus not be available for oxidation anymore ("dead" active material). Even worse, since the electrode is thickening under these circumstances, pressure may build up in the cell and the whole element might be damaged or become non-functional as a result. [21]

There are many ways to prevent or inhibit dendritic growth, the most obvious of which is the selection of electrolyte. If an electrolyte that is suitable for use in a battery forms a

stable SEI when combined with an alkali metal electrode, it should be possible to create a functioning cell from these components. A scheme showing the difference in sodium metal deposition between a stable SEI and an unstable SEI is shown in figure 4. While the stable SEI allows for the expansion of the anode while remaining on the electrode surface, the irregular SEI breaks up and has to be continually rebuilt due to direct contact between the electrolyte and fresh Na. This may also result in significant capacity losses. [20] The main goal of this work was to find a liquid electrolyte that can provide a stable SEI on sodium metal.

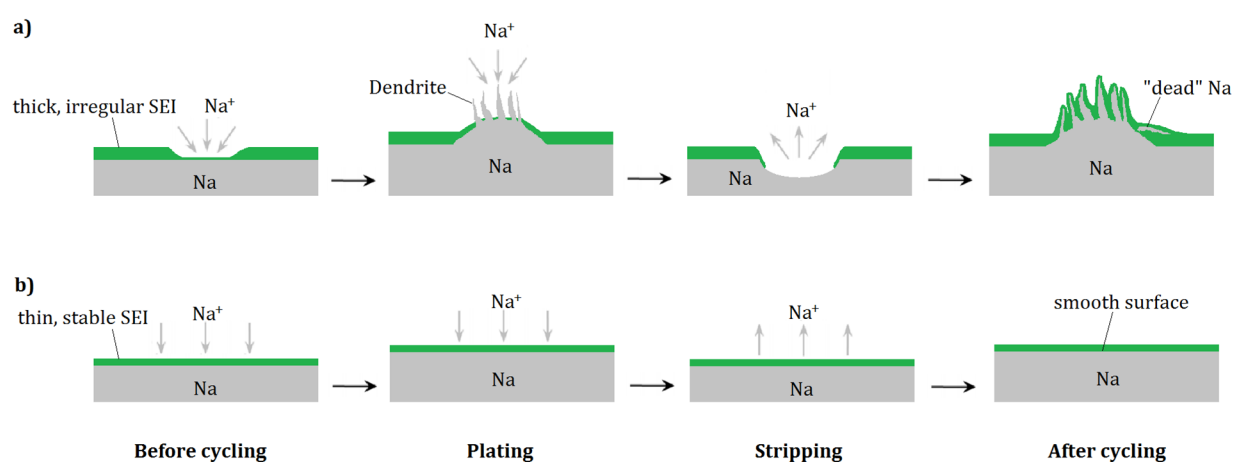


Figure 4: Schemes showing the difference between (a) dendritic and (b) non-dendritic sodium plating and stripping.

Solid state electrolytes provide another possibility of dealing with dendrites. These systems often consist of an ionically conductive ceramic layer, which acts as the electrolyte and separator at the same time while providing very high structural stability and low reactivity vs. alkali metals. Unfortunately, solid state electrolytes have their own range of problems, two of the most important of which are low ionic conductivity and low contact area between electrode and electrolyte. For this reason, ceramic electrolytes so far have only been used extensively in high temperature (HT) batteries such as HT-Na-S where these disadvantages can be remedied (see also ch. 2.2.2). In order to keep all active materials in their liquid phase, the HT-Na-S system operates at above 300 °C. Because of this, no dendrites can be formed. Furthermore, the contact area between

electrolyte and liquid sodium metal as well as the ionic conductivity of the ceramic electrolyte increase drastically. [3]

2.3 Cathodes

While there is a whole range of available cathodes for lithium-based systems, sodium-based systems only have a limited number of compatible cathodes. Two of these have been chosen for this work in order to create full cells. This chapter is supposed to give a short overview of their most important properties. It is important to note that while sulfur cathodes were formulated and manufactured by the author, cathodes and the synthesis thereof were not a focus of this work.

2.3.1 Sodium Nickel Cobalt Manganese Oxide (NaNCM) Cathodes

Layered compounds with the general formula LiMO_2 have been studied extensively in the past as Li-intercalation cathode materials. Recently, a number of investigations have shown that 2D-layered transition metal oxides are also good sodium intercalation materials and serve well in cathodes for Na-ion batteries. [22–25] One group of such materials is sodium nickel cobalt manganese oxides (NaNCMs) with the general formula $\text{Na}_x\text{Ni}_a\text{Co}_b\text{Mn}_c\text{O}_2$. Since the NaNCM cathodes used in this work were synthesized at Helmholtz Institute Ulm (HIU) following the method described by Buchholz et al., they will serve as an example to discuss this class of electrodes. [26] Here, the exact composition of the material was $\text{Na}_{0.66}\text{Ni}_{0.22}\text{Co}_{0.11}\text{Mn}_{0.67}\text{O}_2$.

In figure 5, a representation of the material structure of such a NaNCM cathode is shown. Two layers are present in this stacked P2-type material. These are formed by octahedrally coordinated transition metal cations. The sodium ion is located in the interspace between the transition metal layers and is coordinated by six oxygen anions in a trigonal prismatic configuration. [27]

With these electrodes, specific capacities of about 90 mAh g^{-1} were achieved at HIU in the voltage range of 2.0 V to 4.0 V with 1.0 M NaPF_6/PC as the electrolyte.

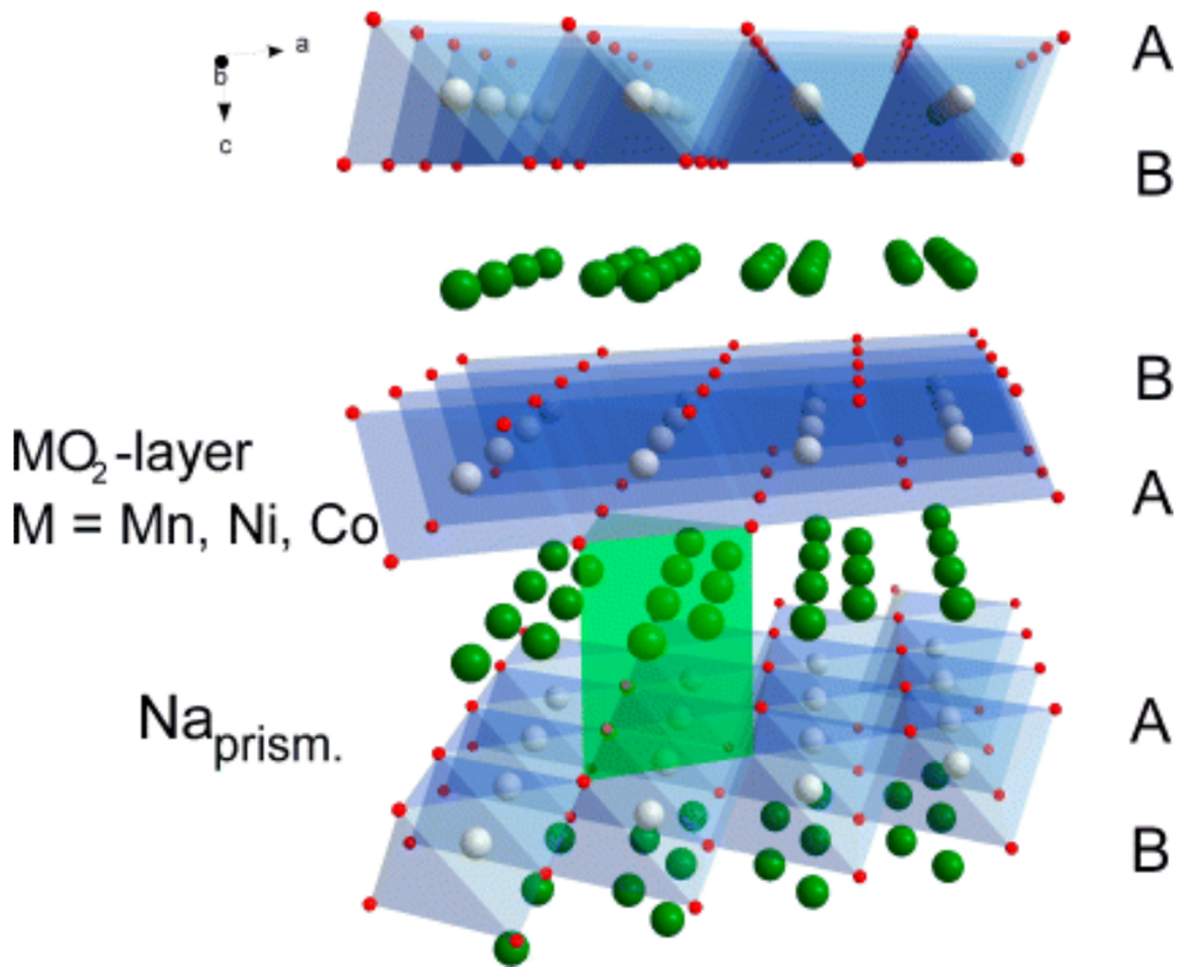


Figure 5: Illustration of the structure of a P2-type NaNCM. [27]

2.3.2 Sulfur Cathodes

Elemental sulfur has one of the highest theoretical specific capacities of all cathode materials at 1672 mAh g⁻¹. This means that in combination with high capacity anode materials such as Li metal and Na metal, energy densities at the cell level of up to 600 Wh kg⁻¹ could be reached. [28] For this reason, Li-S research has increased immensely in popularity over the last decade. Commercial Li-S cells are slowly becoming available but are still suffering from comparably low cycle life. Na-S systems, on the other hand, have only been used in high-temperature configurations so far, as discussed above. Another reason for the allure of this cathode material is its low price which is due to its high availability of 5 billion tons globally. [29]

Li-S

Li-S cells typically combine a Li metal anode with a sulfur cathode. The reaction equation for the system is



and yields a theoretical cell potential of 2.24 V. [30]

However, this conversion goes through multiple steps where several intermediary species with the sum formula Li_2S_n ($1 \leq n \leq 8$) occur. These polysulfides are soluble to different degrees in typical organic electrolyte solvents. A certain degree of solubility is necessary in order to allow for complete active material utilization. However, it has been proposed that entrapment of polysulfides within the cathode structure might be beneficial. [31] A typical discharge and charge profile of a Li-S cell is given in figure 6.

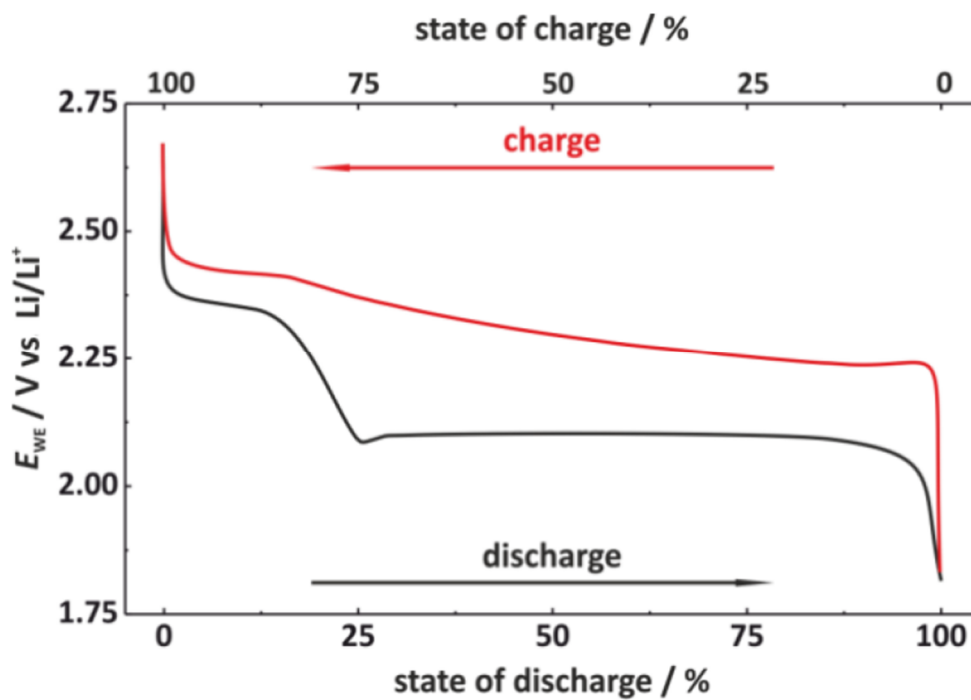


Figure 6: Typical voltage profile of a Li-S cell. [30]

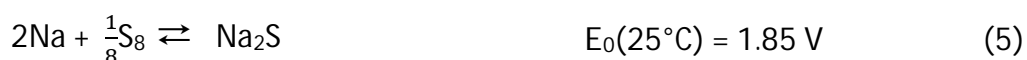
In order to create a functional cathode out of elemental octatomic sulfur, several additives are necessary. Due to sulfur's low electrical conductivity, conductive carbons are used to create a sort of backbone for the cathode. These carbons influence the behavior and performance of the electrode depending on their geometry and properties. [32,33] Among the carbons implemented in this way are amorphous carbon blacks, graphites, carbon nanotubes (CNTs), carbon nanofibers and carbons with a wide variety of porosities. [34] Besides their high electrical conductivity, carbons also allow for polysulfide adsorption.

Furthermore, binders are normally added to the mixture in order to generate structural stability. Polyvinylidene fluoride (PVDF), Polytetrafluoroethylene (PTFE) and styrene-butadiene rubber (SBR) are some of the most commonly used binders. The choice of binder depends on the chosen production process and it has been observed that the binder/cathode mass ratio may influence the electrode performance massively. [35–37] In most cases, the binder makes up about 10 wt% of the cathode (current collector excluded). These components typically lower the sulfur fraction to 40-80 wt%, which equals a decrease in cathode capacity compared to pure sulfur.

Other important parameters of sulfur electrodes are the areal sulfur load and sulfur utilization. While the former determines how much active material is present in a cathode per area unit, the latter describes the fraction of sulfur that is actually used during cycling. While typical areal loads lie between 0.5 and 2.0 mg_s cm⁻², it has been theorized that in order to compete with commercialized systems, sulfur cathodes would need to have at least 3 mg_s cm⁻². [28] In terms of sulfur utilization, low areal load Li-S systems with capacities between 500 and 700 mAh g⁻¹_s after 1000 cycles have been presented in literature, which corresponds to 30-42% of the maximum theoretical capacity. [38–40] During the first few cycles, capacities of 1100 mAh g⁻¹_s are obtainable even in high sulfur load electrodes, but high capacity fade with cycle number is common. [41] One other factor that has been shown to be essential for creating high energy density Li-S cells is electrolyte/sulfur ratio. [28] However, no focus was put on this aspect in this work.

Na-S

For room temperature Na-S systems, only very little research has been done so far, compared to Li-S. Nevertheless, there are a few reports of functional RT-Na-S cells, the majority of which appeared in the last few years. Adelhelm et al. have proposed a series of reactions taking place during an ideal discharge process of a Na-S cell with corresponding theoretical cell potentials calculated from thermodynamic data: [30]



In liquid electrolyte cells, the reaction paths are arguably more complex than this though. Similar to the Li-S system, many polysulfides are highly soluble and metastable phases exist. However, Na_2S_2 and Na_2S are the least soluble compounds in organic solvents, which means that the reaction as described in equation 4 is expected to be a solid state conversion. [30]

While some publications with low sulfur content cathodes have shown maximum capacities as high as 1400 - 1600 mAh g⁻¹ in the first cycle and about 1100 mAh g⁻¹ in the 10th cycle, most research into more conventionally produced electrodes with realistic parameters have struggled to reach more than 500 mAh g⁻¹. [42–46] Many of these publications have made use of tetraglyme in their electrolytes. For example, Ryu et al. have reported maximum specific capacities of about 540 mAh g⁻¹ for cathodes with a sulfur fraction of 60 wt% and unspecified areal load. The cathodes were produced from an acetonitrile suspension which was cast onto an aluminium current collector and were cycled with 1 M NaTf/tetraglyme as the electrolyte. [44] During discharge, only the plateau region at 1.68 V associated with the $\text{Na}_2\text{S}_2/\text{Na}_2\text{S}$ conversion reaction was observed. The publication attributed the capacity values, which were rather low when compared to most Li-S systems, to losses of active material through dissolution in the

electrolyte. Nevertheless, to the knowledge of the author, this represents one of the best results obtained Na-S cells employing conventionally produced cathodes with a sulfur content equal to or above 60 wt%.

2.4 Liquid Nonaqueous Electrolytes

In battery research, a wide variety of liquid electrolytes has been studied in the past. This chapter is meant to give a short overview of the different electrolyte components as well as the typical properties of this class of electrolytes.

2.4.1 Electrolyte Basics

While active electrode materials attract the most attention, the electrolyte arguably has an equally important role to play for the performance of batteries. Ionic conductivity is probably the key electrolyte property since it quantifies the rate at which ions can be transported between electrodes and thus determines the power output of the cell. [47] For example, LP30, an electrolyte commonly used in Li-ion cells, has a conductivity of 12.55 mS cm^{-1} . [48] Ponrouch et al. have argued that an equally important parameter is electrolyte stability or metastability since ideally, there should be no chemical reactions or changes involving the electrolyte during cell operation. They have compiled the following generic list of properties which should be considered when choosing an electrolyte. The list is copied directly from the quoted source. [49]

An ideal electrolyte should be:

- chemically stable – no chemical reactions during cell operation including both within itself, with the separator and electrodes used, and with the current collectors and packaging materials employed,
- electrochemically stable – large separation of high and low onset potentials for decomposition by oxidation or reduction, respectively,

- thermally stable – a wide liquidus range; both the melting and boiling points should be well outside the (internal) operation temperatures, and
- ionically conductive and electronically insulating – to sustain cell operation by facile ion (here Na^+) transport and to minimize self-discharge of the cell, respectively.

Furthermore, there are practical criteria that should be pursued. The electrolyte should:

- have low toxicity and also meet other measures of limited environmental hazard successfully,
- be based on sustainable chemistries, and
- carry as low a total cost of materials and production as possible

In order to achieve these requirements, the right choice of solvent and conducting salt is crucial.

2.4.2 Electrolyte Solvents

For cells with alkali metal anodes, the following solvents can be used: [50]

- dipolar protophobic aprotic solvents such as esters,
- electron donors with low permittivity such as ethers,
- inert solvents such as alkanes and,
- low polarity solvents such as benzene

Solvents from the first group such as EC and PC as well as from the second group such as DIOX and tetraglyme are often used because of their physical properties. In general, a low viscosity is advantageous since it results in a higher ion mobility and thus conductivity. [50]

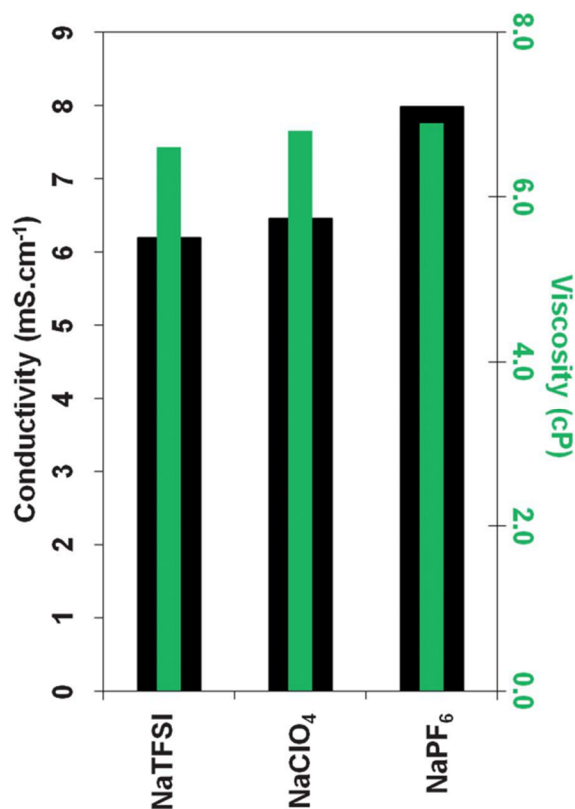


Figure 7: Conductivities and viscosities of several PC-based electrolytes with salt concentrations of 1 M. [48]

2.4.3 Conducting Salts

The second crucial electrolyte component is the salt. Here, the solubility within the solvent(s) used, the stability vs. oxidation/reduction, the chemical stability vs. other materials in the cell, and safety-related aspects, are the most important properties affecting salt selection. [49]

For sodium systems, mostly the same anions are used as in lithium-based systems: PF_6^- , ClO_4^- , BF_4^- , Tf, TFSI, and FSI. Unfortunately, all of these anions have some problems which make them less than perfect for battery applications. While PF_6^- tends to suffer hydrolysis to yield PF_5 , POF_3 , and HF at elevated temperatures and in the presence of moisture, ClO_4^- is a strong oxidant and mostly banned from any practical cell development. Because of its comparatively strong interaction with the cation, BF_4^- creates electrolytes which have fewer charge carriers present and are thus less

conductive. The same problem is present in Tf-based electrolytes, which also tend to corrode aluminium current collectors. This is also the reason why TFSI is rather unpopular, academically. While NaFSI is non-toxic, has high thermal stability and yields high conductivities, it is yet unclear whether it corrodes Al. [49]

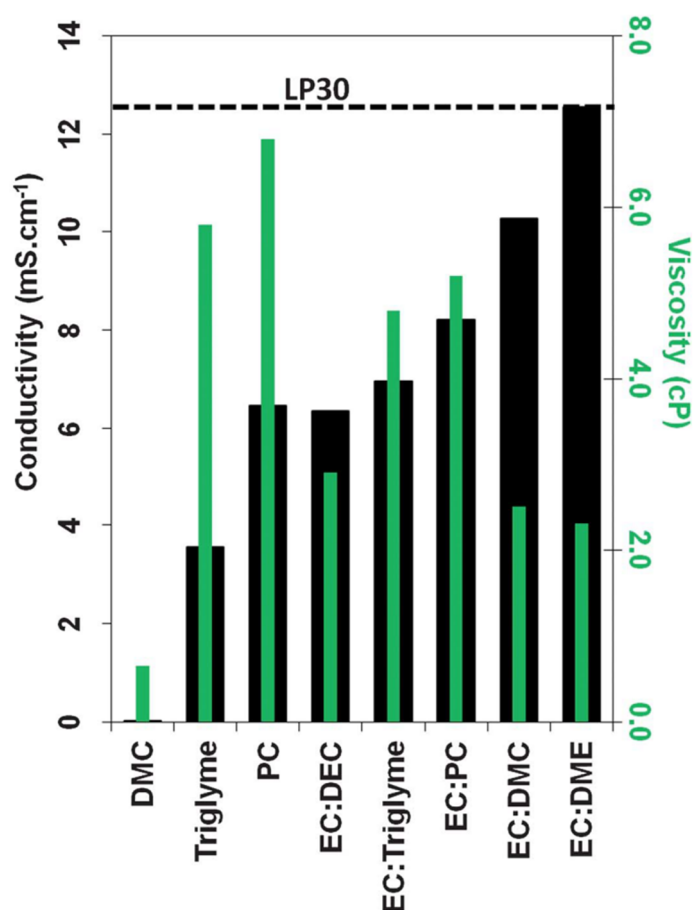


Figure 8: Conductivities and viscosities of several electrolytes based on 1 M NaClO₄ solutions in different solvents and solvent mixtures. [48]

2.4.4 Additives

In order to improve certain electrolyte properties without having to change the basic composition majorly, additives are often used. These components are incorporated in small amounts and are often consumed during the initial cell cycles as they are intended for the formation of interphases at the electrolyte/electrode interfaces. [47]

Additives can target most of the general properties of suitable electrolytes discussed above such as improving chemical and electrochemical stability or decreasing viscosity. [49] For example, in Li-S cells, the addition of small amounts of NaNO_3 to the electrolyte has been shown to majorly influence the aggregation of dissolved polysulfides on the anode (polysulfide shuttle). [51–53]

Perhaps the most important additive is fluoroethylene carbonate (FEC), which is commonly used in carbonate electrolytes and has been shown to improve cell performance in a number of different systems such as Li-ion and Na-ion. [54–57] It has been shown that SEIs formed by FEC containing electrolytes tend to be denser and thinner than those formed in FEC-free electrolytes. [47]

3 Experimental

This chapter is meant to detail the experimental conditions of this work. The specifications of all used equipment, materials and instruments are given. Furthermore, the experimental procedures performed are described and explained.

All tasks that necessitated the use of a dry, oxygen-free environment were performed in an MBRAUN glovebox filled with argon, containing less than 1 ppm of H₂O and O₂ each.

3.1 Materials and Chemicals

An overview of the used materials and their preparation is given in this chapter.

3.1.1 Sodium Metal and Lithium Metal

In an argon atmosphere, a dry sodium stick from Acros Organics (purity \geq 99.8%) was cut into 2x1x0.2 cm³ pieces, which were then inserted into a Mylar foil pouch. This pouch was put into a roll press and the contained sodium was pressed to a thickness of 300 μ m. The resulting thin sodium metal sheet was stored in a sealed container in an argon atmosphere.

For lithium metal anodes, lithium foil (Sigma Aldrich; purity \geq 99.9%) was roll-pressed to a thickness of 300 μ m and stored in a sealed container in an argon atmosphere.

3.1.2 Solvents and Conducting Salts

Solvents

A wide range of different solvents was used in this work. Table 1 gives an overview of these solvents and the companies they were procured from.

Table 1: Solvents used in this work with respective manufacturers.

| Manufacturer | Sigma Aldrich | Merck | BASF |
|--------------|--|-------------------------|--------------------------|
| Solvent | Diethyl carbonate (DEC) | Ethylene carbonate (EC) | Propylene carbonate (PC) |
| | Fluoroethylene carbonate (FEC) | | |
| | Diethylene glycol dimethyl ether (diglyme) | | |
| | Tetraethylene glycol dimethyl ether (tetraglyme) | | |
| | Acetonitrile | | |
| | Tetramethylene sulfone (Sulfolane) | | |
| | 1,3-Dioxolane (1,3-DIOX) | | |
| | 1,2-Dimethoxyethane (DME) | | |

All solvents were dried before use by adding a 3 Å molecular sieve to the storage container of each solvent in order to trap any traces of water. The solvents were stored in an argon-filled glovebox.

Conducting salts

A variety of conducting salts (CS) was tested for use in electrolytes. An overview of these salts and their respective manufacturers is given in table 2.

Table 2: Conducting salts used in this work with respective manufacturers.

| Manufacturer | Sigma Aldrich | Alfa Aesar | Solvionic |
|------------------------|---|---|--|
| Conducting salt | Sodium tetrafluoroborate (NaBF ₄) | Sodium hexafluorophosphate (NaPF ₆) | Sodium bis(trifluoromethane)sulfonimide (NaTFSI) |
| | Sodium trifluoromethanesulfonate (NaTf) | Sodium perchlorate (NaClO ₄) | Sodium bis-(fluorosulfonyl)imide (NaFSI) |
| | Lithium nitrate (LiNO ₃) | | |
| | Lithium bis(trifluoromethane)sulfonimide (LiTFSI) | | |

The salts were dried for 24 h at 80 °C in a vacuum chamber (<10⁻² mbar) before being stored in an argon-filled glovebox.

3.1.3 Electrolytes

By combining the solvents and conducting salts (CS) described in ch. 3.1.2, a range of sodium-based electrolytes was formulated. It was attempted to create electrolytes with a 1.0 M concentration. If the amount of CS corresponding to this concentration did not fully dissolve in a particular solvent, the concentration was lowered to 0.5 M. If the CS still precipitated after that, the concentration was lowered even further to 0.25 M. Mixtures of EC and DEC were always prepared at a volume ratio of 1:1. To some of the formulations, 2 vol% of FEC was added. An overview of the electrolytes created for sodium metal plating and stripping tests is given in table 3.

Table 3: Electrolyte formulations for sodium metal plating/stripping tests with respective concentrations.

| Solvent | Conducting salt concentration / M | | | | | |
|------------|-----------------------------------|-------------------|-------------------|--------|-------|------|
| | NaClO ₄ | NaPF ₆ | NaBF ₄ | NaTFSI | NaFSI | NaTf |
| EC/DEC | 1.0 | 1.0 | 0.25 | 0.5 | 0.5 | 0.5 |
| EC/DEC/FEC | 1.0 | 1.0 | 0.25 | 0.5 | 0.5 | 0.5 |
| PC | 1.0 | 1.0 | 0.25 | 0.5 | 0.5 | 0.5 |
| PC/FEC | 1.0 | 1.0 | 0.25 | 0.5 | 0.5 | 0.5 |
| Diglyme | 0.5 | 0.5 | 0.5 | 0.5 | 0.5 | 0.5 |
| Tetraglyme | 1.0 | 1.0 | 1.0 | 1.0 | 1.0 | 1.0 |

An electrolyte for Li-S tests with the following composition was also prepared:



All electrolytes were mixed and stored in an argon-filled glovebox.

3.1.4 Separators

For most of the cells studied in this work, Whatman GFA glass fiber separators were used. [58] In cells where less separator porosity was required (e.g., cells for SEM examination), celgard 2400 was employed. [59] NKK TF4050, a cellulose separator, was used for cells prepared for SEM examination containing PC-based electrolytes. [60] All separators were cut to size by hole punches and then dried for 24 h in a vacuum chamber ($<10^{-2}$ mbar). Whatman GFA separators were additionally subjected to a temperature of 120 °C during the drying process.

3.1.5 Substrates

Sodium metal plating and stripping were performed on two substrates, stainless steel disks, and copper foil.

The disks were made from EN 1.4404 type stainless steel, had a thickness of 2.5 mm and a diameter of 11.3 mm. Prior to sodium electrodeposition, they were wet-sanded with 800 grit sandpaper, cleaned and dried. This was done in order to ensure a uniform surface. These disks were also used as current collectors for all test cells, independent of other cell parameters.

The other substrate used was Schlenk SE-Cu R360, a galvanostatically treated copper foil with a thickness of 6 - 10 μm , which was cut to size and dried for 24 h under vacuum ($<10^{-2}$ mbar) at 120 °C before use.

3.1.6 NaNCM cathodes

For full cell tests, pre-prepared NaNCM cathodes were provided by Helmholtz Institute Ulm (HIU). These P2-type layered $\text{Na}_{0.66}\text{Ni}_{0.22}\text{Co}_{0.11}\text{Mn}_{0.67}\text{O}_2$ electrodes had been produced following a procedure detailed in literature. [26] They had an active material content of 85 wt% and had exhibited an average specific capacity of 90 mAh g^{-1} for cycling tests between 2.0 V and 4.0 V at a current density of 40 mA per gram of active material at HIU. The cathodes were stored in a sealed container in an argon atmosphere and were cut to size with a hole punch when needed.

3.1.7 Sulfur Cathode Materials

In the framework of a bachelor's thesis, sulfur cathodes were developed with the goal of maximizing sulfur load while maintaining high sulfur utilization. [61] While a wide variety of material combinations were tested, only one of them is presented in this work. It contained the following components:

Table 4: Materials used for making sulfur cathodes with respective manufacturers.

| Material | Manufacturer |
|---------------------------|---------------------|
| Sulfur | Sigma Aldrich |
| PSBR100 [62] | Targray |
| Ketjenblack EC-600 JD[63] | AkzoNobel |
| Porocarb HD3 [64] | Heraeus |
| Porocarb HG3 [64] | Heraeus |
| FC4430 [65] | 3M |

3.1.8 Test Cells

The test cells assembled in this work can be divided into two categories, two-electrode cells, and 3-electrode cells. Both consisted of a glass outer body into which stainless steel (EN 1.4404) plungers and stainless steel discs with a diameter of 11 mm were inserted as current collectors or electrodes. All parts of the cells were cleaned thoroughly and dried under vacuum ($<10^{-2}$ mbar) for 24 h at 120 °C before use. Because of the glass shell, some of the processes taking place inside the cells during tests can be observed with the naked eye (e.g., electrolyte color change). These custom test cells were designed and developed at Fraunhofer ICT.

2-Electrode Cell

Most of the test cells in this work were of this type. The outer shell consisted of a glass tube with an inner diameter of 11.5 mm into which the other components of the cell were inserted. For the counter electrode, Sodium metal foil was cut to size with a hole punch and pressed onto a stainless steel disk which acted as the current collector. On top of this sodium metal sheet, the separator, electrolyte and working electrode (WE) were added. If not specified differently, the counter electrode, WE and separator all had a diameter of 11 mm. As shown in figure 9, a spring ensured good contact between all cell components. Rubber seals on the stainless steel plungers at both ends of the cell insured an airtight environment. The plungers also served as connectors for the testing station.

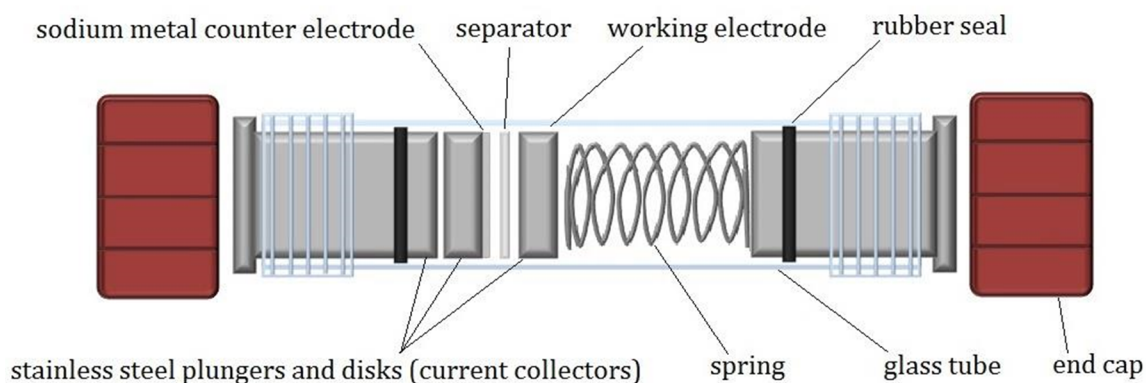


Figure 9: Scheme of a 2-electrode glass cell; inner diameter: 11.5 mm.

3-Electrode Cell

This type of cell had a smaller diameter tube (7.5 mm) attached to the larger tube. This allowed for the installation of a reference electrode which consisted of a small patch of sodium foil mounted on a stainless steel plunger. Otherwise, the design was the same as for the 2-electrode cell. This type of cell was used exclusively for cyclic voltammetry (CV) tests, where a more precise control of cell potential was necessary.

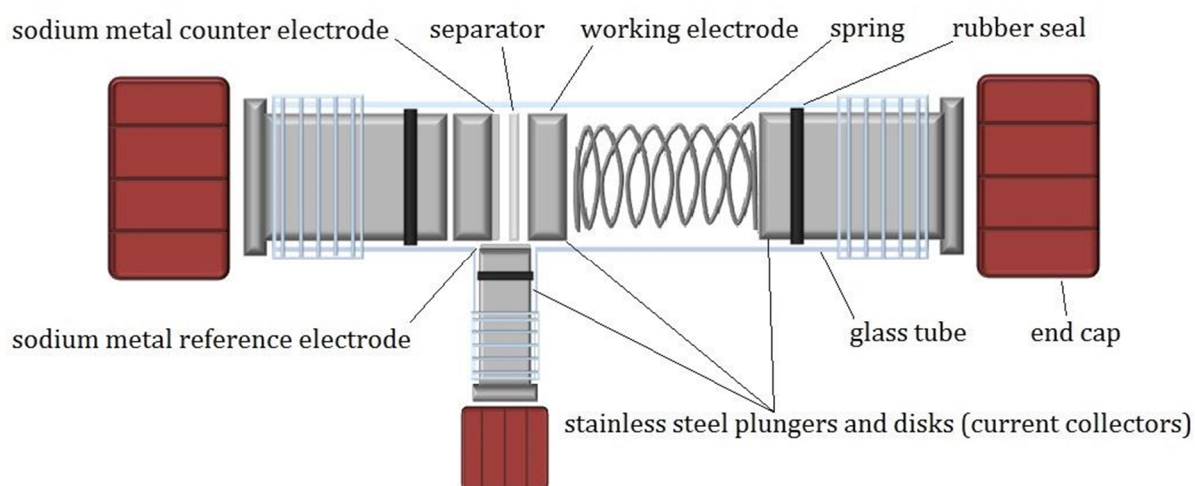


Figure 10: Scheme of a 3-electrode glass cell; inner diameters: 11.5 mm and 7.5 mm.

3.2 Techniques

In this chapter, the various techniques and methods employed in this work are to be explained and detailed. All tests were conducted at room temperature.

3.2.1 Galvanostatic Cycling

Galvanostatic cycling was the main tool used in this work for studying sodium metal plating and stripping as well as full cell performance. For coulombic efficiency tests, 2-electrode cells as shown in figure 9 were built with two Whatman GFA separators between electrodes and an electrolyte volume of 85 μl . The experiments were performed on a Basytec CTS Lab System.

Standard Coulombic Efficiency Test

For this test, constant currents of -0.1 mA and +0.1 mA were applied alternately to the stainless steel WE (electrode area: 1.0 cm^2). The negative current was applied during the discharge step in order to induce sodium ion reduction and thus sodium metal deposition on the WE. This was done for two hours resulting in a maximum deposited areal capacity of 2 mAh cm^{-2} . Afterwards, the positive current was applied during the charge step in order to oxidize and strip the sodium metal from the WE until a voltage of 1.0 V was reached (cutoff potential). The capacity recovered during this step (Q_{charge}) was compared to the theoretical deposited capacity ($Q_{\text{discharge}}$) in order to obtain the coulombic efficiency (CE):

$$CE = \frac{Q_{\text{charge}}}{Q_{\text{discharge}}} * 100\% \quad (1)$$

This cycle was repeated until the cell failed, for example due to a short circuit. It is important to remember that the same processes as described here for the WE also take place on the sodium metal counter electrode, only in reverse (discharge=stripping;

charge=plating). This effectively doubles the chance of dendrite growth. The initial survey of sodium metal plating and stripping out of a wide selection of electrolytes was done using this test procedure.

Aurbach-Test

For the standard coulombic efficiency test described above, sodium metal was plated on and stripped off of stainless steel disks. However, in a sodium metal full cell, these processes would take place on a sodium metal sheet on the anode, similar to what happens on the counter electrode during the standard test. Thus it was necessary to find a CE test that would simulate these conditions in order to examine if the plating and stripping behavior was any different.

Aurbach et. al have proposed a method for determination of coulombic efficiencies for plating and stripping of alkali metals which solves this problem. [66] It consists of depositing a large quantity of alkali metal onto a substrate and subsequently stripping and re-depositing a small fraction of this metal before a last stripping step which removes the metal completely from the substrate again. By comparing the capacities of the first plating step and the last stripping step, it can be determined how much capacity was lost during the smaller capacity cycles and an average CE can be determined. However, this test does not allow for observation of the change of CE with cycle number.

For two of the tested electrolytes, 1.0 M NaPF₆/PC and 1.0 M NaBF₄/tetraglyme, this Aurbach-test was performed in a slightly modified manner. Sodium was deposited and stripped twice at a current density of 0.1 mA cm⁻² over 20 h. This was done in order to determine the effective charge capacity for the large deposit. After a third plating step, the stripping and plating time was reduced to 1 h at the same current and the cell was cycled like this for 10 cycles, finishing with a plating step. Finally, the metal was stripped until the cell reached the cutoff-voltage of 1.0 V which meant that all the sodium metal was stripped from the substrate. The capacity loss over the 10 low capacity cycles (Q_{loss}) could then be calculated through the following relation:

$$Q_{\text{loss}} = \frac{Q_{\text{hc}} - Q_{\text{end}}}{10} \quad (2)$$

where Q_{hc} is the charge capacity during the second high capacity cycle and Q_{end} is the capacity during the final charge step. The coulombic efficiency for the low capacity cycles was then calculated as

$$CE = \frac{Q_{lc} - Q_{loss}}{Q_{lc}} * 100\% \quad (3)$$

where CE is the coulombic efficiency and Q_c is the discharge capacity of the low capacity cycles.

Sodium-Metal/NaNCM Cells

For full cell tests with NaNCM cathodes, the same 2-electrode cell setup as described before was used except that cathodes with a diameter of 11 mm were introduced between the GFA separators and the stainless steel disk on the WE side. The electrolyte volume was 85 μ l.

The measurement protocol was set so that the cells were continually cycled between 2.0 V and 4.0 V at a rate of 40 mA per gram of active material.

Three different electrolyte formulations were tested within these cells:

- 1.0 M NaPF₆/PC
- 1.0 M NaBF₄/tetraglyme
- 0.5 M NaBF₄/0.5 M NaPF₆/tetraglyme

Sodium-Metal/Sulfur Cells

The cells for these tests were analogous to those built for NaNCM tests except that sulfur cathodes prepared as described in ch. 3.2.6 were used. The electrolyte volume was 85 μ l.

For galvanostatic cycling, the lower and upper voltage limits were set as 1.2 V and 2.3 V, respectively. The current density was either 0.144 mA cm⁻² or 0.5 mA cm⁻².

Two electrolytes were tested for use in Na-S cells:

- 1.0 M NaTf/tetraglyme
- 1.0 M NaBF₄/tetraglyme

Lithium-Metal/Sulfur Cells

In the framework of a bachelor's thesis, where sulfur cathodes were developed with the goal of maximizing sulfur load, Li-S cells were built and cycled galvanostatically. [61] These test cells were built analogously to those described in figure 9 and used two layers of celgard 2400 as a separator. On the counter electrode, lithium metal was used instead of sodium metal while sulfur cathodes were inserted between the separator and the stainless steel disk on the WE side of the cell. The electrolyte volume was only 40 μ l since that amount had been shown to be sufficient for this type of cell in the past.

During galvanostatic testing, the cells were cycled at currents of 0.5 mA, 1.0 mA, 2.0 mA, and 3.0 mA in order to examine their reaction to changes in current density. The lower and upper voltage limits were 1.8 V and 2.6 V, respectively.

The electrolyte for the Li-S tests described in this work had the following composition:



3.2.2 Cyclic Voltammetry (CV)

Cyclic voltammetry tests were performed in 3-electrode cells as described as shown in figure 10. Similar to the CE tests, two Whatman GFA separators with a diameter of 11 mm were inserted between the electrodes. However, the electrolyte volume had to be increased to 600 μ l in order to account for the increased dead volume inherent to this cell design.

On a Gamry Reference 3000 potentiostat, the potential of the cells was modulated at a rate of 10 mV s⁻¹ between 0.01 V and 4.5 V for 10 cycles. The starting- and end point of the measurement was the open circuit voltage (OCV) of the cell.

3.2.3 Electrochemical Impedance Spectroscopy (EIS)

In order to determine the conductivity of a selection of electrolytes, EIS was performed on a Gamry Reference 3000 potentiostat with 2-electrode cells. These cells were similar to those shown in figure 9 but had no sodium metal in them. Instead, 11 mm stainless steel disks acted as working- and counter electrodes. Again, two Whatman GFA separators were used. The electrolyte volume was 200 μl .

The measurements were conducted at a perturbation amplitude of 10 mV in the frequency range from 100 Hz to 1 MHz. From the measured real part of the impedance (Z') the conductivity of the electrolyte (κ) was derived through the following formula:

$$\kappa = \frac{1}{Z'} * \frac{d}{A} \quad (4)$$

where d is the distance between the electrodes and A is the electrode surface.

3.2.4 Scanning Electron Microscopy (SEM)

SEM was used to obtain images of sodium metal deposited on various substrates. 2-electrode cells were built as described in figure 9. However, it was not possible to separate the WE cleanly from Whatman separators after sodium had been deposited. Thus, both electrodes were additionally covered with a thinner less porous separator. For tetraglyme- and EC/DEC-based electrolytes, celgard 2400 was used. For PC-based electrolytes, the additional separator was NKK TF4050 since PC does not wet celgard separators. In total, there were 4 layers of separator in the SEM cells (thin separator/GFA/GFA/thin separator). The electrolyte volume was 85 μl .

For deposition on copper, Schlenk SE-Cu R360 copper foil was introduced in between the thin separator and the stainless steel disk on the WE side of the cell.

The measurement protocol was also modified compared to the CE experiments. In order to make an examination by SEM possible even with low-CE electrolytes, a maximum areal capacity of 2 mAh cm^{-2} was deposited and stripped over 10 hours at a current of

0.2 mA for 4 cycles. After the sodium metal plating step of the 4th cycle, the cells were disassembled and the samples were transferred to the microscope in an argon atmosphere.

The SEM used was a Zeiss EVO MA 10 with a tungsten cathode. Images were produced from type I secondary electron (SE1) detection.

Sodium metal deposits out of three different electrolytes were studied:

- 1.0 M NaClO₄/EC/DEC
- 1.0 M NaPF₆/PC
- 1.0 M NaBF₄/tetraglyme

Furthermore, SEM images of the stainless steel and copper substrates were taken in order to evaluate and compare their surface morphology.

3.2.5 X-Ray Photoelectron Spectroscopy (XPS)

For XPS analysis of the SEI created during sodium metal deposition out of 1.0 M NaBF₄/tetraglyme, three-electrode cells were set up in the same way as for the CV experiments (ch. 3.2.2). On a Gamry Reference 3000 potentiostat, the measurement protocol was set up with the exact same parameters as for the CVs except that the process was stopped after the potential had been modified from the OCV of the cell down to 0.1 V vs. Na/Na⁺ during the first cycle. It was hypothesized that SEI formation should have occurred up to this point in the voltage range since it is close to the plating potential of sodium (~0.0 V vs. Na/Na⁺).

Afterwards, the working electrode was removed from the cell in an argon glove box. The surface of the WE was then rinsed twice with pure tetraglyme in order to remove any residual NaBF₄. After it had dried for 30 min, the sample was transferred to a PHI 5000 VersaProbe XPS system while still being protected by an argon atmosphere. In order to scan the sample across an information area of 300 x 500 μm², monochromatic Al Kα (1496 eV) radiation with 50 W excitation energy was used. XPS survey spectra of the

sample were taken at a pass energy of 187 eV. For detail element spectra, the pass energy was set to 29.4 eV. Integration of peak area through Multipeak software with default standard factors was used to perform elemental quantification. The detection angle was 45 ° and the C1s peak at 284.8 eV was used as a calibration point.

In order to create a depth profile of the SEI, the samples were sputtered with a 1 kV Ar laser at a rate of about 1nm min⁻¹ for 3 min, 10 min, and 30 min. Survey and detail spectra of the sample were taken after each sputtering step.

3.2.6 Sulfur Cathode Preparation

Under the guidance of the author of this work, sulfur cathodes were developed in the framework of a bachelor's thesis. [61] While the main focus of that thesis was to create cathodes for Li-S cells with a high areal sulfur load, these electrodes were also used to create Na-S cells for this work.

In order to avoid the use of toxic and expensive solvents such as NMP, which are commonly used in cathode preparation, it was attempted to manufacture sulfur cathodes with a water-based slurry process. While a wide variety of slurry mixtures was tested, only the composition that showed the best results is presented in this work. It consisted of 60 wt% elemental sulfur and 10 wt% each of Ketjenblack EC-600 JD, Porocarb HD3, and Porocarb HG3 conductive carbons. These powders were premixed in a ball mill. The remaining 10 wt% (dry weight SBR) were added in the form of PSBR100 binder dispersion. The components were mixed with 5 ml of a water solution of 0.3 wt% FC4430 dispersion agent in a planetary centrifugal mixer (Thinky Corporation) until a smooth slurry was obtained. This slurry was then coated on a carbon-primed aluminium current collector with an automatic film applicator (Zehntner GmbH) and dried overnight at 60 °C. Cathodes for test cells were cut from the coated foil with hole punches.

4 Results and Discussion

4.1 Electrolyte Screening

In order to start off the evaluation of liquid electrolytes suitable for sodium metal deposition and dissolution, a range of solvents and conducting salts (CS) was selected based on what is commonly used in battery research. [44,47,49,67,68] These electrolytes were then introduced into small two-electrode test cells as described in ch. 3.1.8. Their potential for sodium metal plating and stripping was tested by galvanostatic cycling. In figure 11, a typical voltage and current profile of such a test cell is shown as an example.

In general, after a negative current was applied to the stainless steel working electrode (WE), the voltage dropped from the open circuit potential (OCV) of stainless steel vs. sodium to below 0 V and stabilized around the plating potential, which in the given example was between -0.016 V and -0.018 V. After a deposition time of 2 h, the current was switched to 0.1 mA and the voltage increases to about 0.015 V while the formerly deposited sodium was dissolved. At the same time, sodium metal was replated on the reservoir of the counter electrode. When almost no sodium was left on the WE, the voltage started to increase exponentially before reaching the cutoff potential of 1.0 V, at which point no metallic sodium was left on the surface of the WE while any stable solid electrolyte interphase (SEI) formed during deposition should have persisted. The coulombic efficiency (CE) was then determined by the ratio of charge capacity (Q_{charge}) to discharge capacity ($Q_{\text{discharge}}$) through the following formula:

$$CE = \frac{Q_{\text{charge}}}{Q_{\text{discharge}}} * 100\% \quad (5)$$

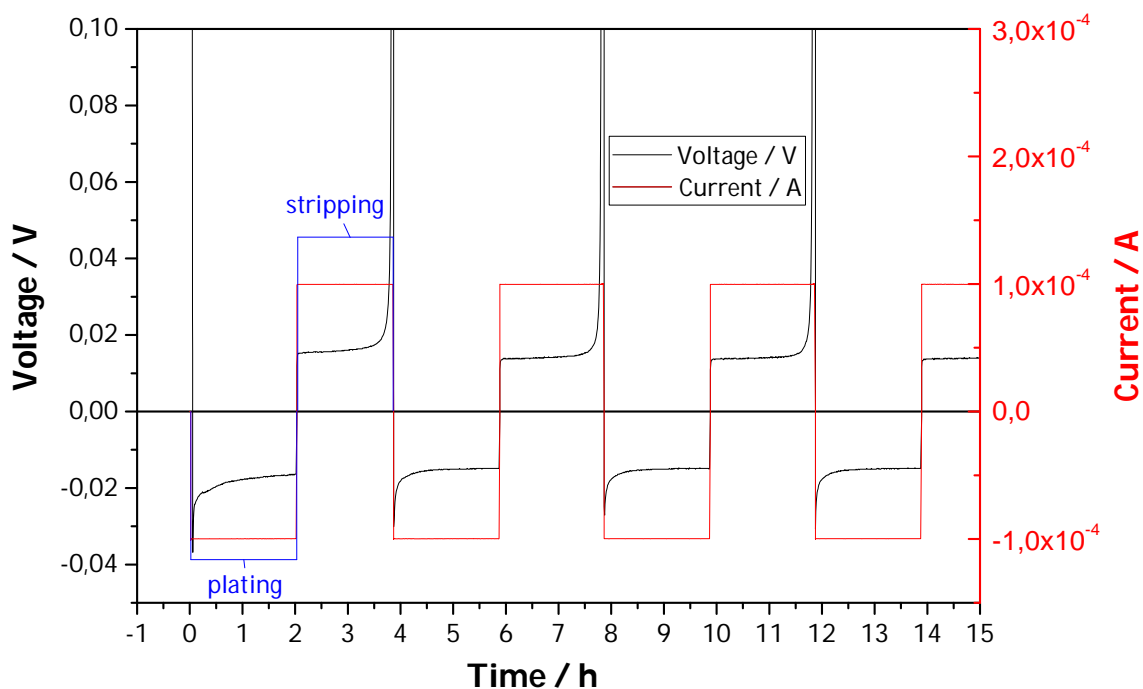


Figure 11: Voltage and current over time of a two-electrode cell containing 1.0 M NaBF₄/tetraglyme during galvanostatic plating and stripping of sodium metal on a 1.0 cm² stainless steel substrate; $V_{\max} = 1.0$ V.

4.1.1 Unsuitable Solvents

After cell assembly, it became apparent that acetonitrile and sulfolane were not suitable for use in combination with sodium metal, as it could be observed with the naked eye that an instantaneous reaction took place as soon as any electrolyte containing one of these solvents came into contact with the metallic sodium of the counter electrode. Through the glass hull of the cell, it was possible to see gas formation and dissolution of the sodium metal. Thus, it was decided to refrain from further examination of these electrolytes. With all other solvents, no violent reactions were observed and it was possible to assemble and cycle multiple test cells with each electrolyte.

4.1.2 Coulombic Efficiency

In figure 12, an overview of the coulombic efficiency (CE) for the first cycle of sodium metal plating and consecutive stripping is given for all tested electrolytes. Because of the large number of electrolyte formulations, the results are grouped by solvent used. In general, it can be seen that none of the studied electrolytes exhibits a CE above 92% during the first cycle. This is most easily explained by SEI-formation taking place for the first time, as well as potential side reactions. [47] While there are major differences between the CEs of the different electrolytes even during the first cycle, some general trends can be observed.

First off, almost all electrolytes containing fluoroethylene carbonate (FEC) performed better than their non-FEC counterparts. The highest CEs of close to or slightly above 90% were achieved with tetraglyme electrolytes containing NaClO_4 , NaBF_4 or NaTf as well as with NaBF_4 in diglyme. Carbonate-based electrolytes, on the other hand, did not reach a coulomb efficiency above 80% with the best performing combination being 1.0 M NaPF_6 in PC/FEC. The electrolytes containing the solvent combination of EC/DEC/FEC showed the best overall compatibility with metallic sodium since all cells reached a CE of between 58 and 75%. Lastly, it was observed that the combination of TFSI salt with tetraglyme and diglyme yielded the lowest CEs while other electrolytes containing the same CS performed normally.

In figure 13, the CE for the 20th cycle of the same cells is shown. Again, multiple trends can be observed. First off, when carbonate electrolytes are considered, the addition of FEC seems to generally improve the CE. Furthermore, 20th cycle CE has improved from CE in the first cycle for almost all FEC containing electrolytes while it is worse for most carbonate electrolytes without FEC. Thus it can be assumed that FEC does indeed increase electrolyte performance for sodium metal anodes. Two electrolytes, NaBF_4 in EC/DEC/FEC and in PC, actually show CEs above 90%. The best CE overall, above 99%, is reached by NaBF_4 and NaTf in tetraglyme as well as by NaBF_4 in diglyme. Cells containing NaClO_4 in tetraglyme, which had shown the best CE in the first cycle, failed due to short circuits after only a few cycles. The same occurred for all electrolytes containing tetraglyme except those mentioned above, which showed exceptionally high CEs.

Another important aspect of these measurements was the observation that all PC based electrolytes which didn't contain FEC performed comparatively poorly, with none of them reaching a CE above 20% in the 20th cycle. This is of particular interest, considering that many publications on sodium based systems use either NaClO₄/PC or NaPF₆/PC for their half-cell tests. [48,69,70] As a low CE may indicate that side reactions between the electrolyte and metallic sodium are taking place, it is possible that half-cell tests of Na-ion materials using these electrolytes and sodium metal as a counter electrode could be influenced by the products of these side reactions. These products would presumably not be present in a full cell not containing metallic sodium. To give a concrete example: If a cathode material performs badly in a half-cell test vs. sodium in NaClO₄/PC, this might be due to decomposition products from the reaction between the electrolyte and sodium metal influencing the cathode material. These same reaction products would probably not be present in a cell with hard carbon as the anode.

Based on the results of these galvanostatic cycling tests, a few of the electrolytes were chosen for a more in-depth examination.

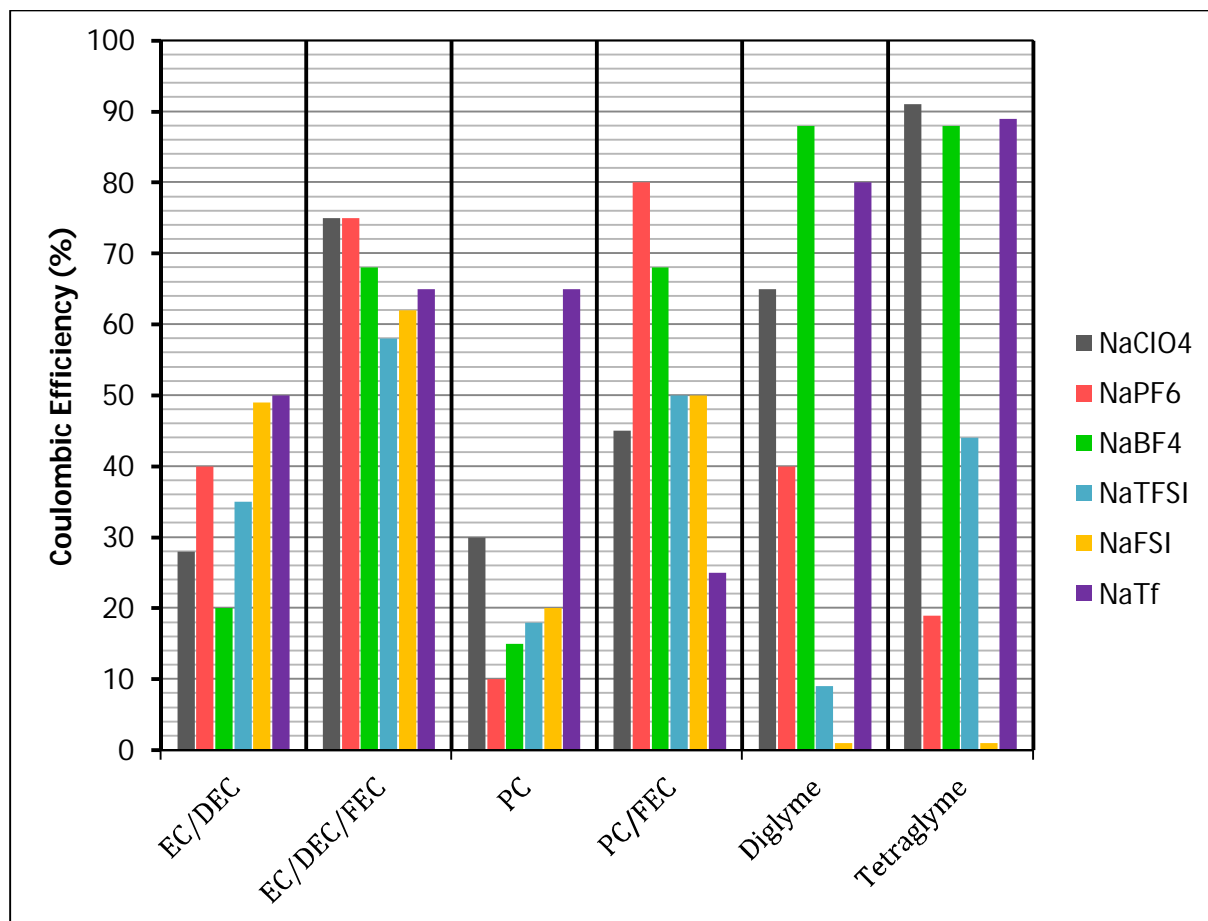


Figure 12: Coulombic efficiency of first cycle for sodium metal deposition and dissolution in a range of liquid electrolytes; 0.1 mA cm^{-2} ; 2 h ; $V_{\text{max}} = 1.0 \text{ V}$.

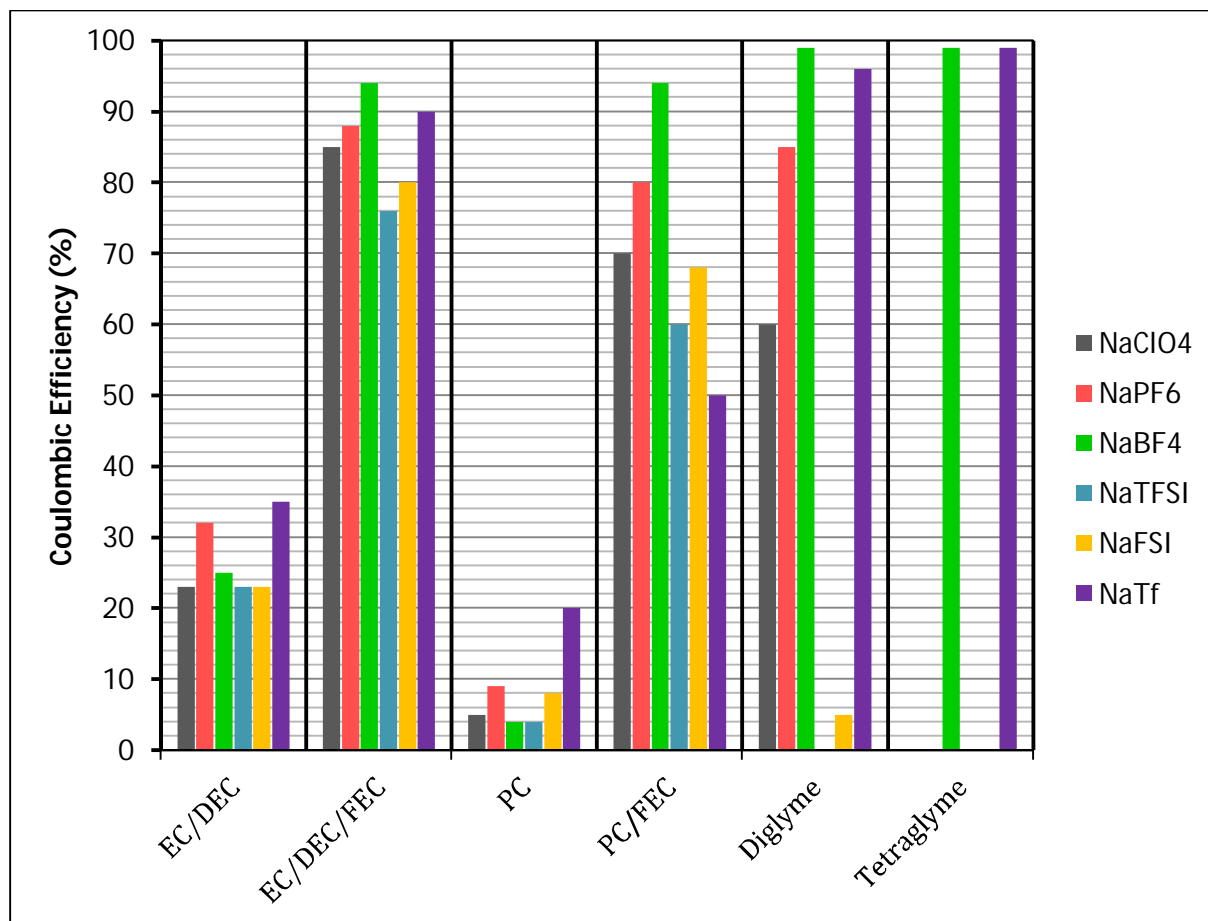


Figure 13: Coulombic efficiency of 20th cycle for sodium metal deposition and dissolution in a range of liquid electrolytes; a CE of 0% indicates a critical test failure before the 20th cycle; 0.1 mA cm⁻²; 2 h; $V_{\max} = 1.0$ V.

4.1.3 Galvanostatic Cycling Profiles of Select Electrolytes

In order to further analyze the differences between the tested electrolytes, out of these 36 formulations, 6 were selected for an in depth discussion of their galvanostatic cycling profiles. Their compositions are given in table 5.

Table 5: Electrolyte formulations selected for further examination with respective concentrations; green indicates high CE, red indicates low CE.

| Solvent | Conducting salt concentration / M | | | |
|------------|-----------------------------------|-------------------|------|-------------------|
| | NaClO ₄ | NaPF ₆ | NaTf | NaBF ₄ |
| EC/DEC | 1.0 | | | |
| EC/DEC/FEC | | | | 0.25 |
| PC | | 1.0 | | |
| Diglyme | | | | 0.5 |
| Tetraglyme | | | 1.0 | 1.0 |

In [figure XX4](#), a comparison of the CEs of these electrolytes is given, with the exception of NaBF₄/tetraglyme, which is discussed separately. For three of the featured electrolytes, a very high CEs above 90% were observed over more than 100 cycles. However, even the best performing carbonate electrolyte was clearly less stable than the glyme-based electrolytes with a CE varying between 90 % and almost 100% over a few cycles. Furthermore, the CE of this electrolyte took almost 20 cycles to reach these high levels which would lead to high capacity losses in a full cell. The two glyme-based electrolytes, on the other hand, reached CEs above 95% after only 2 cycles, with NaTf/tetraglyme yielding more stable results than NaBF₄/diglyme.

The other two carbonate electrolytes featured here, NaClO₄/EC/DEC and NaPF₆/PC, exhibited low CEs which only diminished with each cycle. Here, the latter showed an overall lower CE but at a consistent level while the former's CE varied a lot between cycles. This variation, which was also observed in the cell with NaBF₄/EC/DEC/FEC as the electrolyte, is best explained by the formation of mossy sodium metal with thin dendritic structures. These structures may break or otherwise lose contact with the bulk of the electrode during cycling which would lead to a loss in capacity and a low CE.

During a later cycle, these disconnected structures might regain contact to the electrode due to pressure buildup, for example. In this case, a higher amount of sodium metal would be available for stripping during the subsequent stripping step which would lead to an increased CE for that cycle.

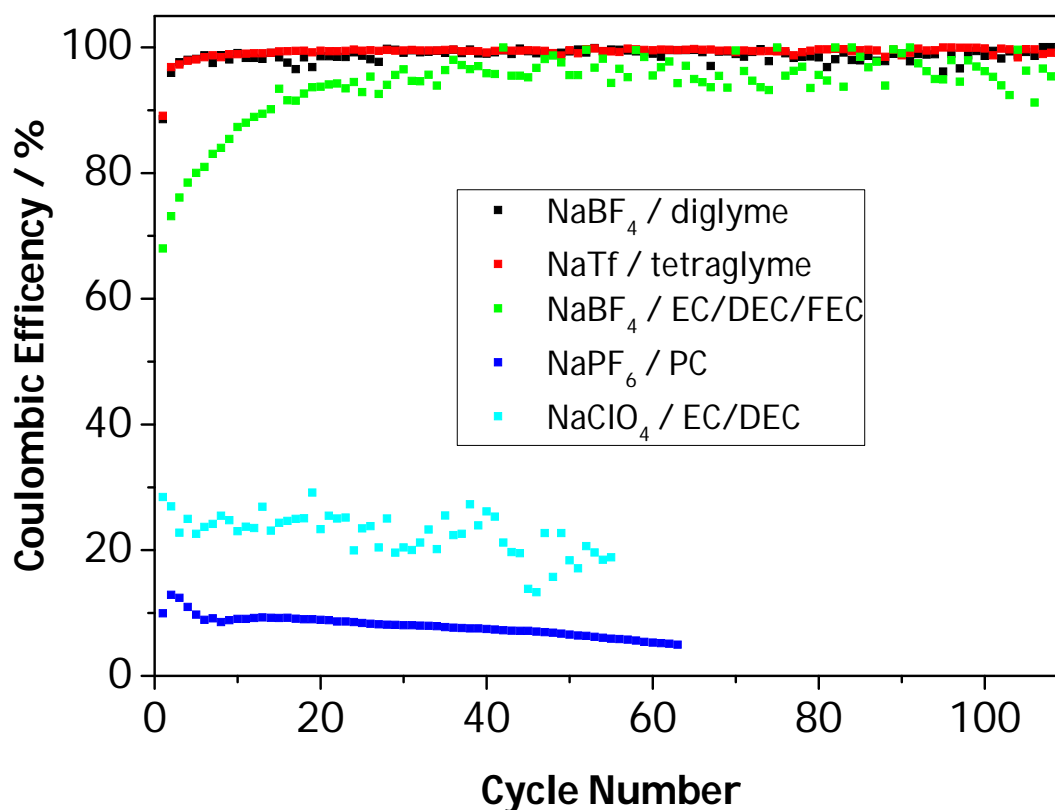


Figure 14: Coulombic efficiency for sodium metal plating and stripping in 2-electrode cells containing a variety of electrolytes; 0.1 mA cm^{-2} ; 2 h; $V_{\text{max}} = 1.0 \text{ V}$.

One of the possible reasons for a low CE is the occurrence of electrolyte-sodium reactions during the plating and stripping process. These reactions include the formation of the SEI, which may vary significantly in thickness and stability between electrolytes. [47,71] Furthermore, if the SEI is not stable enough, continuous direct contact between electrolyte and sodium metal may take place and thus, ongoing reactions between the two, due to sodium's high reactivity. [30,72] Another reaction that might occur is electrochemical electrolyte decomposition due to instability of the electrolyte under the conditions present in the cell. [48]

All these factors influence the potentials at which the plating and stripping of sodium metal take place. These potentials, under ideal conditions, should be close to 0.0 V (V vs. Na/Na⁺). Hereafter, the galvanostatic test voltage profiles for the selected electrolytes are discussed. It is important to note that for these tests, contrary to intuition, a discharge step (i.e., the application of a negative current and subsequent occurrence of a negative voltage) equals reduction and deposition of sodium on the working electrode. During the charge step, on the other hand (i.e., positive current and voltage), the formerly deposited sodium is oxidized and stripped from the WE.

0.5 M NaBF₄/diglyme

After an initial drop to -0.05 V during the discharge step of the first cycle, the potential stabilizes around -0.02V. Similar behavior was also observed for the other electrolytes and is consistent with an activation-overpotential for the initial sodium metal deposition. Low overpotentials persisted throughout the test and were also observed during the charge step. In the first charge step, the cutoff potential of 1.0 V was reached after 0.176 mAh cm⁻² or 88% of the full discharge capacity of 0.20 mAh cm⁻². However, within 11 cycles, the charge capacity reached almost 100% of the discharge capacity which indicates a stable and persistent SEI. This was further corroborated by the consistently low overpotentials. However, as seen in the CE profiles, the charge capacity varied slightly over time and reached no more than 0.193 mAh cm⁻² during the 81st cycle, for example.

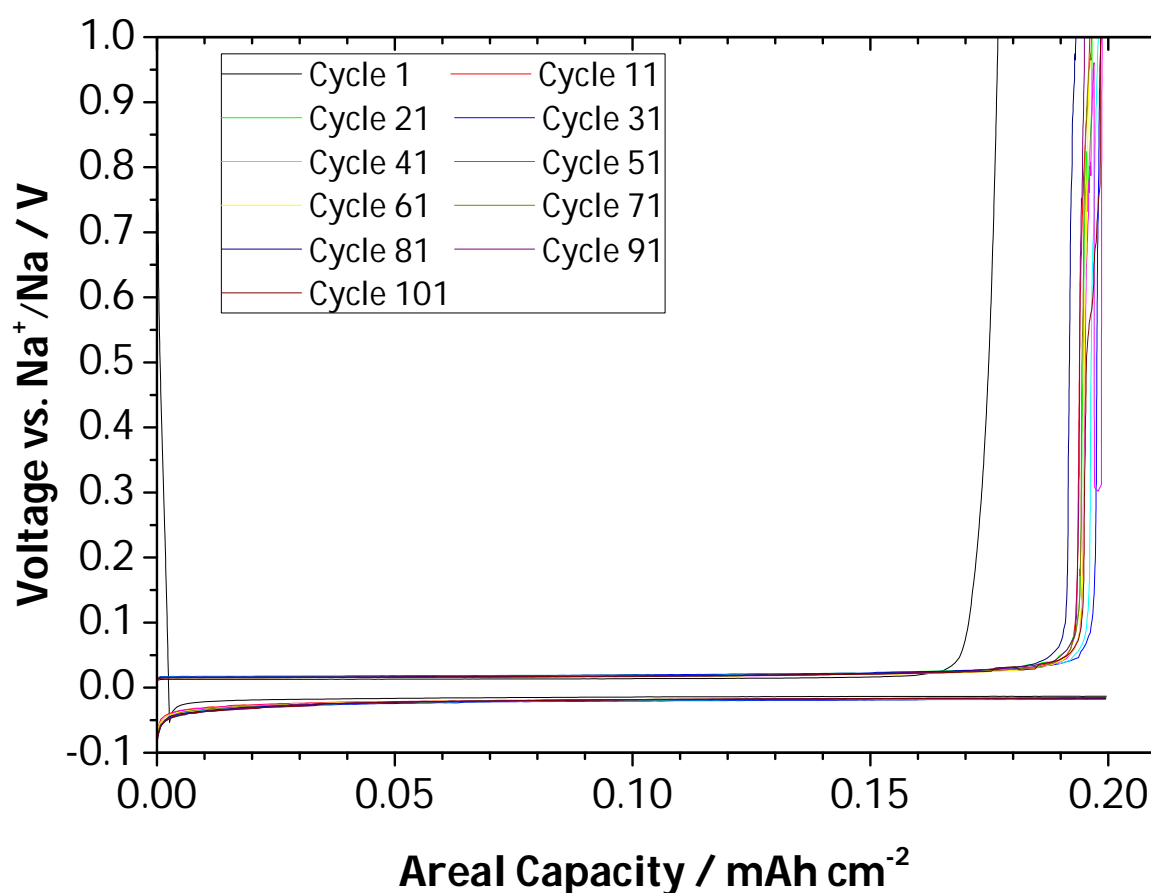


Figure 15: Voltage profile for select cycles of sodium metal plating and stripping in a 2-electrode cell containing 0.5 M NaBF₄/diglyme; 0.1 mA cm⁻²; 2 h; V_{max} = 1.0 V.

1.0 M NaTf/tetraglyme

The voltage profile for this electrolyte was very similar to that of NaBF₄/diglyme with the exception of the charge capacities during the later cycles which reached values close to 100% of the full discharge capacity more consistently.

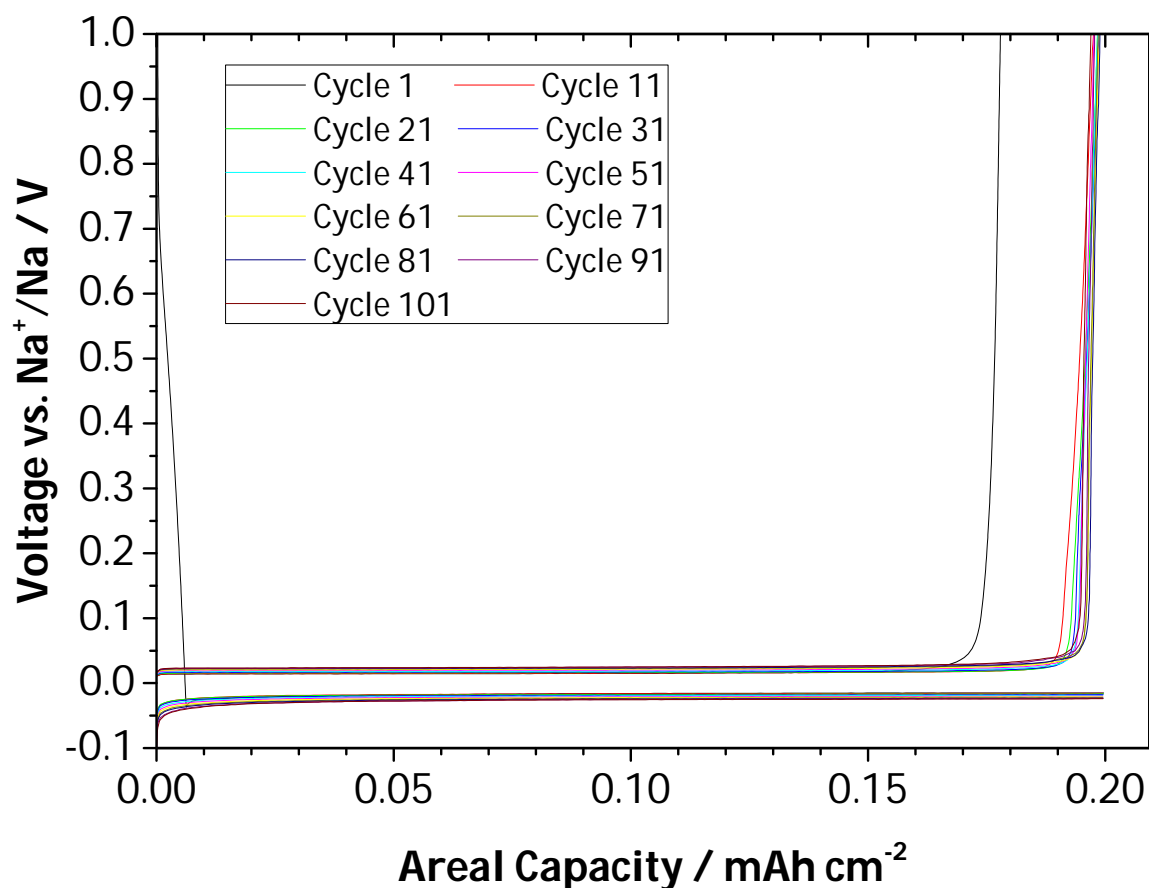


Figure 16: Voltage profile for select cycles of sodium metal plating and stripping in a 2-electrode cell containing 1.0 M NaTf/tetraglyme; 0.1 mA cm⁻²; 2 h; V_{max} = 1.0 V.

0.25 M NaBF₄/EC/DEC/FEC

While it was possible to reach high charge capacities with this electrolyte, their strong variation, as well as the observed potentials, indicate a less than optimal SEI. During the first cycle, the potential initially dropped as low as -0.24 V and stabilized around -0.12 V which is still significantly higher than what was found for the two electrolytes discussed before. Interestingly, during later cycles, the discharge potential would remain relatively

stable at -0.05 to -0.07 V but would start to increase to -0.14 to -0.17 V at some point during the sodium plating process. This suggests an increase in resistance which could be explained by a buildup of non-conductive material on the WE either in the form of decomposition products, mossy sodium or a thick, unstable SEI. Apparently, this buildup is then removed again during the subsequent charge step since the potential returns to its former low level. The charge step potentials, in general, were relatively stable at 0.09 to 0.05 V. A premature increase only occurred during the 11th cycle, for which no plausible explanation was found. One possible explanation for the comparatively high potentials observed for this electrolyte could be polarization due to low CS concentration.

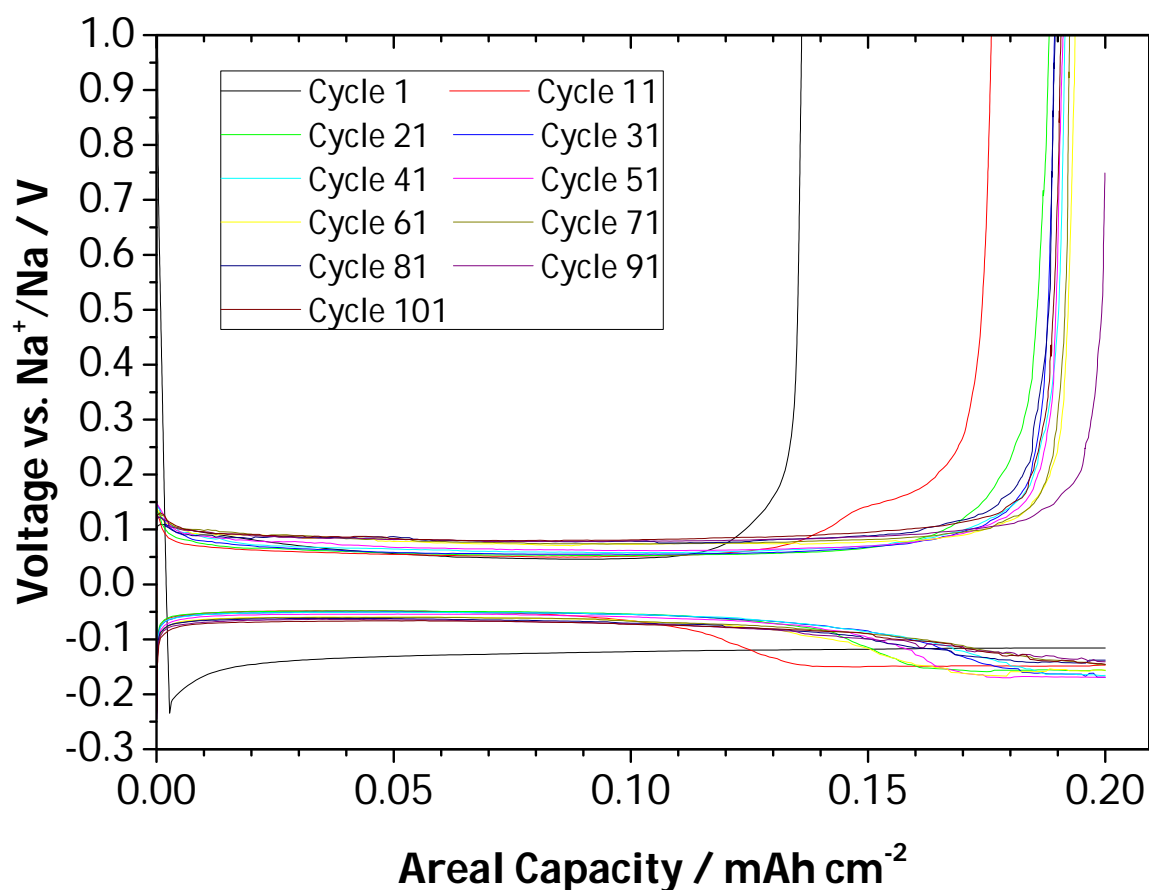


Figure 17: Voltage profile for select cycles of sodium metal plating and stripping in a 2-electrode cell containing 0.25 M NaBF₄/EC/DEC/FEC; 0.1 mA cm⁻²; 2 h; V_{max} = 1.0 V.

1.0 M NaClO₄/EC/DEC

NaClO₄/EC/DEC serves as an example of a low-CE electrolyte. Interestingly, after the initial activation overpotential, the discharge potential started off relatively low at -0.02 V during the first cycle. Nevertheless, the first cycle charge capacity was only 0.055 mAh cm⁻² or about 28% of the discharge capacity. In the following cycles, the discharge potentials increased significantly to about -0.12 V with a peak voltage of -0.16 V occurring at a capacity of 0.015 mAh cm⁻². This peak indicates the formation of a thick and unstable SEI early during the discharge step which was rebuilt by the system for every cycle. While the charge step potentials also increased from the first cycle onwards, the difference was not as significant as observed in the discharge step.

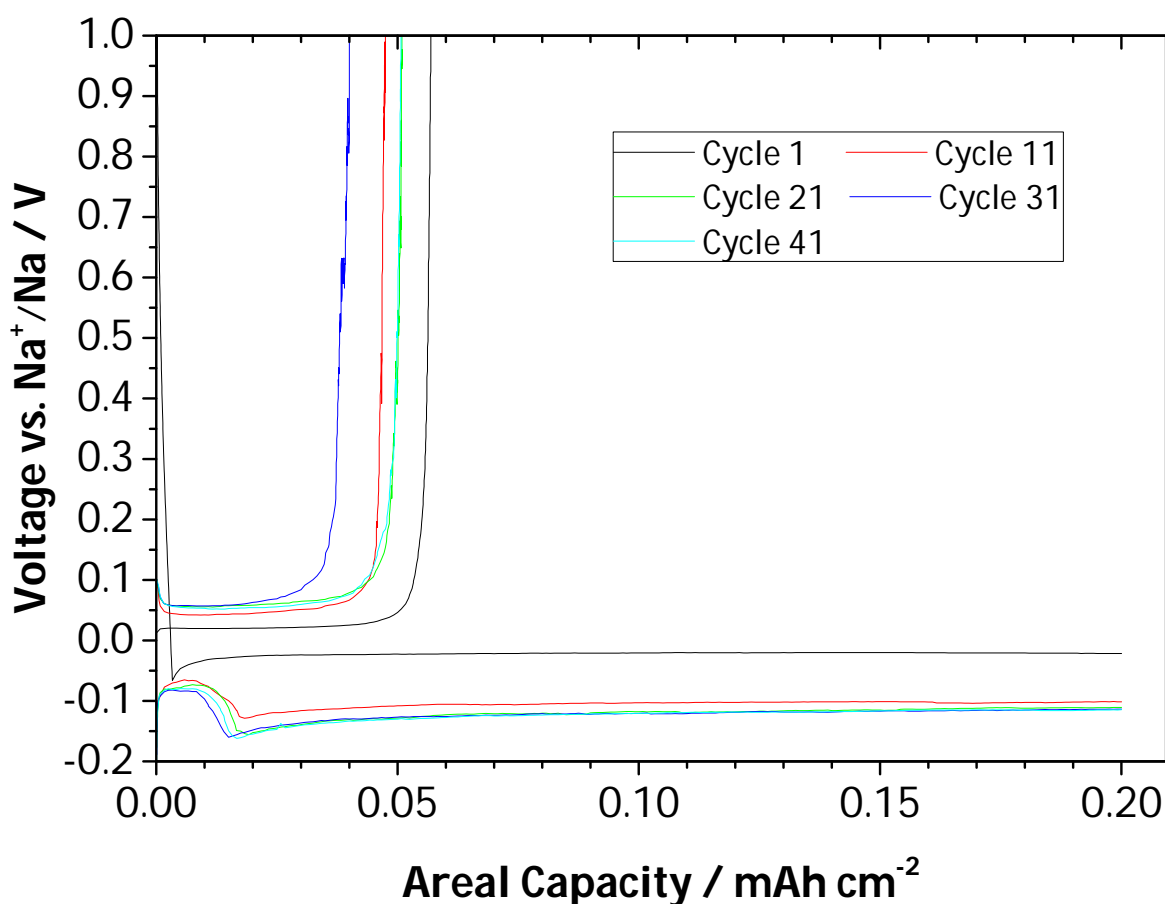


Figure 18: Voltage profile for select cycles of sodium metal plating and stripping in a 2-electrode cell containing 1.0 M NaClO₄/EC/DEC; 0.1 mA cm⁻²; 2 h; V_{max} = 1.0 V.

1.0 M NaPF₆/PC

This electrolyte is of particular interest since it has been shown in literature to be well suited for application with NaNCM cathodes. [69] In terms of its suitability for use in conjunction with sodium metal anodes, however, it was found to exhibit a very low CE. Cells with this electrolyte exhibited strong overpotentials of more than 0.2 V from the first cycle, which only increased with cycle number. This indicates the formation of a weak, thick SEI which is reformed for each cycle and cannot protect the deposited sodium metal from continuous reaction with the electrolyte. Furthermore, the formation of dendritic structures during the sodium plating is highly probable due to current fluctuations caused by an irregular SEI. In many of the experiments in this work, this electrolyte was used as a low-CE example for the sake of comparison.

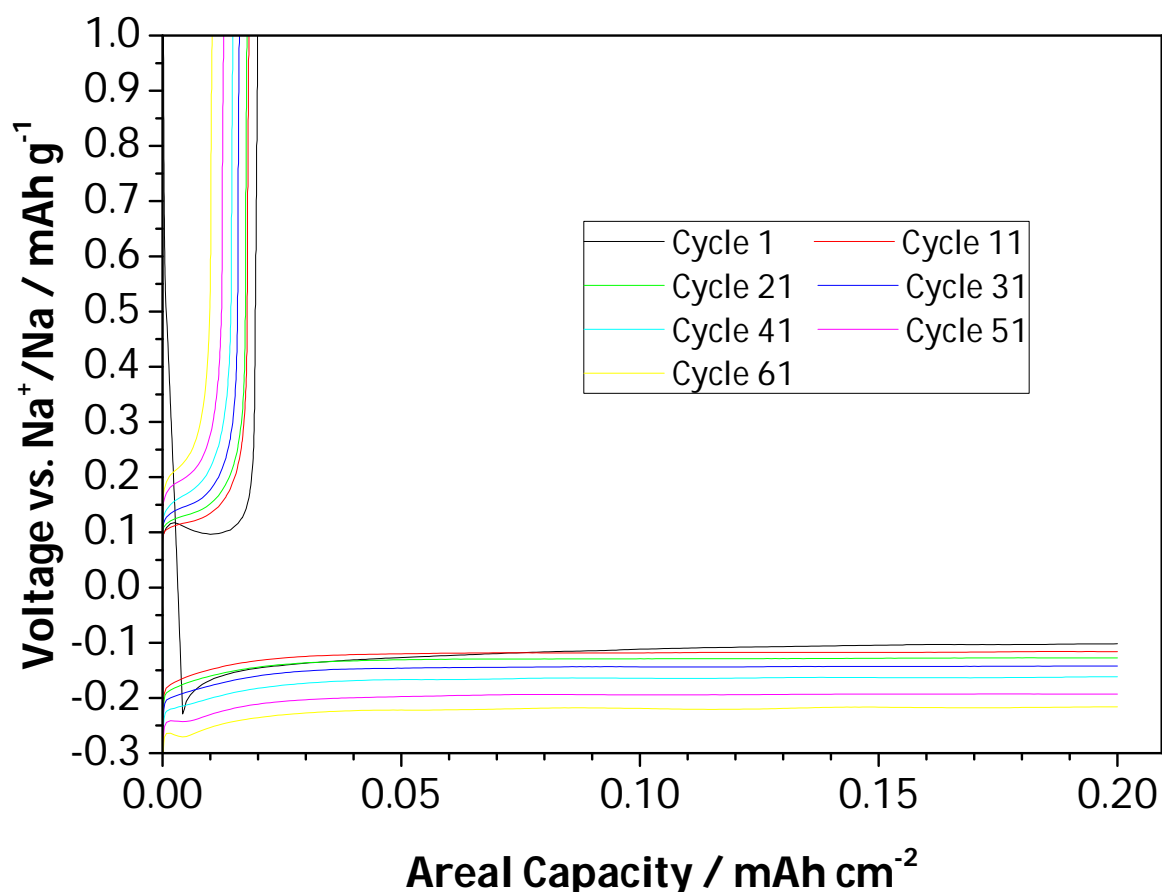


Figure 19: Voltage profile for select cycles of sodium metal plating and stripping in a 2-electrode cell containing 1.0 M NaPF₆/PC; 0.1 mA cm⁻²; 2 h; V_{max} = 1.0 V.

1.0 M NaBF₄/tetraglyme

Out of all the electrolytes tested in this work, this formulation showed the highest coulombic efficiencies combined with the best cycling stability. Indeed, a CE around 99.9% was observed over more than 200 cycles, which was impossible with all other electrolytes (fig. XX11). Considering the voltage profile, the cells exhibited extremely low overpotentials of 0.01 V to 0.02 V for the whole test. The findings suggest that this electrolyte creates an exceptionally stable SEI with minimal dendrite formation. Because of these promising results, a lot of focus was put on this particular electrolyte formulation and on its potential application in energy storage.

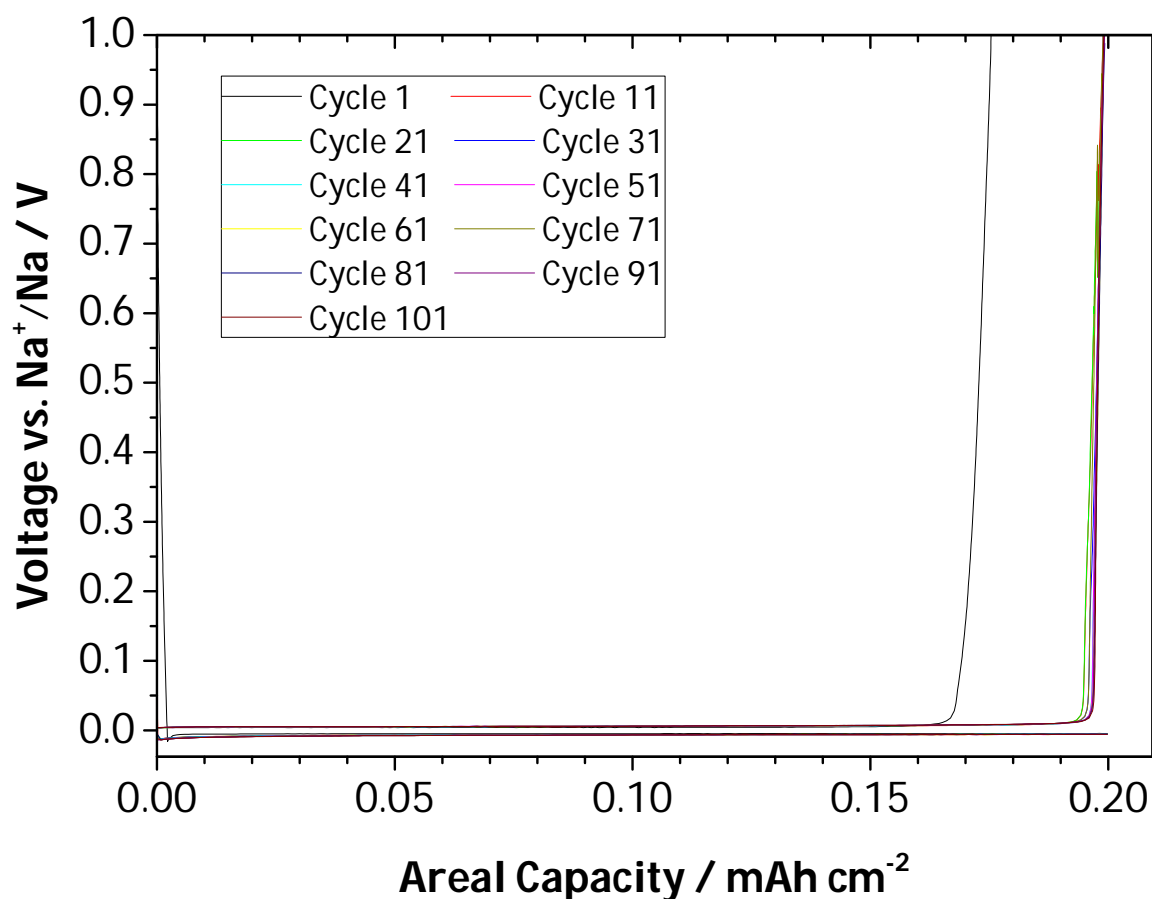


Figure 20: Voltage profile for select cycles of sodium metal plating and stripping in a 2-electrode cell containing 1.0 M NaBF₄/tetraglyme; 0.1 mA cm⁻²; 2 h; V_{max} = 1.0 V.

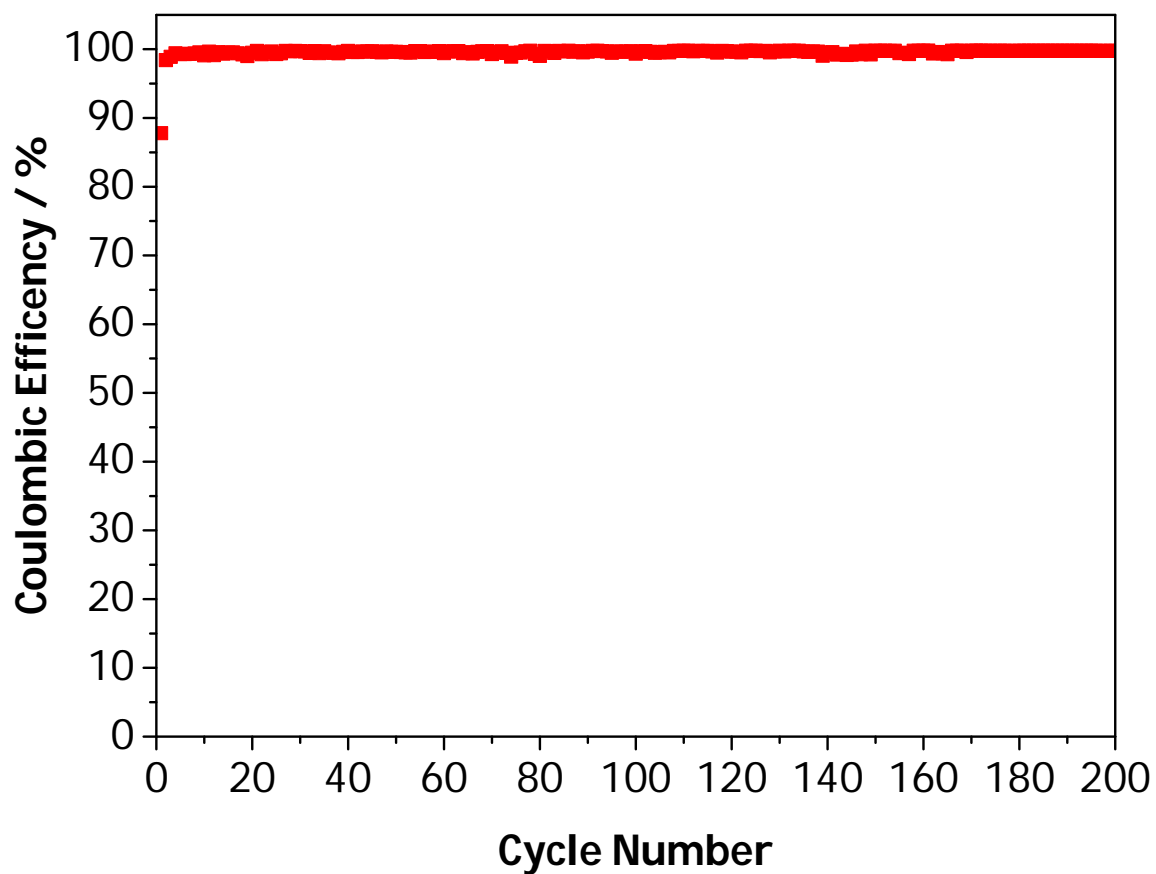


Figure 21: Coulombic efficiency for sodium metal plating and stripping in a 2-electrode cell containing 1.0 M NaBF₄/tetraglyme; 0.1 mA cm⁻²; 2 h; V_{max} = 1.0 V.

4.1.4 Additional galvanostatic testing

For most of the tests performed in this work, sodium metal was plated on and stripped off of stainless steel substrates. In a battery cell, however, these processes would take place on sodium metal which would have been placed in the cell during assembly. Thus it was necessary to determine if the results found during testing on stainless steel substrates were transferable to plating and stripping on and from sodium metal. In order to do so, the Aurbach test procedure described in ch. 3.2.1 was used for test cells containing 1.0 M NaBF₄/tetraglyme and 1.0 M NaPF₆/PC.

As a reminder, for these tests, the capacity loss over 10 low capacity cycles (Q_{loss}) was calculated through the following relation:

$$Q_{\text{loss}} = \frac{Q_{\text{hc}} - Q_{\text{end}}}{10} \quad (6)$$

where Q_{hc} is the charge capacity during the second high capacity cycle and Q_{end} is the capacity during the final charge step. The coulombic efficiency for the low capacity cycles was then calculated as

$$CE = \frac{Q_{\text{lc}} - Q_{\text{loss}}}{Q_{\text{lc}}} * 100\% \quad (7)$$

where CE is the coulombic efficiency and Q_{lc} is the capacity of the low capacity cycles.

For 1.0 M NaBF₄/tetraglyme, the charge capacities of the individual cycles of one Aurbach test cell are shown in figure 22. The charge capacity Q_{end} of the last charge step for cells with this electrolyte was equal to the charge capacity observed during the second high capacity step (Q_{hc}). This would indicate a CE of 100% for the low capacity cycles, which is impossible. The explanation for this phenomenon is that the coulombic efficiency increased between the second and third high capacity cycle. Thus, Q_{hc} would in reality be higher than anticipated the calculated CE would be lower than 100%. Since the charge capacity during the second cycle at 0.198 mAh was already very close to the theoretical maximum value of 0.200 mAh, the difference between Q_{hc} and the actual

charge capacity of the third cycle should be negligible and a true CE of 99.9% can be assumed.

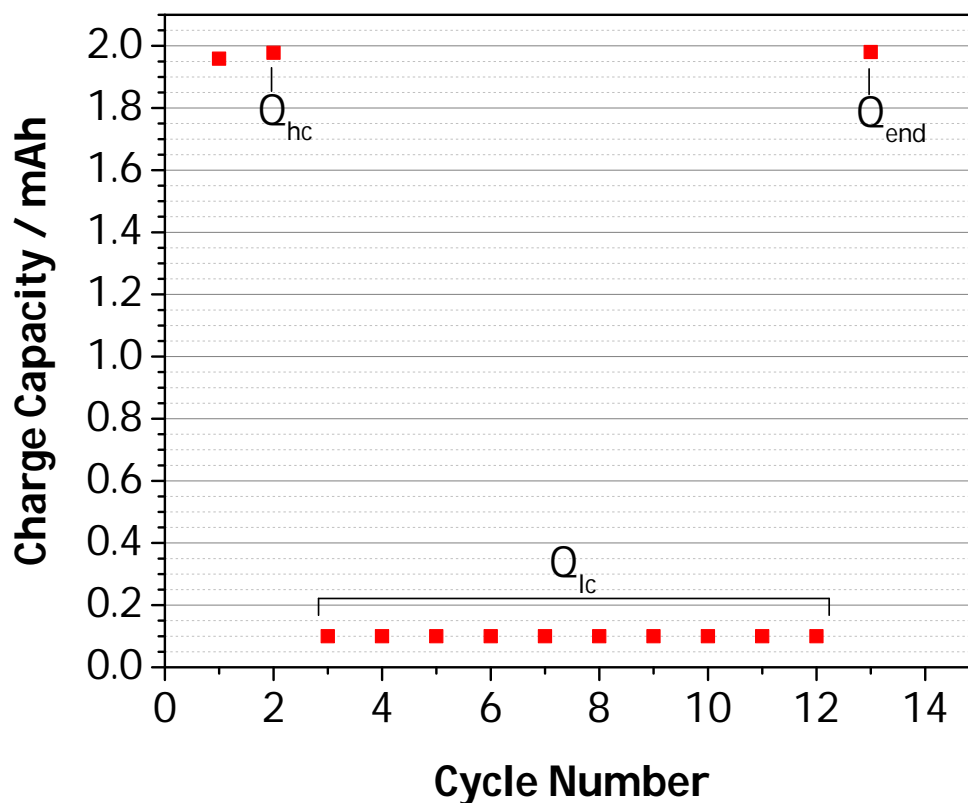


Figure 22: Charge capacities during modified Aurbach test for sodium metal plating and stripping in a 2-electrode cell containing 1.0 M NaBF₄/tetraglyme; 0.1 mA cm⁻²; V_{max} = 1.0 V.

For 1.0 M NaPF₆/PC, the charge capacities of the individual cycles of one Aurbach test cell are shown in figure 23. Unfortunately, for the high capacity cycles the CE at 13% was so low that the resulting capacity Q_{hc} was only about 0.26 mAh or about 2.6 times as much as Q_{lc} . This meant that while a full charge step was possible during the first low capacity cycle, almost all sodium metal was stripped from the substrate before the second low capacity cycle (cycle 4 in the diagram). From that point onwards, the calculation of a CE following formulas 6 and 7 becomes meaningless. Nevertheless it can safely be assumed that the CE for sodium metal plating and stripping on and off of

already present sodium metal is very low since an excess of 160% of was depleted within 2 cycles.

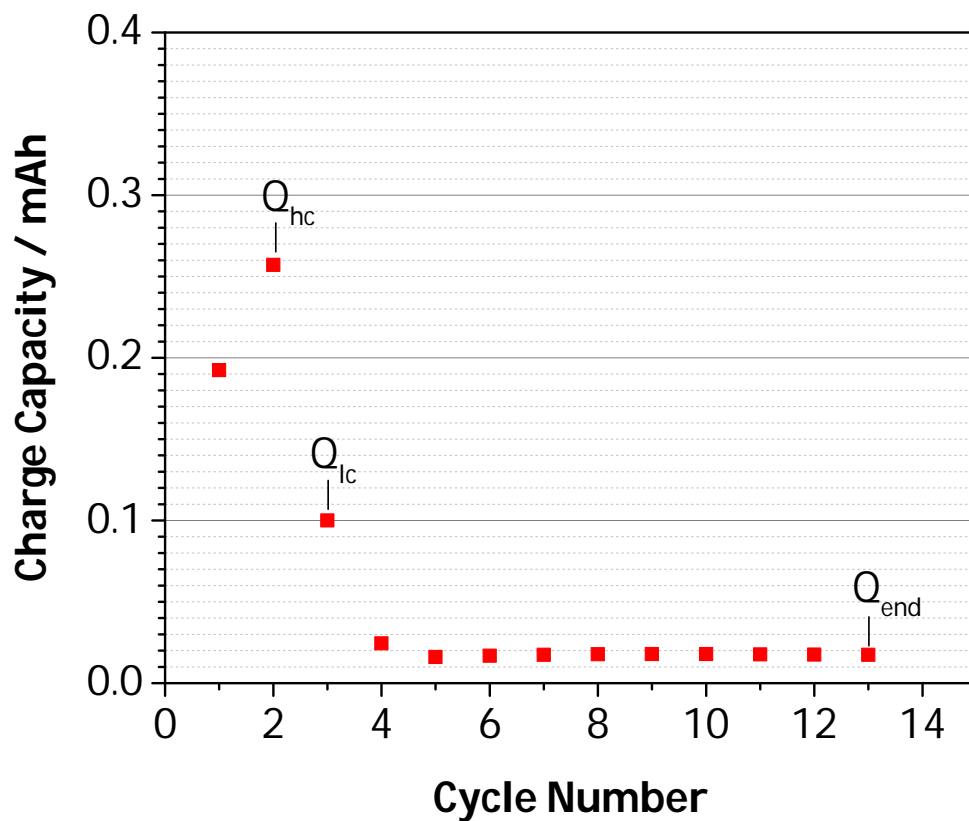


Figure 23: Charge capacities during modified Aurbach test for sodium metal plating and stripping in a 2-electrode cell containing 1.0 M NaBF₄/tetraglyme; 0.1 mA cm⁻²; V_{max} = 1.0 V.

4.2 Electrolyte Stability

4.2.1 Stability Comparison

Cyclovoltammetry (CV) tests were performed for a selection of electrolytes in order to determine their electrochemical potential windows. Furthermore, CVs can give insight into the processes taking place when the cell potential is first lowered to the point of SEI formation, just before sodium deposition takes place.

All tests were performed with three-electrode-cells with a Na/Na⁺ reference electrode. The CV starting and end point for each cycle was the open circuit voltage (OCV) while the potential range was set to 0.01 - 4.5 V. Please note that all potential difference values discussed in this chapter are given in V vs. Na/Na⁺. A total of 10 cycles at a rate of 10 mV s⁻¹ was recorded for each CV. An overview of the tested electrolytes is given in table 6.

Table 6: Electrolyte formulations examined by CV with respective concentrations; green indicates high CE, red indicates low CE.

| Solvent | Conducting salt concentration / M | | | | |
|------------|-----------------------------------|-------------------|------|-------------------|-------|
| | NaClO ₄ | NaPF ₆ | NaTf | NaBF ₄ | NaFSI |
| PC | 1.0 | 1.0 | 0.5 | 0.25 | 0.5 |
| PC/FEC | | 1.0 | | | |
| Tetraglyme | | 1.0 | 1.0 | 1.0 | 1.0 |

A comparison of the 10th cycle of the CVs for tetraglyme-based electrolytes and PC-based electrolytes is given in figures 24 and 25, respectively. It was observed that all electrolyte formulations, except those containing NaTf and NaFSI, were stable over the whole potential range of the experiment. Independent of solvent, NaTf showed elevated oxidation currents above 4.0 V. For the two electrolytes containing NaFSI, reduction- and oxidation currents occurred at onset potentials of 1.5 V and 3.7 V respectively. The high reduction current for NaFSI/tetraglyme could be one explanation for the low CEs achieved with electrolytes containing this salt.

Throughout the tests, it was observed that the first cycle differed significantly from the rest of the CV. This was true for most electrolytes. This may either be due to SEI formation taking place or impurities being present in the electrolyte.

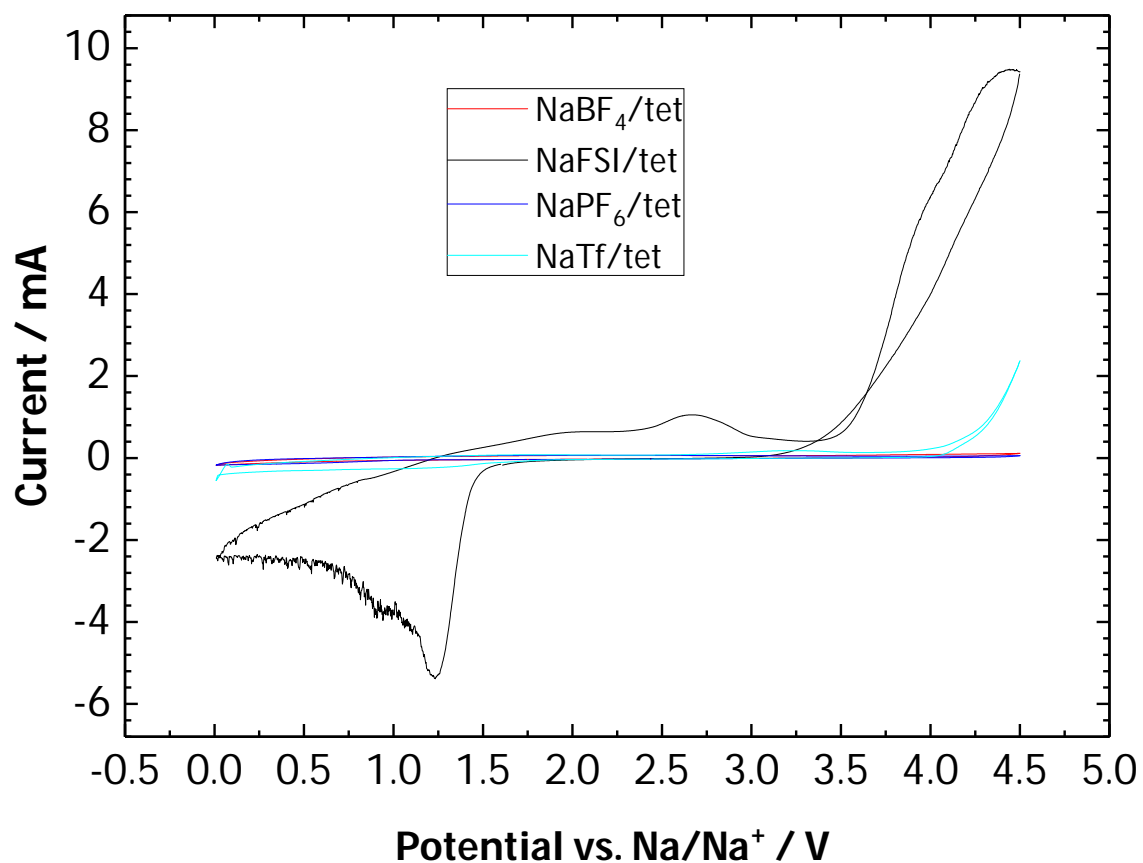


Figure 24: 10th cycle CVs (10 mV s⁻¹) for a variety of tetraglyme-based electrolytes obtained in three-electrode cells with a stainless steel working electrode (1.0 cm²).

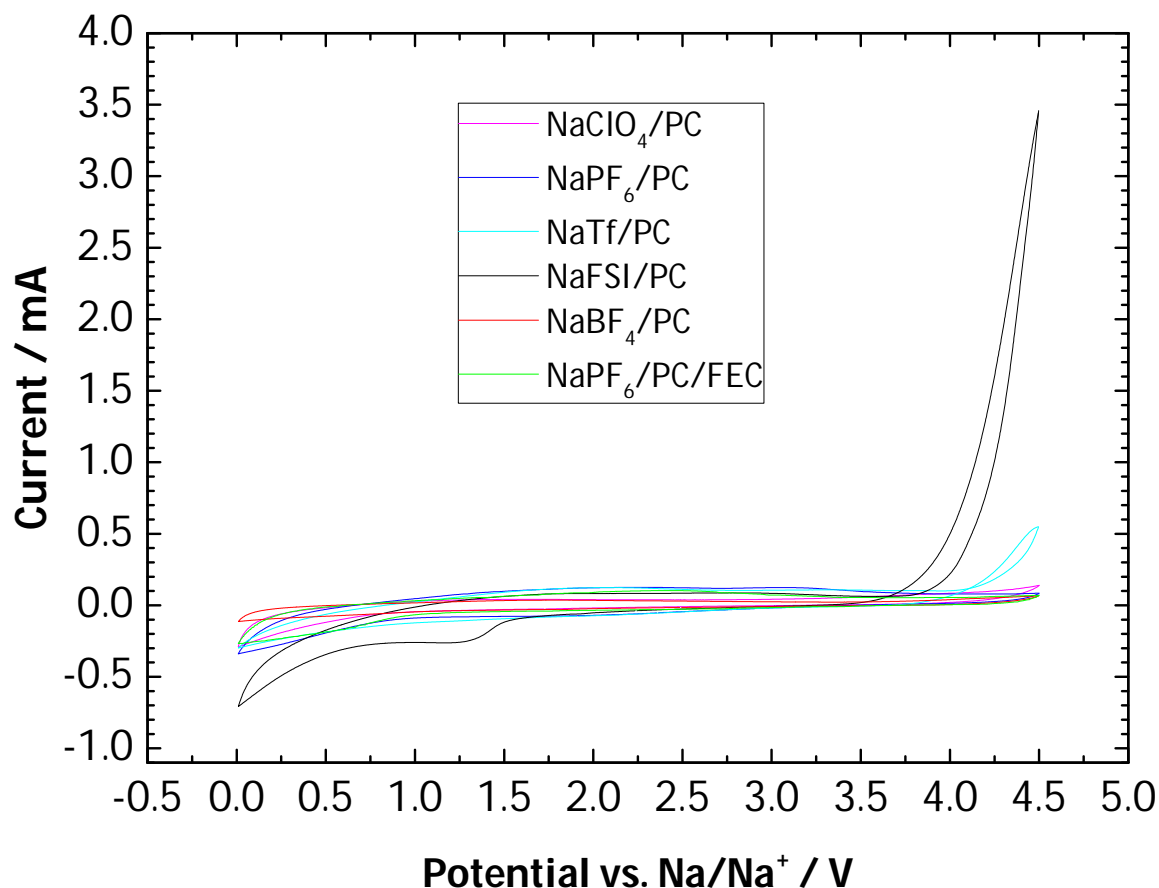


Figure 25: 10th cycle CVs (10 mV s⁻¹) for a variety of PC-based electrolytes obtained in three-electrode cells with a stainless steel working electrode (1.0 cm²).

4.2.2 Cyclic Voltammetry Discussion

In order to show the differences between the electrolytes, a closer look at representative CV profiles of some of the studied electrolytes is given. It is important to note that the absolute current values for the following CVs are not necessarily indicative of stability since there are differences in conductivity between the studied electrolytes as discussed in ch. 4.3.

NaBF₄/tetraglyme

The CV for this electrolyte showed that it was stable over the whole potential range tested in this experiment. There were no major peaks present and the observable currents decreased with increasing cycle number. The highest currents observed occurred during the first cycle, where SEI formation would take place for the first time. However, the overall shape of the first cycle is mostly congruent with the rest of the CV. The lack of high reductive currents at the bottom of the potential range might be indicative of the formation of a thin, stable SEI which persists throughout the experiment.

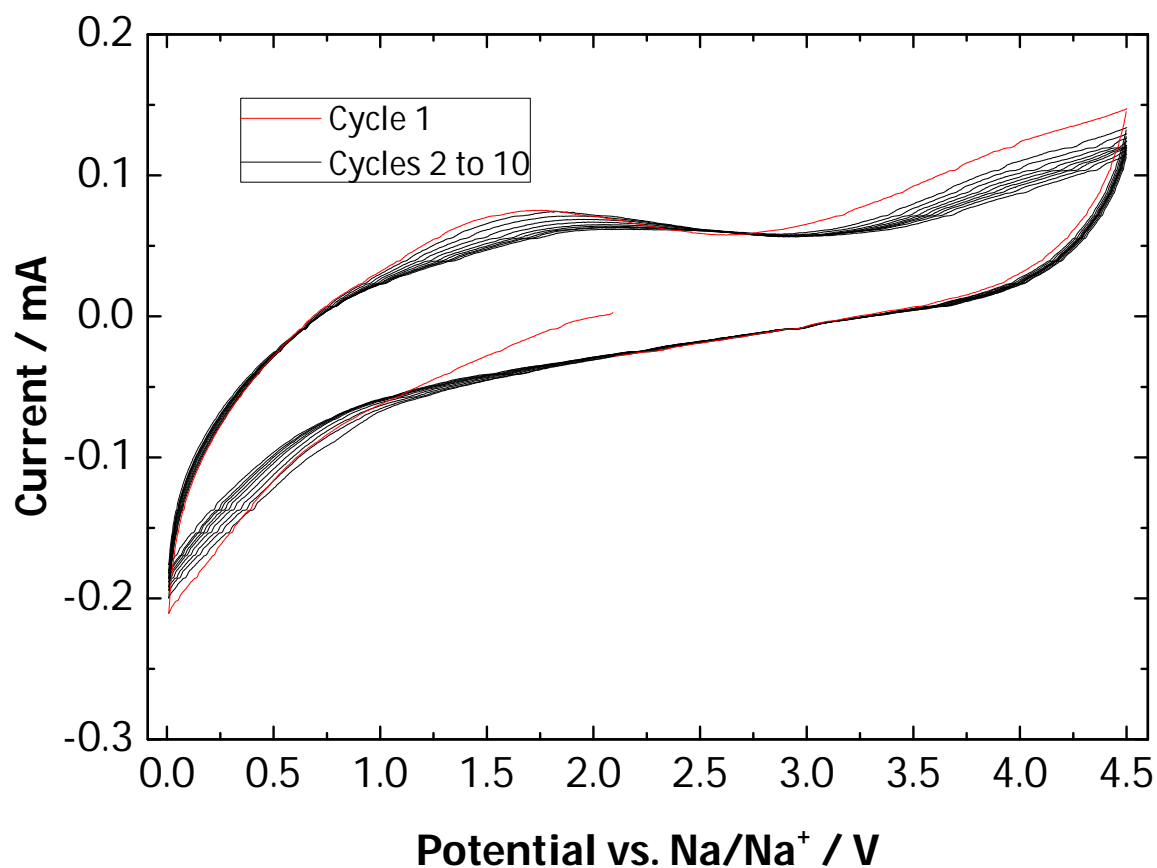


Figure 26: CV for 1.0 M NaBF₄/tetraglyme (10 cycles, 10 mV s⁻¹, 1.0 cm⁻²).

NaTf/tetraglyme

While this electrolyte looked to be stable during the first cycle, oxidative peaks started to appear in subsequent cycles at the top of the potential range. These oxidative currents increased with each cycle and resulted in corresponding reductive peaks at the other end of the potential range. Nevertheless, the electrolyte looks to be stable up to about 4.0 V which means that it could be usable for low operating voltage applications such as Na-S cells.

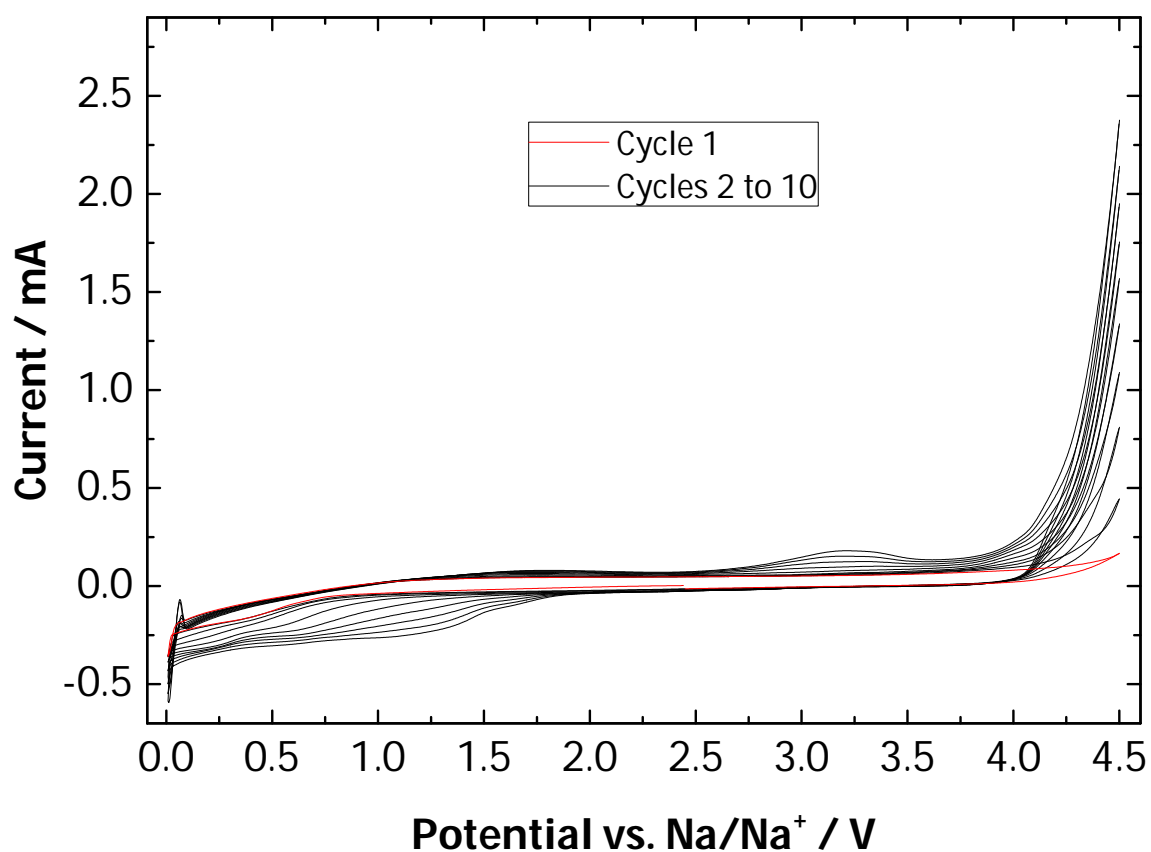


Figure 27: CV for 1.0 M NaTf/tetraglyme (10 cycles, 10 mV s⁻¹, 1.0 cm²).

NaPF₆/tetraglyme

When compared to NaBF₄/tetraglyme, this electrolyte showed a stronger increase in reductive current from about 0.7 V during the first cycle. Afterwards, this reductive current decreases with each cycle as the onset potential of the reduction shifts up to 1.0 V. The relatively higher reductive current might indicate a more extensive SEI formation taking place. However, this reductive peak was still relatively narrow. The electrolyte was stable over the whole potential range.

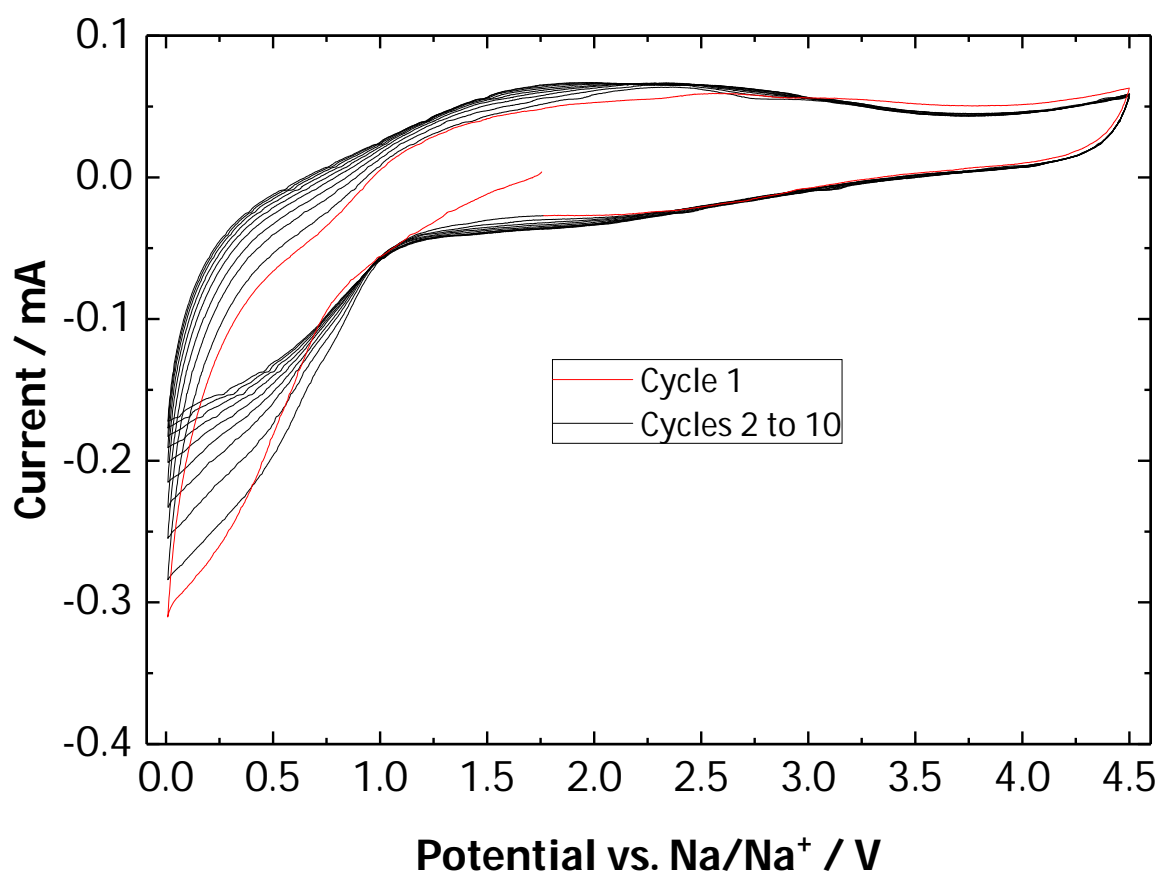


Figure 28: CV for 1.0 M NaPF₆/tetraglyme (10 cycles, 10 mV s⁻¹, 1.0 cm²).

NaPF₆/PC and NaPF₆/PC/FEC

For NaPF₆/PC, the CV was very similar to that of NaPF₆/tetraglyme with the highest current occurring during reduction in the first cycle. When FEC was introduced to the electrolyte, the onset potential of the reduction peak in the first cycle shifted from 0.8 V to 2.1 V and the whole peak broadened extensively. This large reductive peak mostly disappeared in the second cycle, with the overall shape of the CV returning to that of the electrolyte without FEC. This indicates that FEC plays a major role in the SEI formation during the first cycle but otherwise doesn't influence the behavior of the electrolyte much in this experiment. The only other difference was a broad, weak oxidative peak at 2.4 V that increased with every cycle which might also be caused by the addition of FEC. Both electrolytes were stable over the whole potential range.

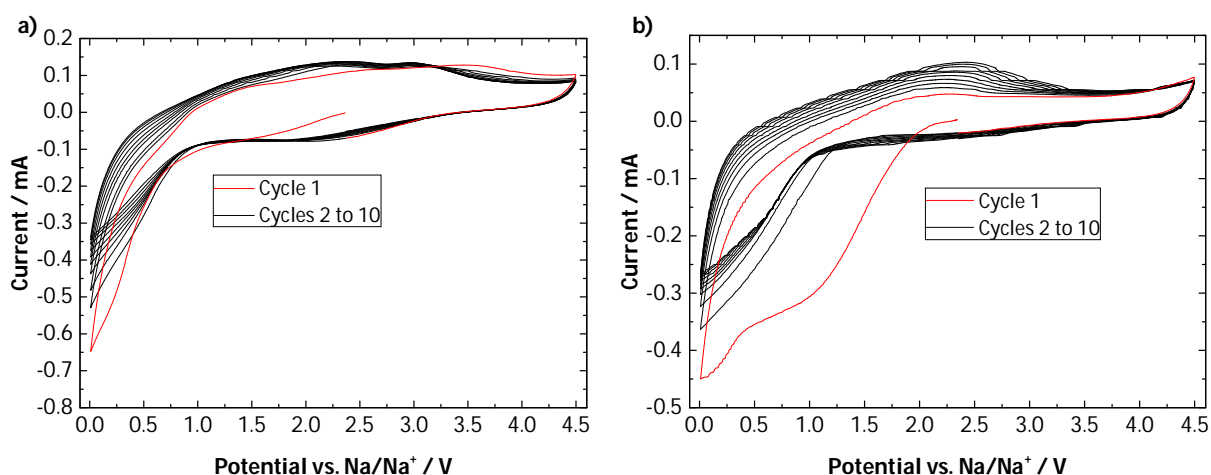


Figure 29: CVs for (a) 1.0 M NaPF₆/PC and (b) 1.0 M NaPF₆/PC/FEC (10 cycles, 10 mV s⁻¹, 1.0 cm²).

NaClO₄/PC

For NaClO₄/PC, an electrolyte which is commonly used in Na-ion research, the CV resembled that of the electrolytes containing NaPF₆ as the conducting salt. [48,70] It was noted that the onset potential of the reductive current during the first cycle was relatively high at 0.9 V, which resulted in a comparatively wide peak. This, once again, might indicate a more extensive SEI formation.

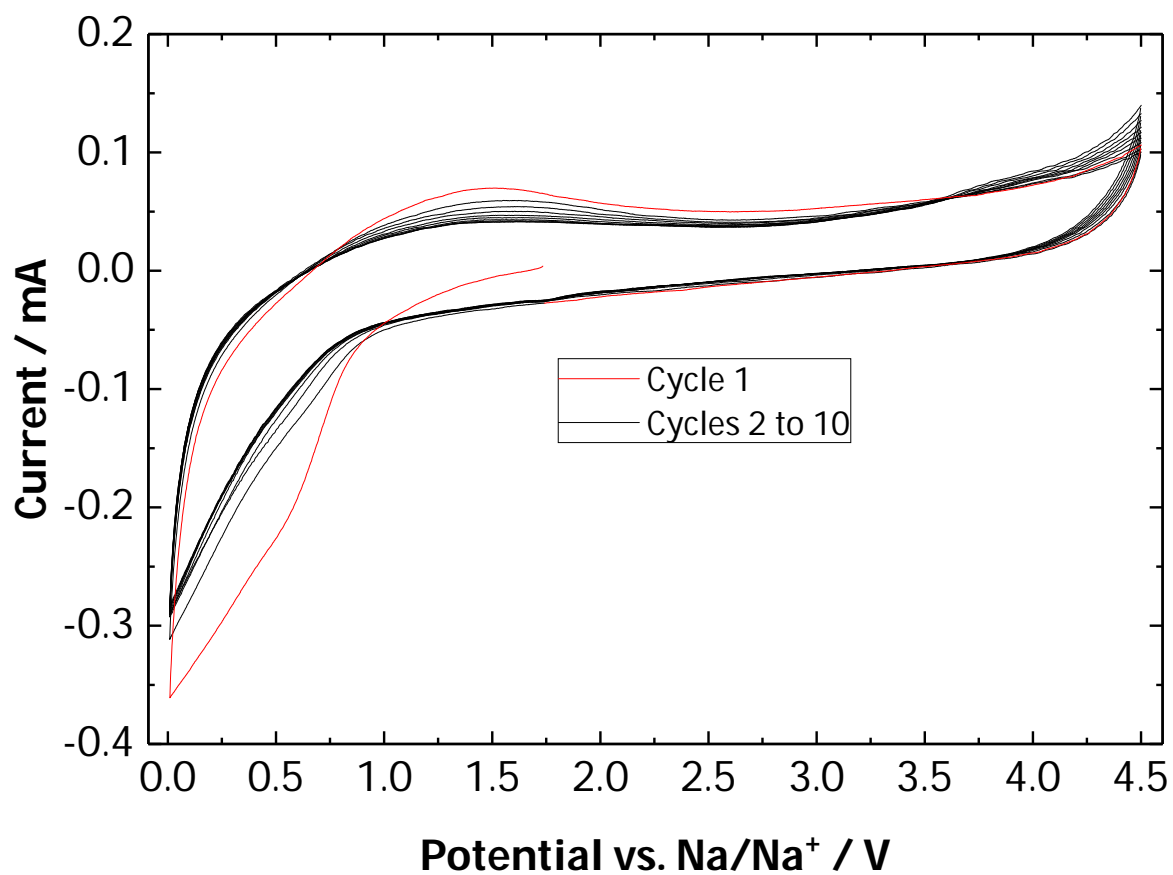


Figure 30: CV for 1.0 M NaClO₄/PC (10 cycles, 10 mV s⁻¹, 1.0 cm²).

4.3 Electrolyte Conductivity

Ionic conductivity tests at room temperature were performed through electrochemical impedance spectroscopy (EIS) on the same electrolyte formulations as tested in ch. 4.2, which are listed with concentrations in table 7 for the sake of overview.

Table 7: Electrolyte formulations tested for ionic conductivity by EIS with respective concentrations; green indicates high CE, red indicates low CE.

| Solvent | Conducting salt concentration / M | | | | |
|------------|-----------------------------------|-------------------|------|-------------------|-------|
| | NaClO ₄ | NaPF ₆ | NaTf | NaBF ₄ | NaFSI |
| PC | 1.0 | 1.0 | 0.5 | 0.25 | 0.5 |
| PC/FEC | | 1.0 | | | |
| Tetraglyme | | 1.0 | 1.0 | 1.0 | 1.0 |

Ionic conductivity is related to impedance through the following formula:

$$\kappa = \frac{1}{Z'} * \frac{d}{A} \quad (8)$$

Where κ is the conductivity, Z' is the real part of the impedance, d is the distance between electrode surfaces and A is the electrode surface area. Since d is difficult to measure for the cell used, it was decided to determine a calibration factor:

$$k_{\text{cal}} = \frac{d}{A} = \kappa_{\text{cal}} * Z'_{\text{cal}} \quad (9)$$

This factor was obtained by comparing the impedance measured for 1.0 M NaClO₄/PC (Z'_{cal}) to its conductivity reported in literature, which is 6.4 mS cm⁻¹ (κ_{cal}). [48] This leads to a calibration factor k_{cal} of 0.058 cm⁻¹. When this factor is applied to the impedance of 1.0 M NaPF₆/PC, an ionic conductivity of 7.7 mS cm⁻¹ is obtained which is in relatively good accordance with the conductivity reported for this electrolyte in the same source (7.9 mS cm⁻¹). Thus it can be assumed that the calibration is accurate. An overview of the

conductivity of the studied electrolytes is given in figure 31. It is notable that the electrolytes with the lowest CEs exhibited the highest conductivity in this experiment. In general, PC-based electrolytes had a higher conductivity than tetraglyme based ones, independent of the conducting salt. Furthermore, it was observed that the addition of FEC lowered the conductivity of the NaPF₆/PC electrolyte. The smallest conductivity in this study, however, was that of 1.0 M NaBF₄/tetraglyme, which incidentally exhibited the highest CE and stability of all tested electrolytes. Its conductivity was less than a quarter of that of 1.0 M NaClO₄/PC. It was even lower than that of 0.25 M NaBF₄/PC even though it had 4 times the concentration of conducting salt. Another electrolyte which had exhibited high CE in previous experiments, 1.0 M NaTf/tetraglyme, showed the second lowest conductivity of the tested electrolytes. While a high conductivity is generally a favorable electrolyte property for reasons of power density, it was not the determining factor for sodium metal plating- and stripping efficiency. However, a low conductivity may be an inhibiting factor when it comes to full cell application since the necessary C-rates might not be obtainable. This is especially true for high capacity systems such as Na-S.

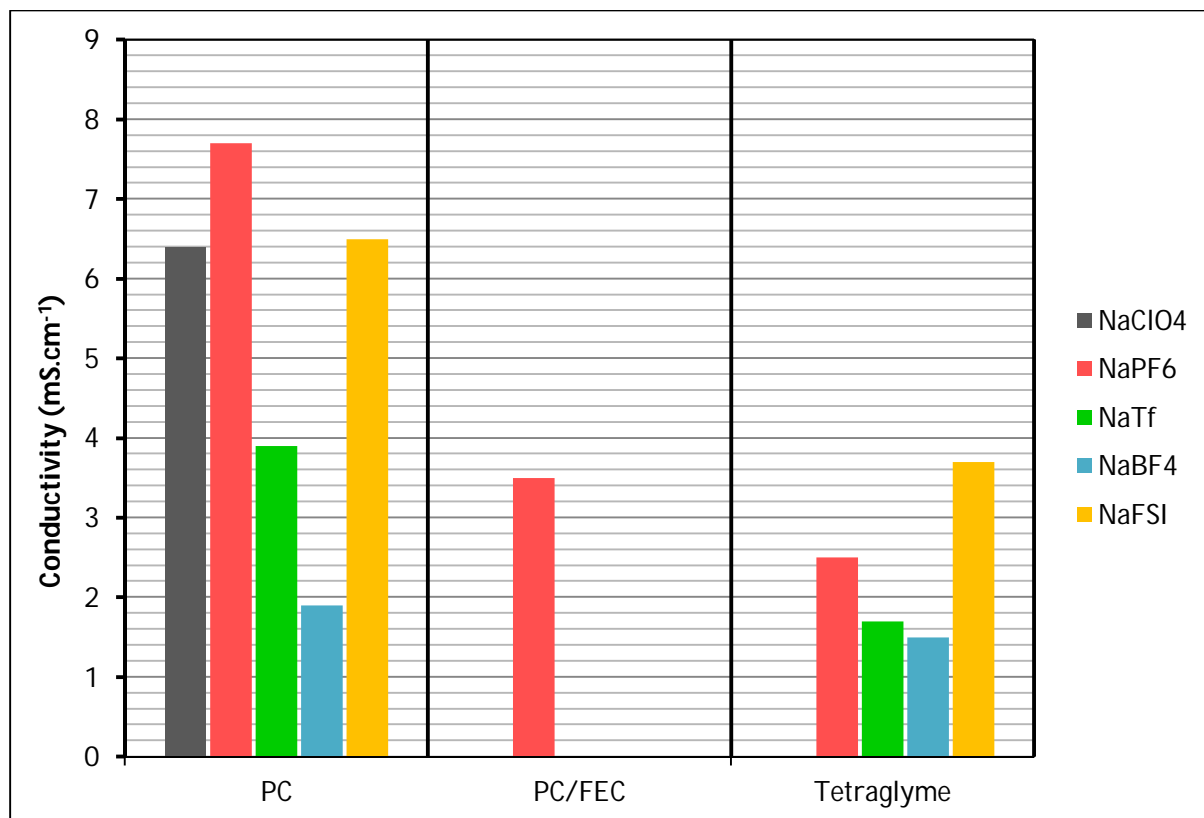


Figure 31: Ionic conductivity of a range of electrolytes at room temperature; the conductivity of NaClO₄/PC was sourced from literature and served for calibration purposes; conducting salt concentration may vary between electrolytes.

4.4 Sodium Deposition Comparison by SEM

For observation of sodium metal deposition behavior by scanning electron microscopy (SEM), special test cells were assembled as described in ch. 3.2.4. In order to make examination by SEM possible even with low-CE electrolytes, a maximum areal capacity of 2 mAh cm⁻² was deposited and stripped over 10 hours at a current of 0.2 mA for 4 cycles onto different substrates. After the sodium metal plating for the 4th cycle, the cells were disassembled and the samples were transferred to the SEM in an argon atmosphere before being examined.

4.4.1 Sodium Deposition on Stainless Steel

For each electrolyte, images at 3 different magnifications are given in order to be able to analyze and discuss the overall appearance of the deposit as well as details of its morphology.

Stainless steel substrate

The stainless steel substrates that the sodium metal was deposited on were wet-sanded with 800 grit sandpaper, cleaned and dried prior to deposition. In order to examine their surface, SEM pictures of one of the stainless steel disks without sodium metal on it were taken. At a magnification of 1000x, sanding marks are clearly visible on the surface of the steel. These intersecting scratches create a surface roughness that should facilitate nucleation and subsequent sodium metal deposition but may also promote dendrite formation according to literature. [73,74]

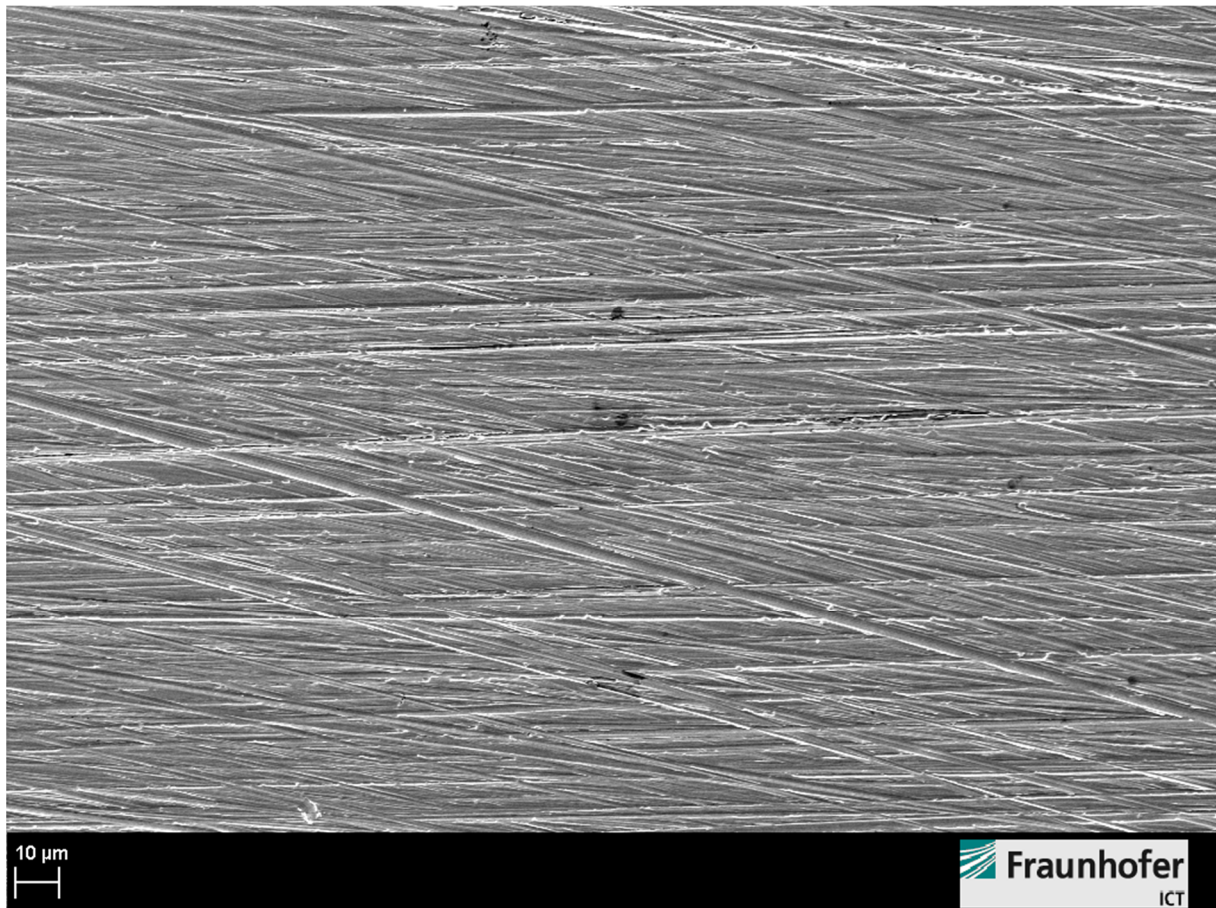


Figure 32: SEM image of a wet-sanded stainless steel disk used as a substrate for sodium metal deposition; magnification 1000x.

1.0 M NaClO₄/EC/DEC

At 60x magnification, the deposited sodium metal looked mostly uniform and even, with no major irregularities visible. However, patterns indicating a variance in depth did show up as a network of white lines in the image (fig. 33).

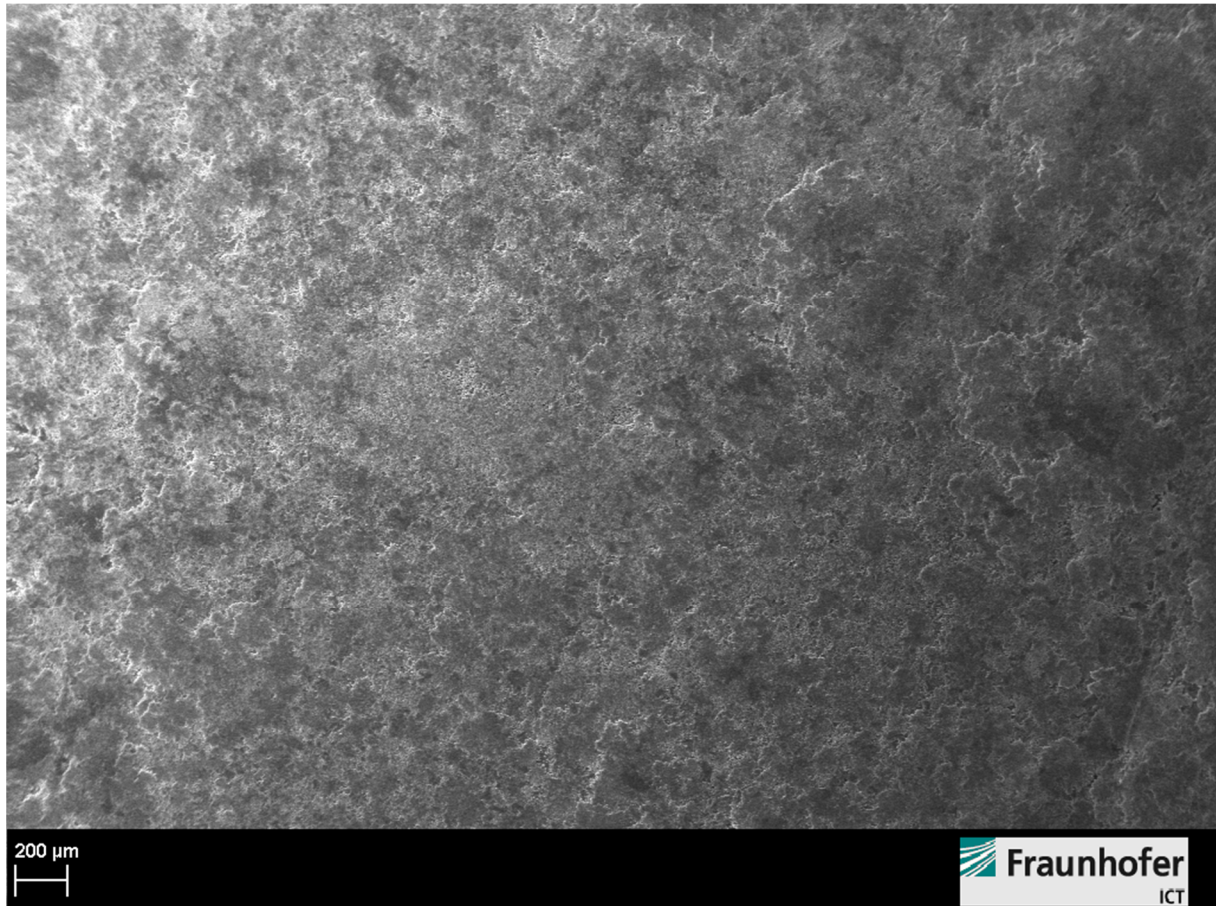


Figure 33: SEM image of metallic sodium deposited out of 1.0 M NaClO₄/EC/DEC onto a stainless steel disk; magnification 60x; 0.2 mA cm⁻²; 10 h; 4th cycle.

At 850x magnification (fig. 34), it became clear that the sodium metal was at least partially dendritic and had a "mossy" appearance. The deposition seemed to mostly form layers of metal upon one another, which became more and more dendritic towards the outer edges. Overall, there was a wide range of structures visible which would indicate a comparatively bad SEI and could explain the observed low CE.

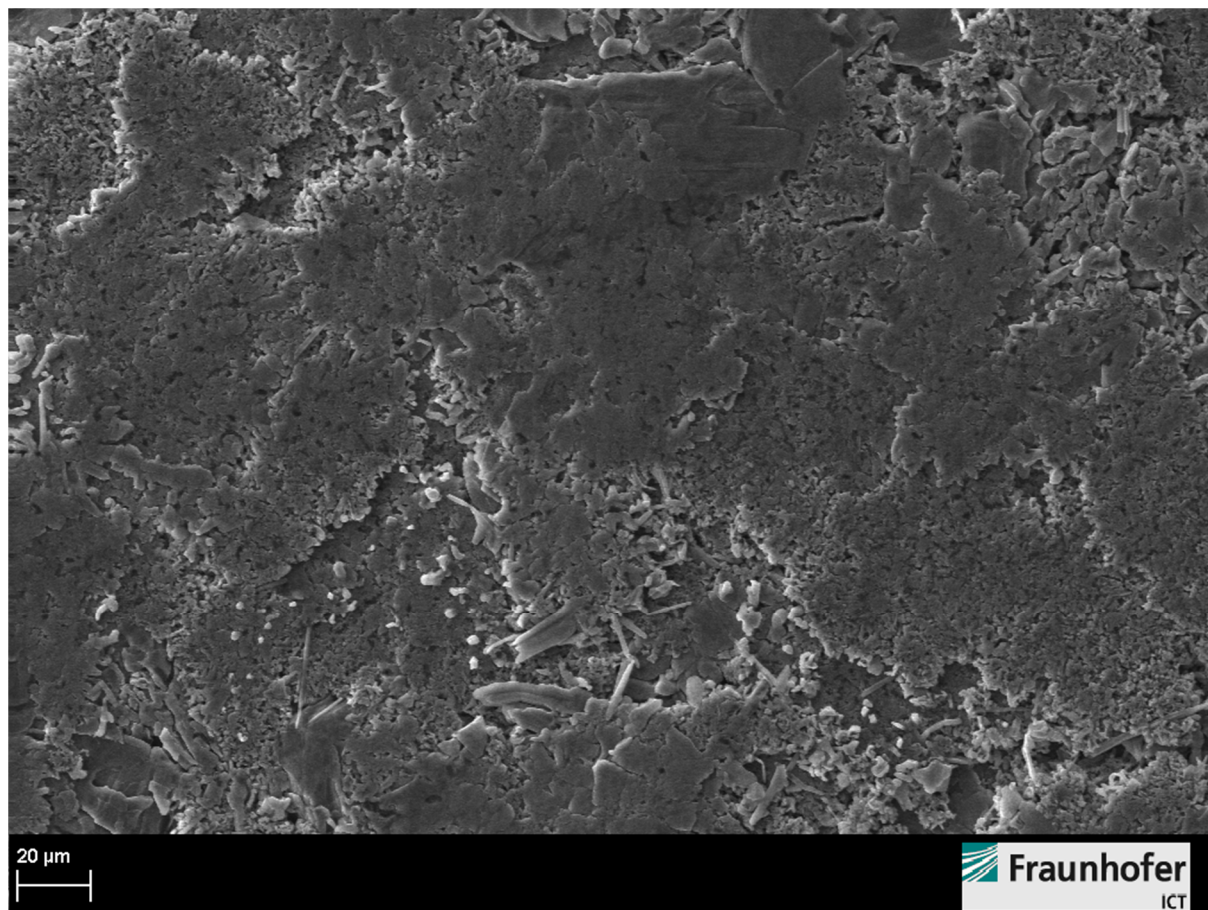


Figure 34: SEM image of metallic sodium deposited out of 1.0 M NaClO₄/EC/DEC onto a stainless steel disk; magnification 850x; 0.2 mA cm⁻²; 10 h; 4th cycle.

By increasing the magnification even further to 5000x (fig. 35), the dendritic sodium structures could be observed in more detail. While there were some areas where the metal was deposited as a uniform plate, most of it formed a lattice of structures between 1 and 10 μm in length. While there were no single dendrites visible that were disconnected from the bulk of the anode, it is safe to assume that a structure such as the one observed in these images would be detrimental to sodium deposition performance. On one hand, parts of the dendritic lattice could easily be detached, which would lead to a permanent loss of capacity. On the other hand, the observed structure has a very high surface-to-bulk ratio which would necessitate a lot of SEI formation at the cost of capacity. Last but not least, there would be a possibility of separator penetration by dendrites in a full cell built with this electrolyte.

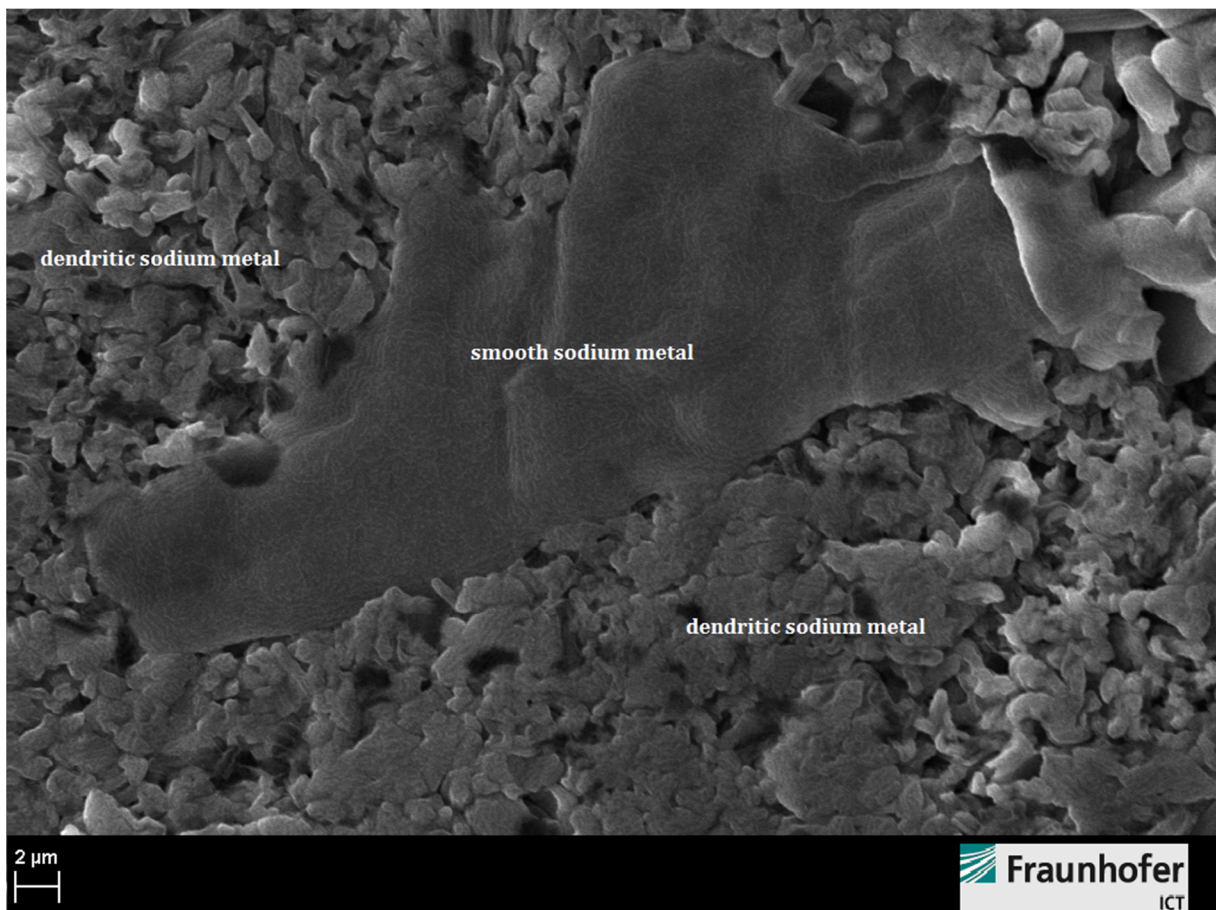


Figure 35: SEM image of partially dendritic metallic sodium deposited out of 1.0 M $\text{NaClO}_4/\text{EC}/\text{DEC}$ onto a stainless steel disk; magnification 5000x; 0.2 mA cm^{-2} ; 10 h; 4th cycle.

1.0 M NaPF₆/PC

In figure 36, metallic sodium deposited out of 1.0 M NaPF₆/PC is shown at a magnification of 60x. It was noticeable that while large parts of the surface seemed to be smooth and uniform, areas with a large degree of unevenness were present. When compared to metallic sodium out of NaClO₄/EC/DEC, the surface appeared a lot less uniform.

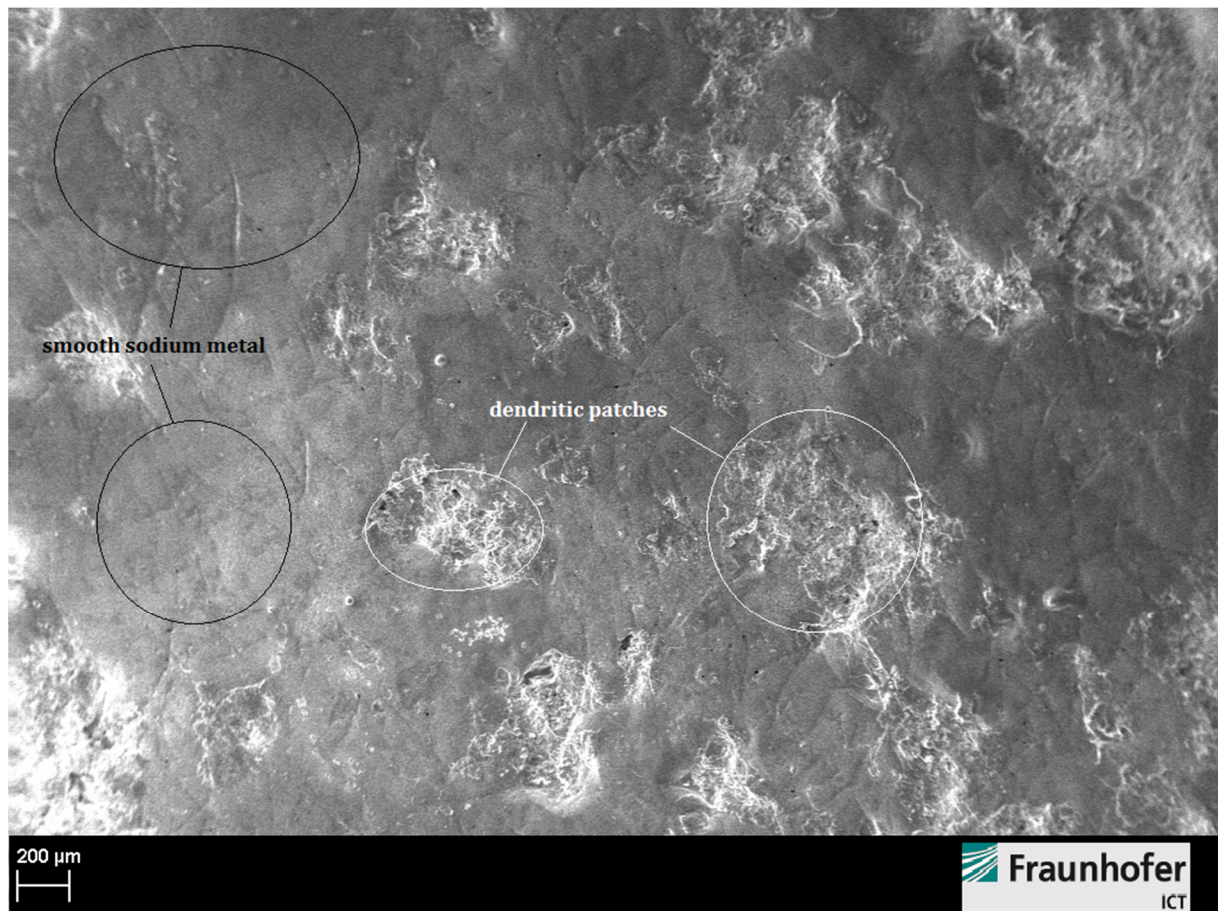


Figure 36: SEM image of metallic sodium deposited out of 1.0 M NaPF₆/PC onto a stainless steel disk; magnification 60x; 0.2 mA cm⁻²; 10 h; 4th cycle.

In order to study the two distinct forms of deposited sodium present in this sample more closely, a comparison image at magnification 850x is given in figure 37. In the relatively uniform area, small beadlike structures were visible that were distributed evenly across the surface. These structures were probably small growths of sodium metal which might have been the beginnings of dendrites and had a diameter of roughly 1 μm . In the uneven areas, dendritic growth was observed with structures between 1 and 20 μm in length. Thus, the dendrites seemed to be more pronounced and less “moss-like” than in the sample deposited out of $\text{NaClO}_4/\text{EC}/\text{DEC}$.

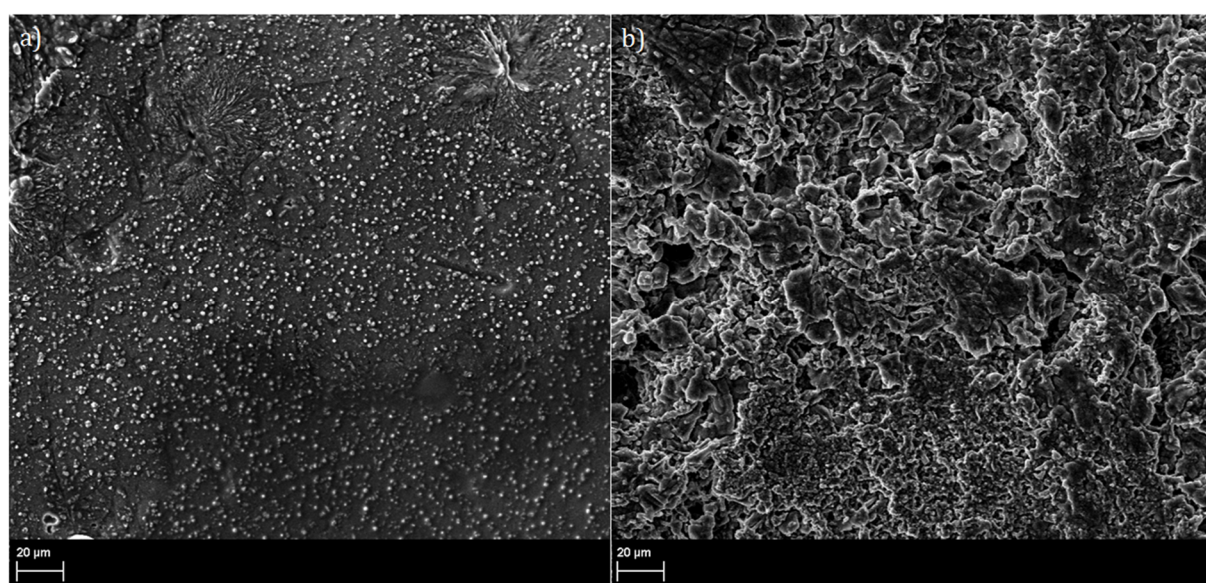


Figure 37: SEM comparison of metallic sodium deposited out of 1.0 M NaPF_6/PC onto two different areas of a stainless steel disk; (a) smooth area with small dendrites; (b) dendritic area; magnification 850x; 0.2 mA cm^{-2} ; 10 h; 4th cycle.

At a magnification of 5000x, the differences became even clearer, as shown in figure 38. The deposited sodium almost had a crystalline structure with needles protruding from the bulk and holes extending into the metal layer. It is clear that an even metal deposition out of this electrolyte is only partly possible under these conditions and that a cell which made use of this electrolyte and a sodium metal anode would risk short circuit formation because of the dendritic growth present. Furthermore, the observed patterns are in agreement with and serve as an explanation for the observed low CEs for cells with this electrolyte.

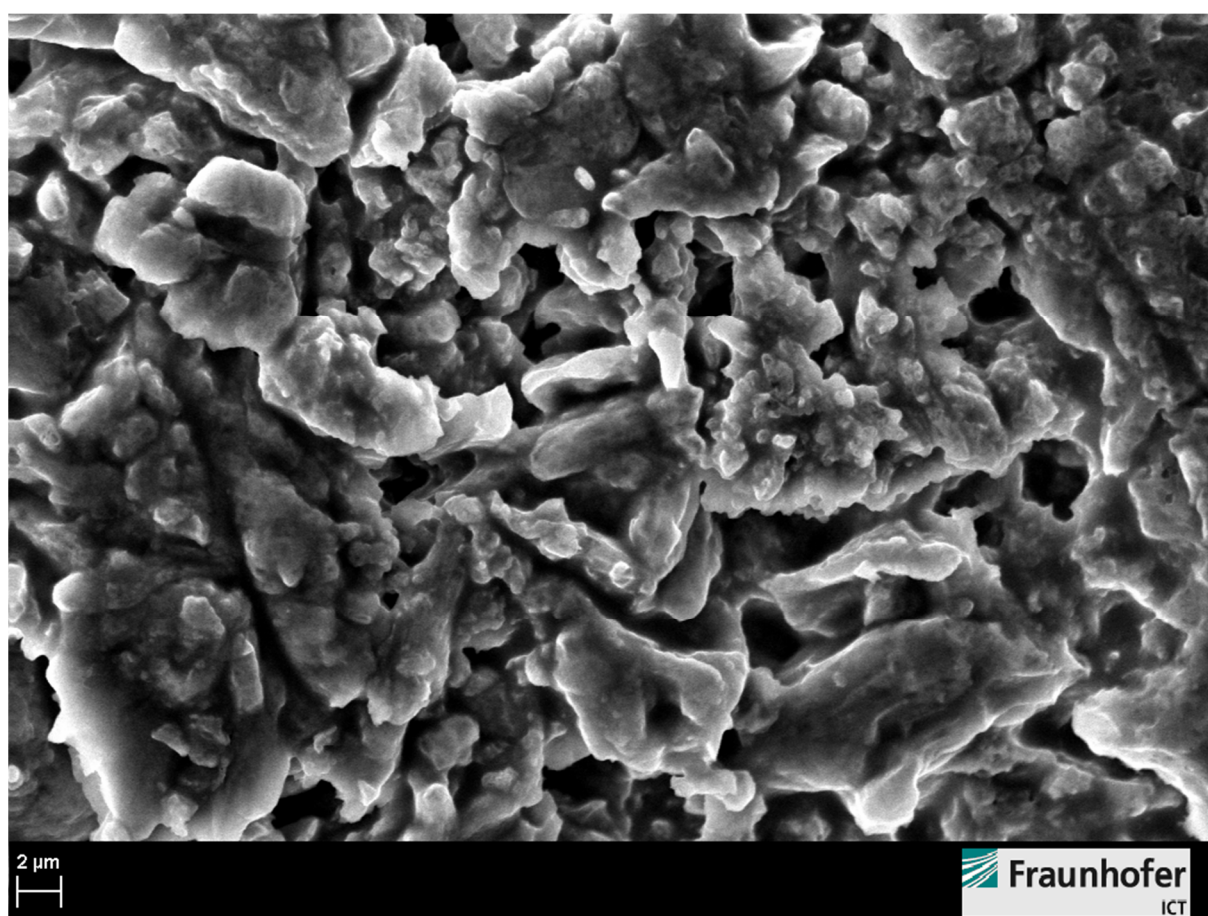


Figure 38: SEM image of dendritic metallic sodium deposited out of 1.0 M NaPF₆/PC onto a stainless steel disk; magnification 5000x; 0.2 mA cm⁻²; 10 h; 4th cycle.

1.0 M NaBF₄/tetraglyme

In figure 39, sodium metal deposited out of 1.0 M NaBF₄ onto a stainless steel disk is shown at a magnification of 60x. The surface of the sample had a very even and uniform appearance with no major irregularities visible.

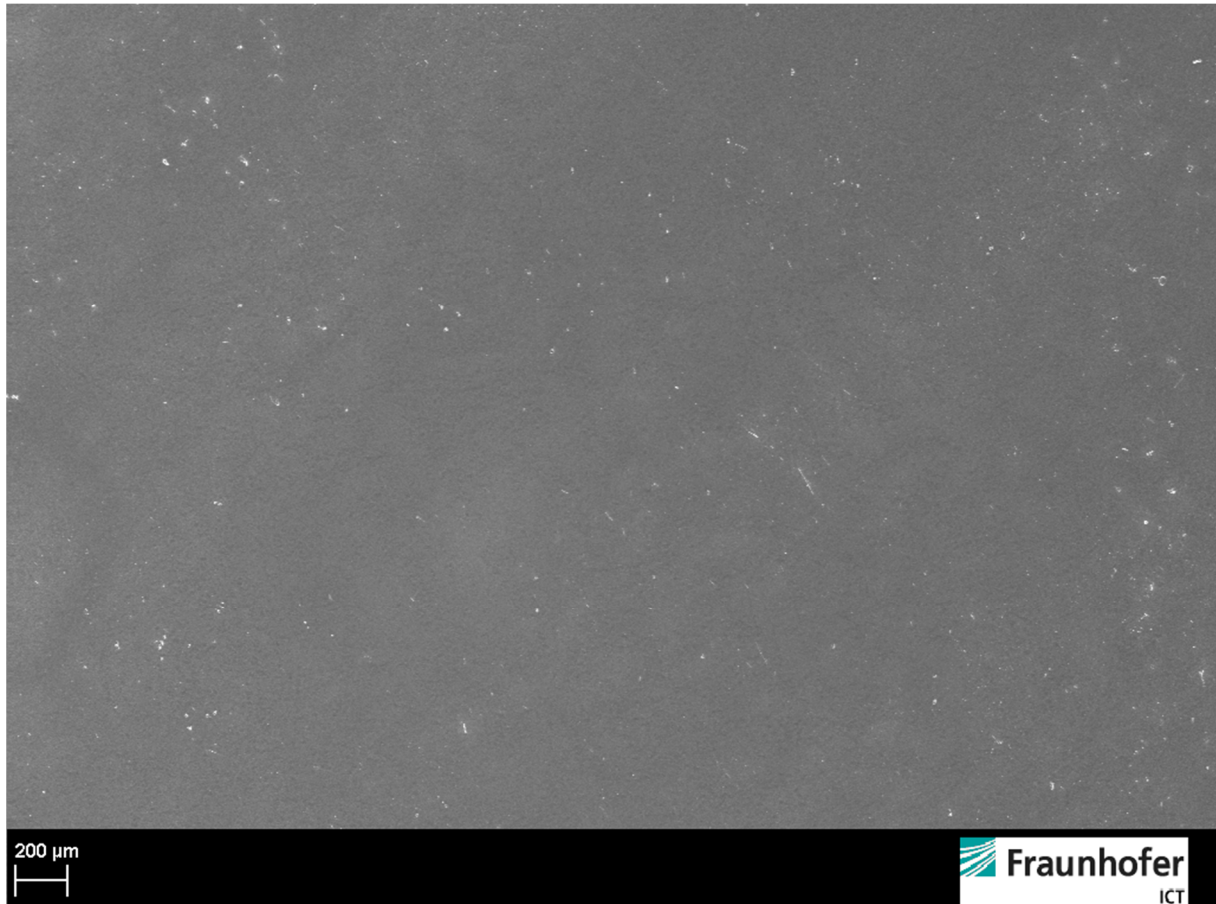


Figure 39: SEM image of smooth metallic sodium deposited out of 1.0 M NaBF₄/tetraglyme onto a stainless steel disk; magnification 60x; 0.2 mA cm⁻²; 10 h; 4th cycle.

Since the sample appeared so uniform, the image at 850x magnification was omitted here. Even at a magnification of 5000x (fig. 40), the deposited sodium metal appeared as an even surface with no dendritic structures present, neither needle-like nor “mossy”. Furthermore, no holes in the surface were visible. This, once again, is in good agreement with the findings of the galvanostatic cycling tests (ch. 4.1) which showed that this electrolyte yielded high coulombic efficiencies over many cycles.

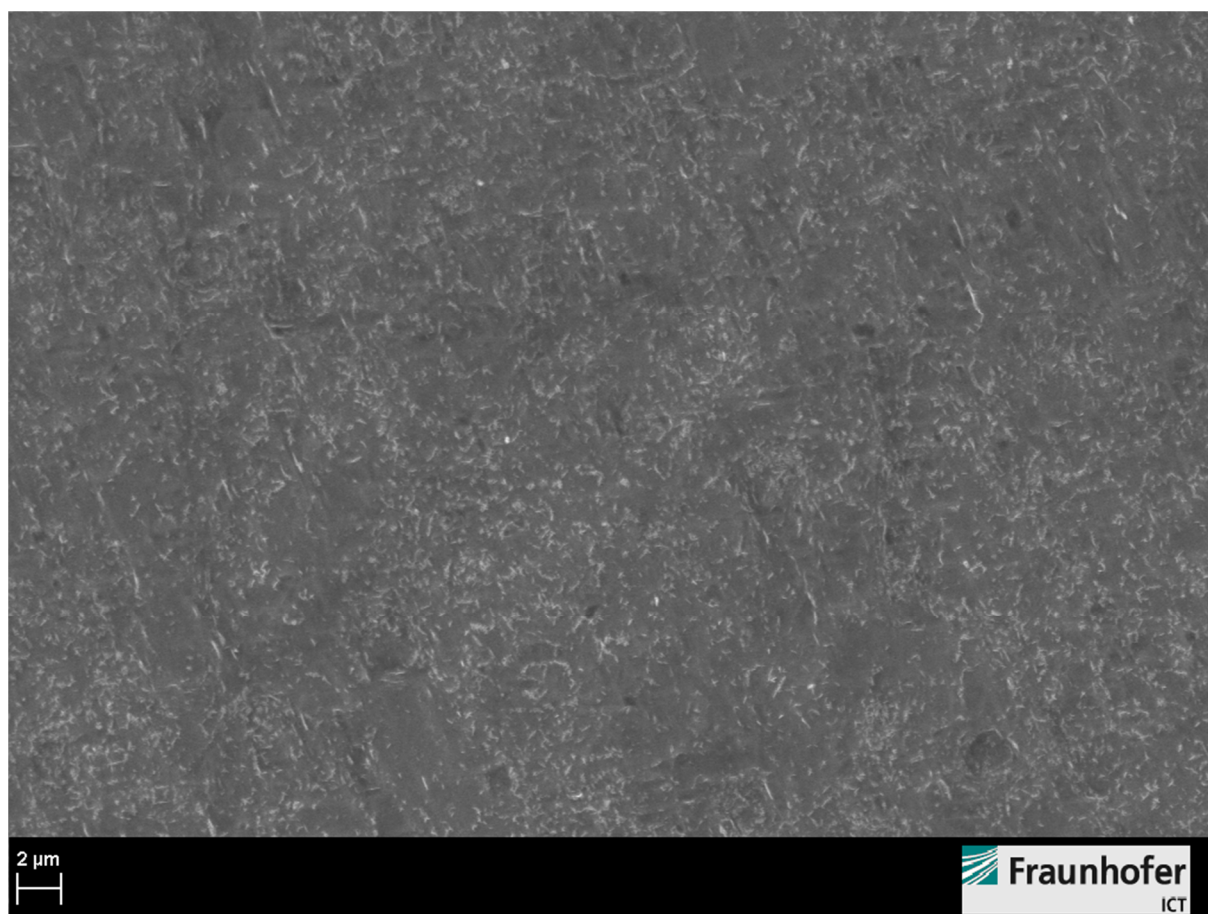


Figure 40: SEM image of smooth metallic sodium deposited out of 1.0 M NaBF₄/tetraglyme onto a stainless steel disk; magnification 5000x; 0.2 mA cm⁻²; 10 h; 4th cycle.

Counter electrode analysis

For two of the tested electrolytes, 1.0 M NaBF₄/tetraglyme and 1.0 M NaPF₆/PC, in addition to the sodium deposited on the working electrode, the remaining metal on the counter electrode was also examined by SEM. This side of the test cells had sodium stripped away from it in the last cycle of the test so that any dendrites formed in the preceding cycles should not be present anymore except if a permanent separation from the bulk had taken place.

In figure 41, a comparison of the two counter electrodes is given at a magnification of 60x. The sample from the NaBF₄/tetraglyme cell was mostly smooth with small irregularities only. There were a few pieces of debris present, probably stemming from the glass fiber separator. However, the sample from the NaPF₆/PC cell had patches of dendritic growth of up to 500 μm in diameter as well as holes in the sodium metal that showed up as dark spots in the image.

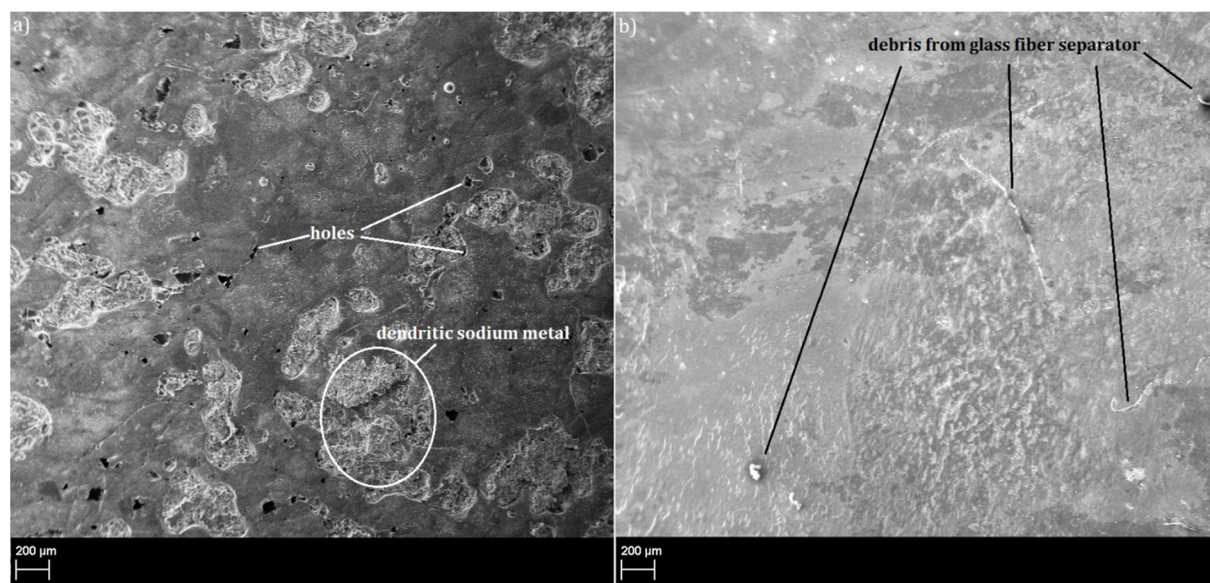


Figure 41: SEM comparison of metallic sodium counter electrodes out of cells containing (a) 1.0 M NaPF₆/PC and (b) 1.0 M NaBF₄/tetraglyme; magnification 60x; 0.2 mA; 10 h; 4th cycle.

When the magnification was increased to 1000x, the differences between the two samples became even more obvious. While the NaBF_4 /tetraglyme sample was rather smooth with a few creases, the NaPF_6 /PC sample had dendritic growth within the patches that are described above. Those patches seem to protrude deep into the electrode and are highly heterogeneous in their structure. This shows that the interaction between sodium metal and the electrolyte is not only impeding plating onto and stripping off of stainless steel but is also relevant for the same processes taking place on already present sodium metal. Furthermore, it is interesting to note that the effects of inferior sodium metal deposition seem to persist even after stripping has taken place.

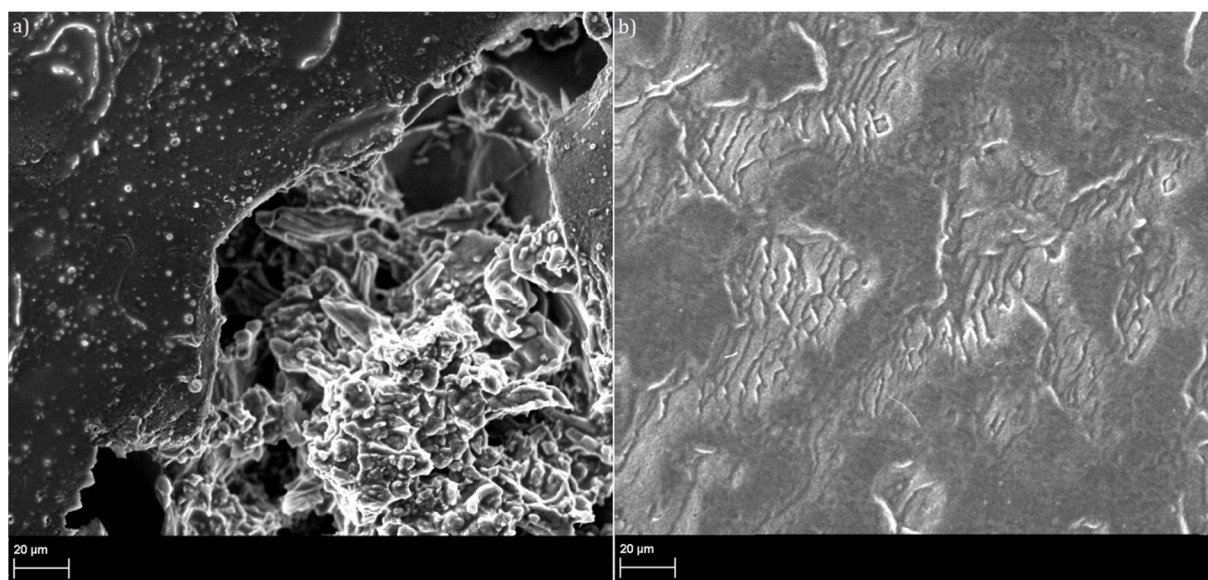


Figure 42: SEM comparison of metallic sodium counter electrodes out of cells containing (a) 1.0 M NaPF_6 /PC and (b) 1.0 M NaBF_4 /tetraglyme; magnification 1000x; 0.2 mA; 10 h; 4th cycle.

4.4.2 Sodium Deposition on Copper Foil

For two of the tested electrolytes, 1.0 M NaBF₄/tetraglyme and 1.0 M NaPF₆/PC, in addition to sodium deposition onto a stainless steel disk, deposition onto copper foil mounted on a stainless steel disk was also tested. The parameters were the same as for deposition on stainless steel, i.e., a current of 0.2 mA cm⁻² over 10 hours for a maximum areal capacity of 2 mAh cm⁻². The coulombic efficiencies for these tests are shown in [figure XX33](#). Even though the areal capacity was increased by a factor of 10 over previous tests, the CE for 1.0 M NaPF₆/PC was very low. For 1.0 M NaBF₄/tetraglyme, the CE was above 98% for the third cycle. This means that the CEs observed in this test were similar to those observed in the sodium electrodeposition tests on stainless steel substrates.

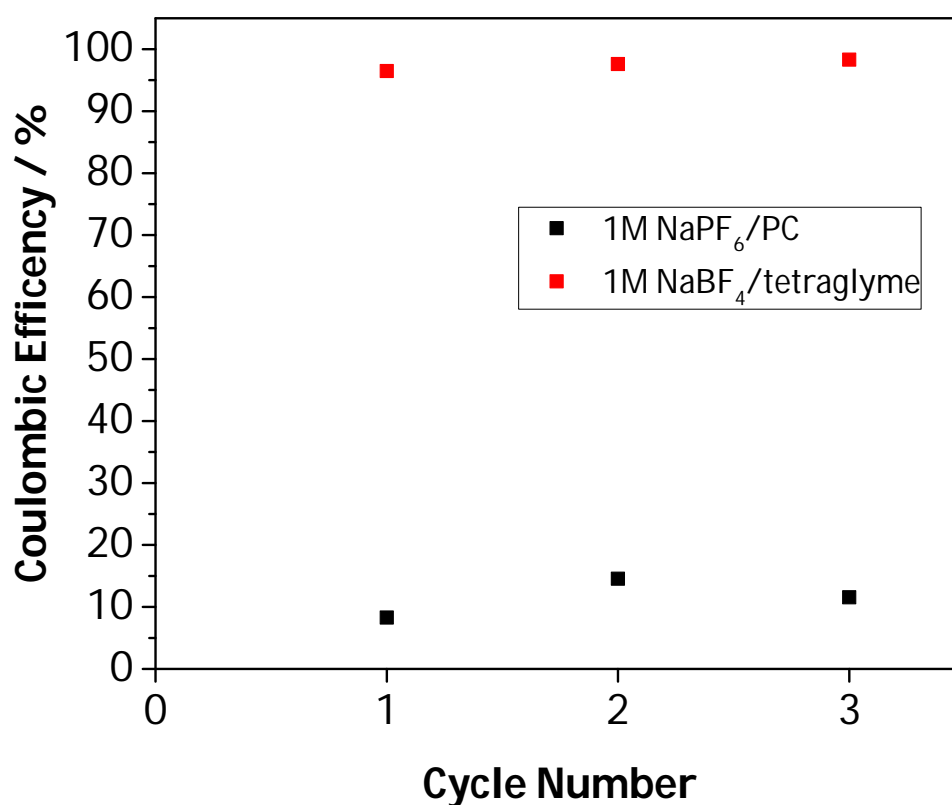


Figure 43: Coulombic efficiencies for long-term metal deposition onto copper substrate out of two different electrolytes; 0.2 mA cm⁻²; 10h.

In order to determine how the change of substrate affected the sodium metal deposition, SEM images of sodium deposited in this way were taken. An SEM image of the surface of a pristine copper substrate is shown in figure 44. When compared to the stainless steel substrate (fig. 32) the surface appears rougher and is covered with small particles with a diameter between 0.2 and 4.5 μm . These particles formed straight parallel lines of varying thickness. According to literature, this surface roughness should facilitate sodium metal nucleation. Because of the relative heterogeneity of the copper particles, they might also have enhanced dendrite formation with larger ones acting as current focal points and thus as seeds for dendrite growth. [73,74]

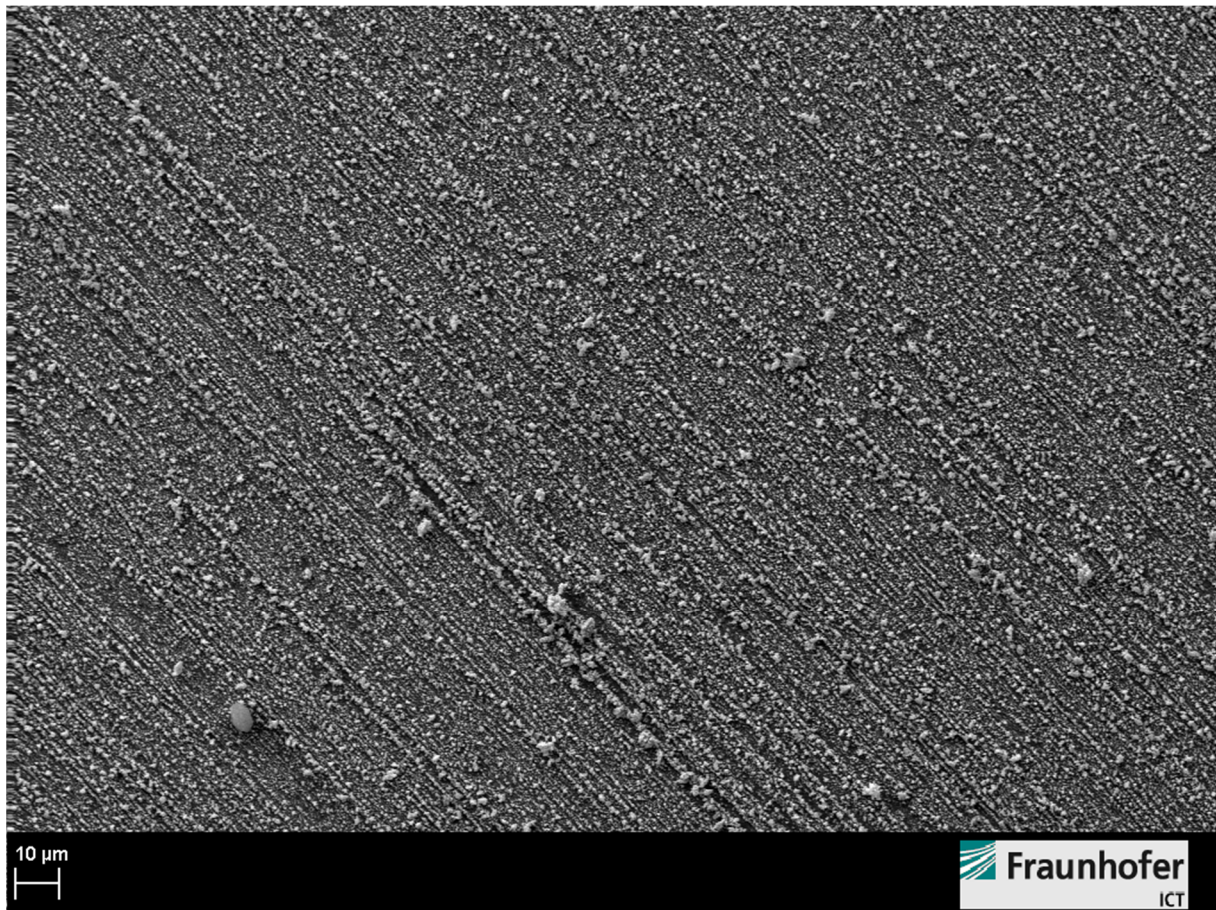


Figure 44: SEM image of copper foil (Schlenk SE-Cu R360) used as a substrate for sodium metal deposition; magnification 1000x.

When comparing the sodium metal deposition onto copper at a magnification of 1000x (fig. 45), the differences between the two deposits immediately become obvious, once again. For the NaPF_6/PC cell, the deposited sodium metal was completely dendritic with holes protruding down to the surface of the copper substrate even after deposition of sodium metal had taken place over 10 h at 0.2 mA. The formed dendrites had a length of up to 15 μm . The $\text{NaBF}_4/\text{tetraglyme}$ cell, on the other hand, yielded a mostly smooth surface. The only observable disturbances in this even surface were straight, parallel lines which arguably stem from the copper substrate, which also exhibited these lines. It is probable that the resulting differences in height carried through during the uniform deposition of sodium metal out of this electrolyte. Once again, these findings are in good agreement with the observed coulombic efficiencies and indicate that the deposition behavior of the studied electrolytes is mostly independent of substrate.

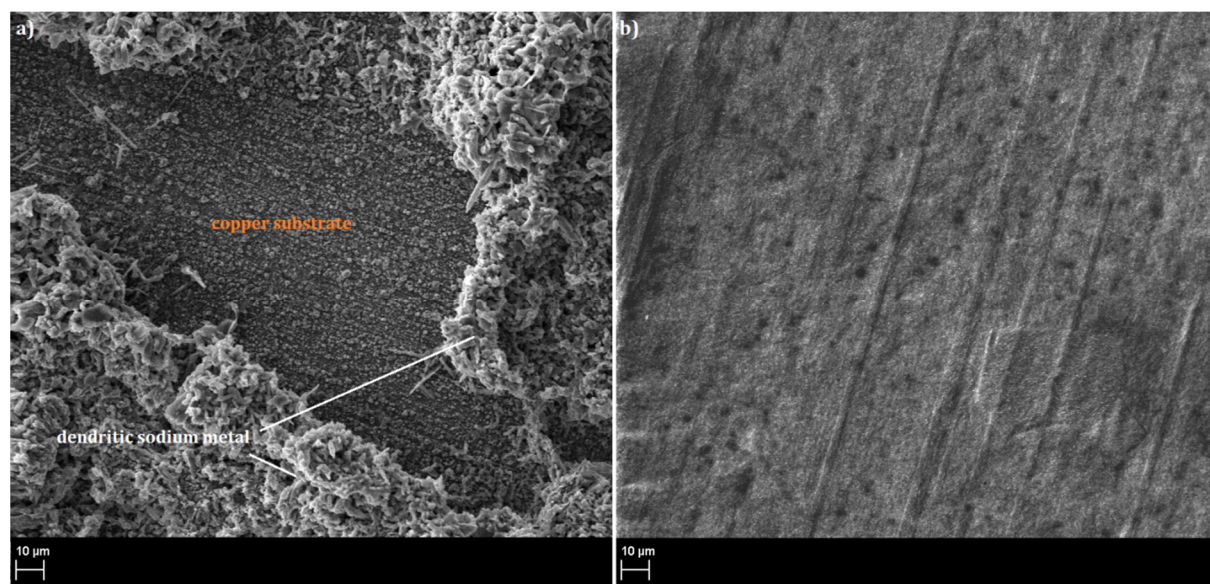


Figure 45: SEM comparison of sodium metal deposited onto a copper substrate out of (a) 1.0 M NaPF_6/PC and (b) 1.0 M $\text{NaBF}_4/\text{tetraglyme}$; magnification 1000x; 0.2 mA; 10 h; 4th cycle.

4.5 SEI Examination by XPS

For 1.0 M NaBF₄/tetraglyme, X-ray photoelectron spectroscopy (XPS) analysis of the SEI created during sodium deposition was performed. In order to do so, a three-electrode cell was set up in the same way as for the CV experiments, with a stainless steel disk as the working electrode and sodium foil as the counter- and reference electrodes. At a rate of 10 mV s⁻¹, the potential of the cell was lowered from the OCV to 0.1 V vs. Na/Na⁺. It was hypothesized that SEI formation should have occurred up to this point in the present voltage range, since it is close to the plating potential of sodium (~0.0 V vs. Na/Na⁺). Thus, the potential scan was stopped and the sample was extracted, washed and examined.

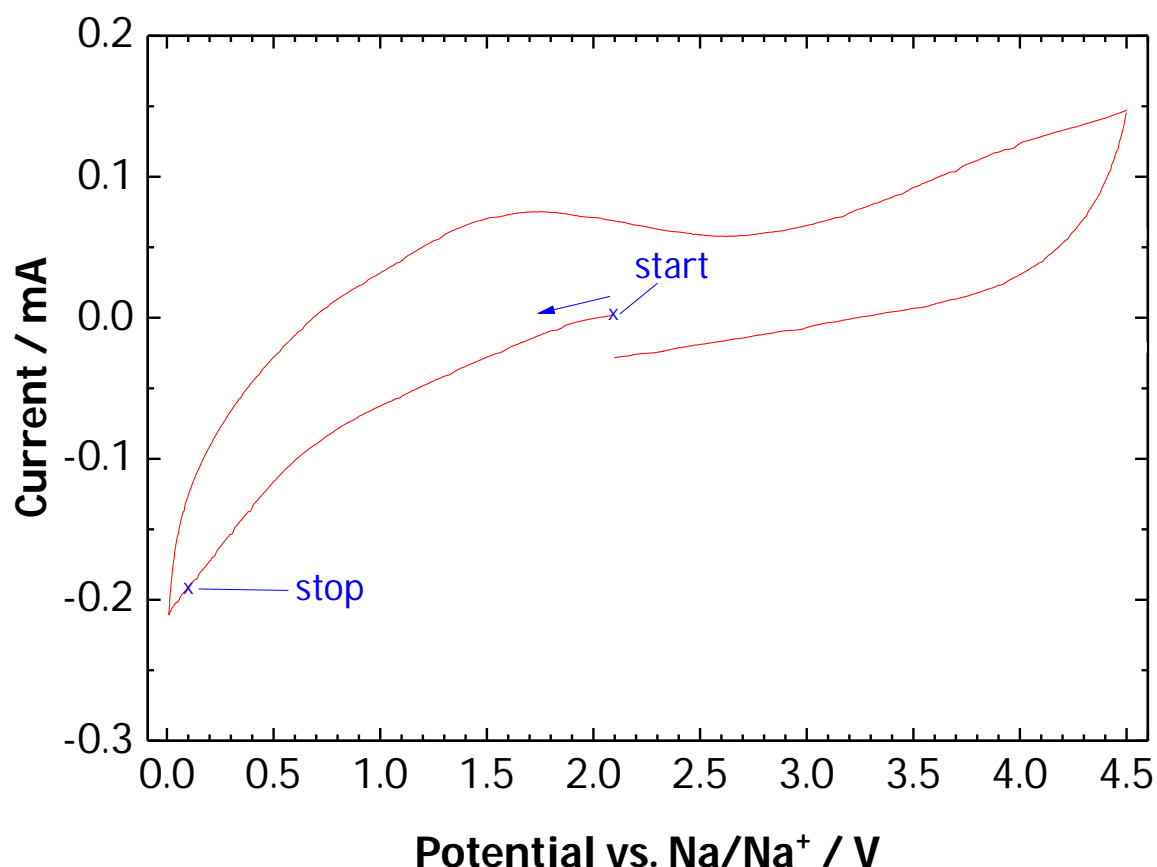


Figure 46: First cycle of a CV for 1.0 M NaBF₄/tetraglyme with indication of test cycle protocol for XPS cells (10 mV s⁻¹).

4.5.1 Overview Survey Spectra

In figure 47a, the survey XPS spectrum for the untreated sample is given which shows the approximate element distribution on the surface. It was observed that the surface consisted mainly of sodium, oxygen, and carbon, with no iron being detected, which indicates that a layer covering the stainless steel plate, presumably the SEI, was present.

After the surface spectrum was recorded, a depth profile of the sample was taken by sputtering at a rate of approximately 1 nm min^{-1} with an Ar laser. The sputtering times were 3 min, 10 min, and 30 min (fig.47b-c). After the initial removal of 3 nm off the surface layer, elements pertaining to the stainless steel like iron, chromium, and molybdenum started to appear while the peaks for C, O, and Na diminished. At the same time, fluoride became apparent in the survey spectrum, which disappeared again after 10 min of sputtering along with most of the intensity of the C, O, and Na peaks. From 10 min to 30 minutes of sputtering, the spectrum stayed mostly identical, with the only major change being that Na disappeared completely.

This depth profile indicates that the SEI created in this experiment had a thickness of only 3 – 10 nm. In comparison, a study of SEI's formed on lithiated graphite electrodes revealed SEI thicknesses of more than 30 nm for various electrolytes. [75]

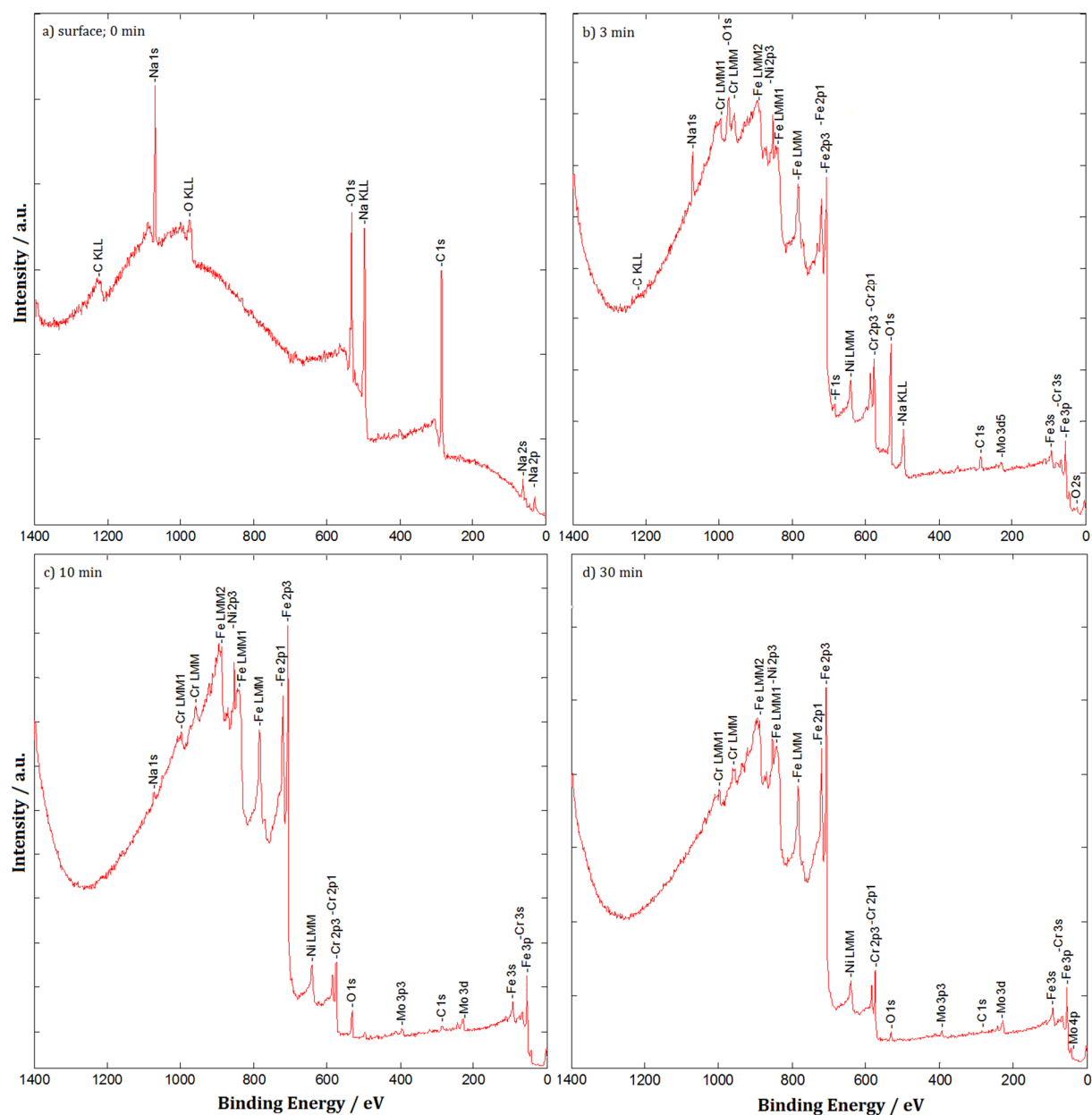


Figure 47: XPS spectrum and depth profile of a surface layer deposited electrochemically out of 1.0 M NaBF₄/tetraglyme onto a stainless steel disk after a) 0 min, b) 3 min, c) 10 min and d) 30 min of sputtering.

4.5.2 Detail Element Spectra

The C 1s, O 1s, Na 1s and F 1s spectra for 0 min and 3 min of sputtering were examined in detail in order to determine the compounds which made up the SEI and their depth distribution. An overview of the fitted peaks and the associated species is given in table 8. The peak assignment was based on data from the NIST X-ray photoelectron spectroscopy database. [76]

Table 8: Electrolyte formulations tested for ionic conductivity by EIS with respective concentrations; green indicates high CE, red indicates low CE.

| Sputtering time | 0 min | 3 min | | |
|-----------------|---------------------|--------|-----------------|------------------------|
| Spectrum | Binding energy / eV | | Peak assignment | Species |
| C 1s | 288.5 | 287.2 | C-O | RONa |
| | 284.9 | 284.8 | C-C, C-H | RONa |
| O 1s | 536.0 | - | Na KLL | Auger peak |
| | - | 534.0 | C-O | RONa |
| Na 1s | 531.5 | 530.5 | Na-O | Na ₂ O |
| | 1071.3 | 1071.9 | Na-O, Na-F | Na ₂ O, NaF |
| F 1s | 686.7 | - | B-F | NaBF ₄ |
| | 683.7 | 684.5 | Na-F | NaF |

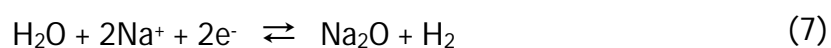
At 0 min of sputtering, the C 1s spectrum could be fitted with 2 peaks at 288.5 eV (C-O) and 284.9 eV (C-C, C-H). These two peaks are consistent with sodium alkoxides (RONa), a common reduction product of ether electrolytes. [71] However, a corresponding C-O peak could not be identified in the O 1s spectrum although it might have overlapped with a Na KLL Auger peak identified at 535.9 eV. [77] Furthermore, the O 1s spectrum showed a peak at 531.5 eV (Na-O) while the F 1s spectrum exhibited a weak peak at 683.7 eV (Na-F). When combining these analyses with the Na 1s spectrum, it is deduced that the Na 1s peak at 1071.3 eV consisted of 2 overlapping peaks of Na-O and Na-F, which would be consistent with tabulated values for Na₂O and NaF. [76] The F 1s peak at 686.7 eV was most likely due to residual NaBF₄ on the SEI surface.

After 3 minutes of sputtering, the overall intensity of the C 1s peaks diminished and their ratio was inverted with the C-O peak being stronger than the C-C/C-H peak. This would indicate a decrease in chain length of the sodium alkoxides at the deeper levels of the SEI. In the O 1s spectrum, the Na KLL Auger peak disappeared and the C-O peak at 339.9 eV became apparent while the overall amount of sodium decreased, which is also apparent in the Na 1s spectrum. For F 1s, the NaBF₄ related peak disappeared and the Na-F peak became more intense which suggests a higher concentration of NaF.

The presence of NaF in the SEI could be explained by decomposition of NaBF₄:



The formation of Na₂O could be due to reaction of sodium with trace amounts of residual water in the electrolyte or with O₂ in the Ar atmosphere of the glovebox (<1.0 ppm):



In conclusion, the formed SEI seemed to be comparatively thin with a high concentration of organic compounds like sodium alkoxides at the surface and inorganic compounds like NaF and Na₂O in its deeper layers. In the past, a high concentration of inorganic compounds has been shown to result in thin and stable SEI's in Li-ion systems. [71,75]

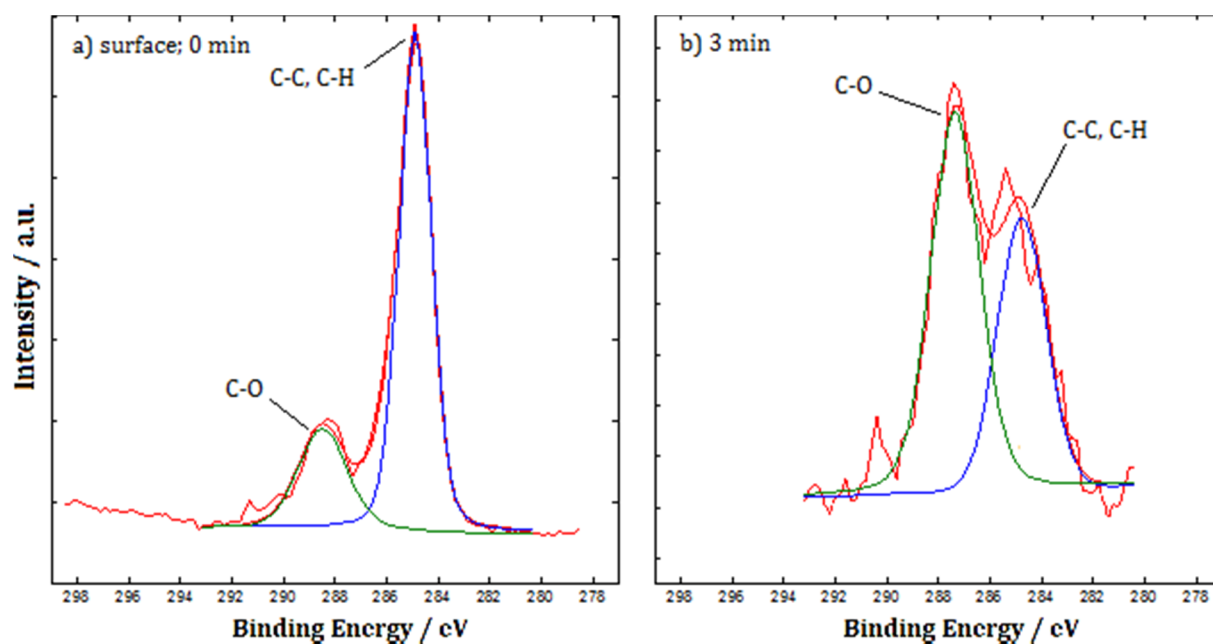


Figure 48: C 1s spectra of a surface layer deposited electrochemically out of 1.0 M NaBF₄/tetraglyme onto a stainless steel disk after a) 0 min, b) 3 min of sputtering.

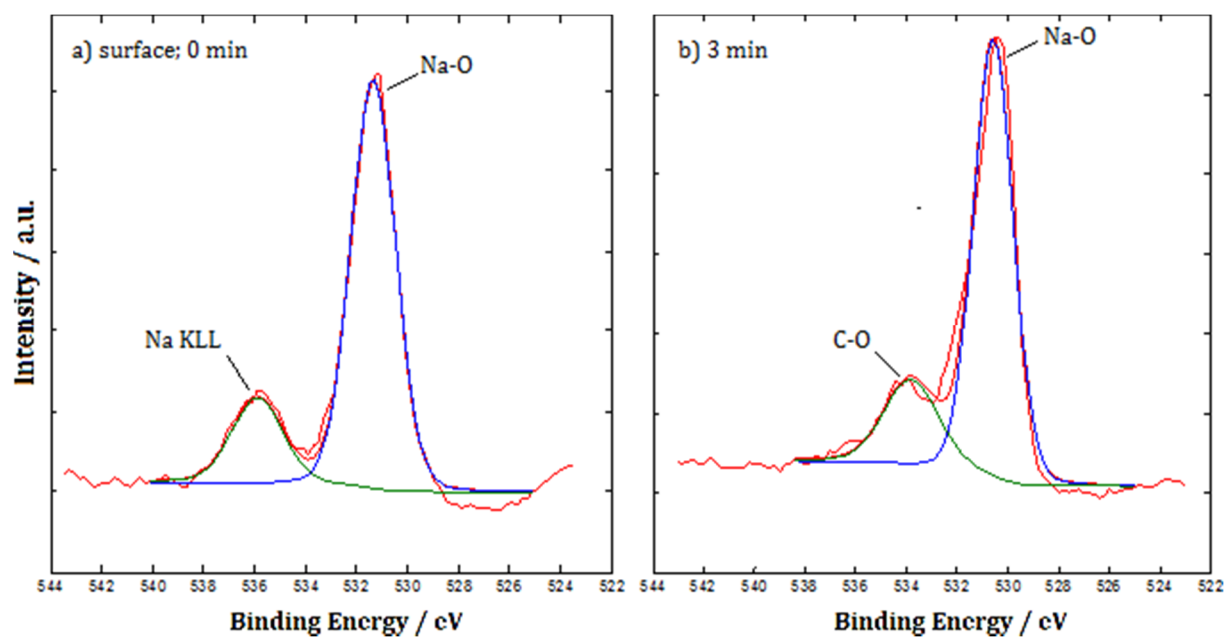


Figure 49: O 1s spectra of a surface layer deposited electrochemically out of 1.0 M NaBF₄/tetraglyme onto a stainless steel disk after a) 0 min, b) 3 min of sputtering.

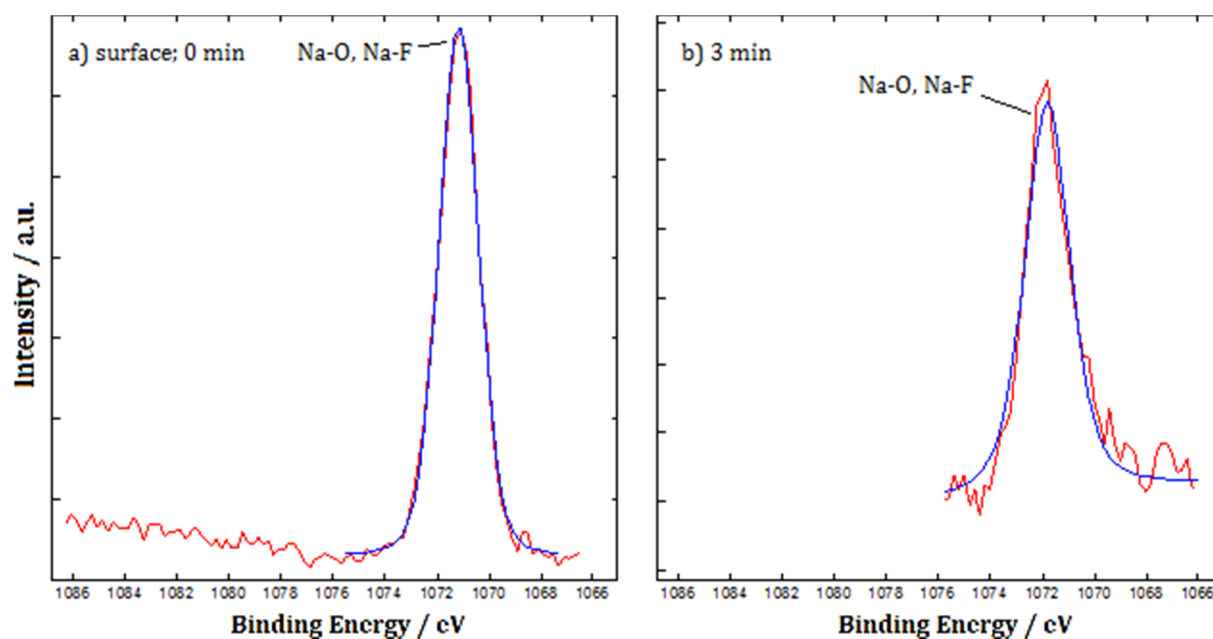


Figure 50: Na 1s spectra of a surface layer deposited electrochemically out of 1.0 M NaBF₄/tetraglyme onto a stainless steel disk after a) 0 min, b) 3 min of sputtering.

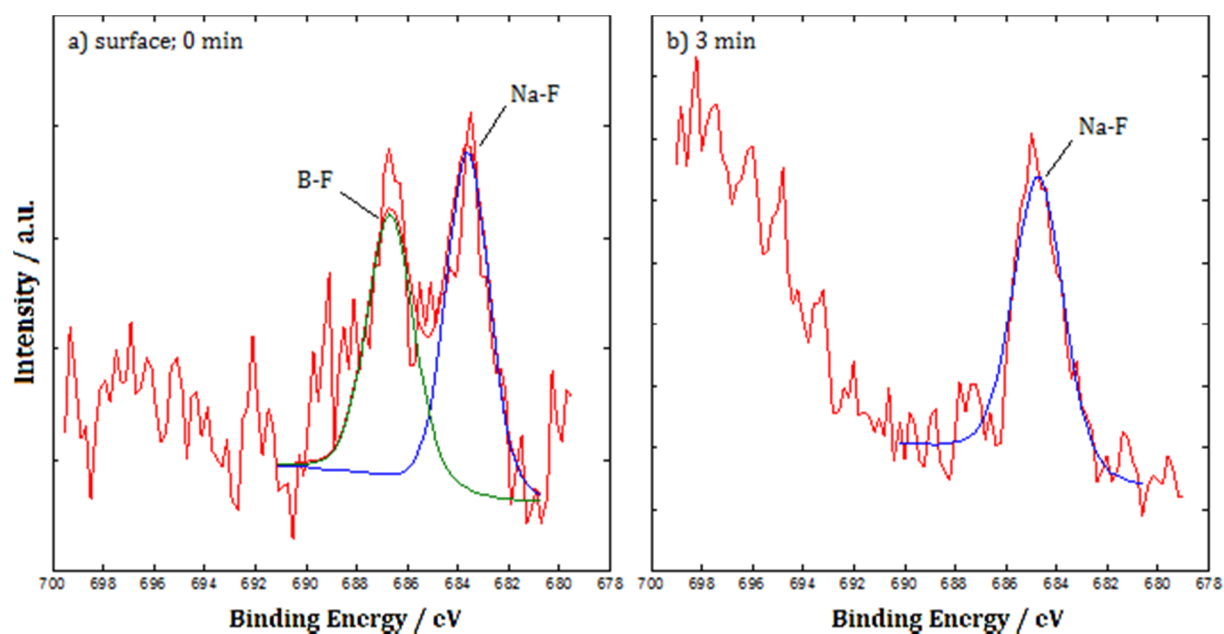


Figure 51: F 1s spectra of a surface layer deposited electrochemically out of 1.0 M NaBF₄/tetraglyme onto a stainless steel disk after a) 0 min, b) 3 min of sputtering.

4.6 Sodium Metal/NaNCM Cells

4.6.1 NaBF₄/tetraglyme and NaPF₆/PC

In order to test if 1.0 M NaBF₄/tetraglyme, the electrolyte with the highest coulombic efficiency for metal deposition observed in this work, was suitable as a battery electrolyte, full cells with a sodium metal anode and a NaNCM cathode were prepared. As a reference, comparable cells employing 1.0 M NaPF₆/PC as the electrolyte were tested as well since this electrolyte has been proven to yield good results in conjunction with the NaNCM cathodes provided by Helmholtz Institute Ulm (HIU). [69] The cells were cycled between 2.0 V and 4.0 V at a current of 40 mA per gram of active material. The capacity- and CE-profile of a cell containing 1.0 M NaPF₆/PC as the electrolyte is shown in figure 52. The cell starts out with a specific capacity of around 88 mAh g⁻¹ which increases slightly over the first 50 cycles to about 92 mAh g⁻¹ before starting to drop off after around 170 cycles and reaching a minimum of about 87 mAh g⁻¹ after 350 cycles. During the whole test, the CE was above 99.8% which was in agreement with previous testing at HIU as were the observed specific capacities.

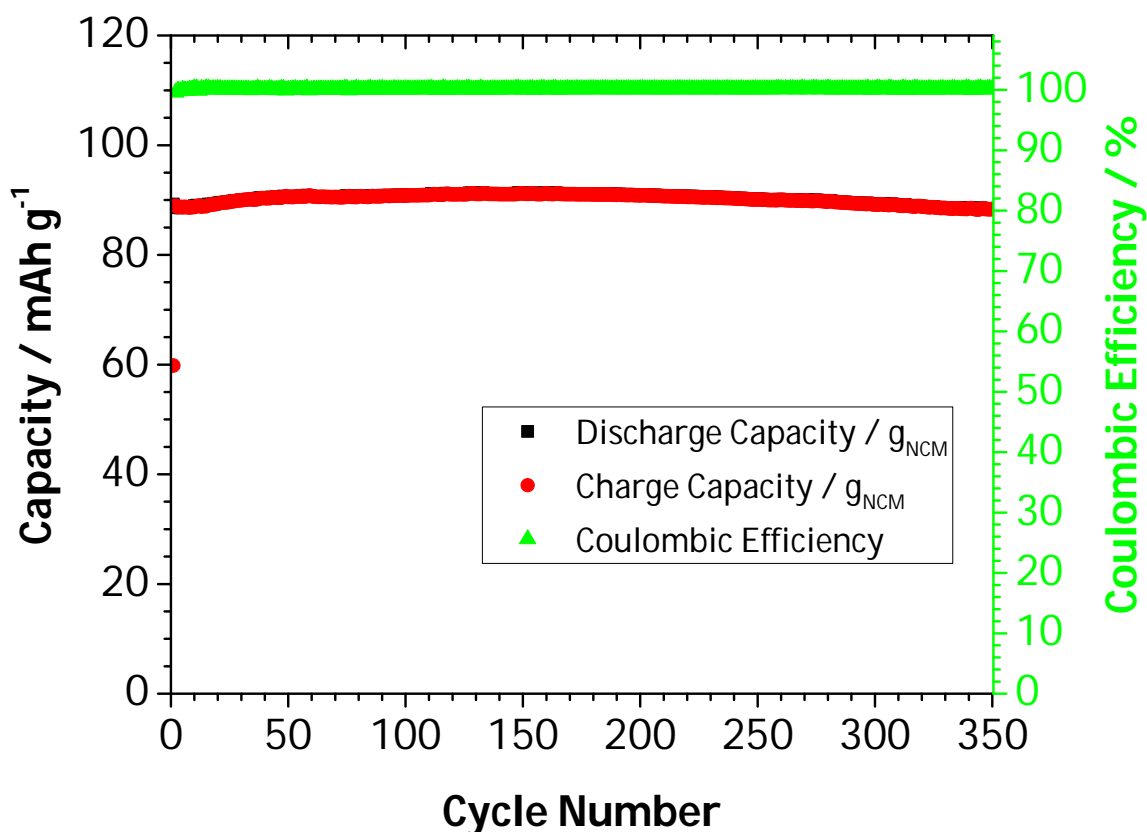


Figure 52: Capacity and coulombic efficiency vs. cycle number for a metallic sodium/NaNCM two-electrode full cell with 1.0 M NaPF₆/PC as the electrolyte; cycled between 2.0 V and 4.0 V at 80 mA g⁻¹.

The capacity- and CE-profile for a similar cell containing 1.0 M NaBF₄ as the electrolyte is shown in figure 53. In comparison, the initial capacity of the cell is approximately equivalent to that of the cell containing NaPF₆/PC at 91 mAh g⁻¹. As cycling continues, though, the specific capacity declines at a steady rate and reaches a minimum of about 75 mAh g⁻¹ after 350 cycles. This behavior is also mirrored in the CE which, at about 99.0% after the first few cycles, is still very high, but doesn't reach the same level as exhibited by the reference cell. This behavior was observed in all tested cells containing the NaBF₄/tetraglyme electrolyte. Thus, this electrolyte doesn't seem to be suited very well for full cells containing NaNCM cathodes since the drop-off in capacity is too severe. However, it is noteworthy that these cells were able to be cycled for a few hundred cycles without failure.

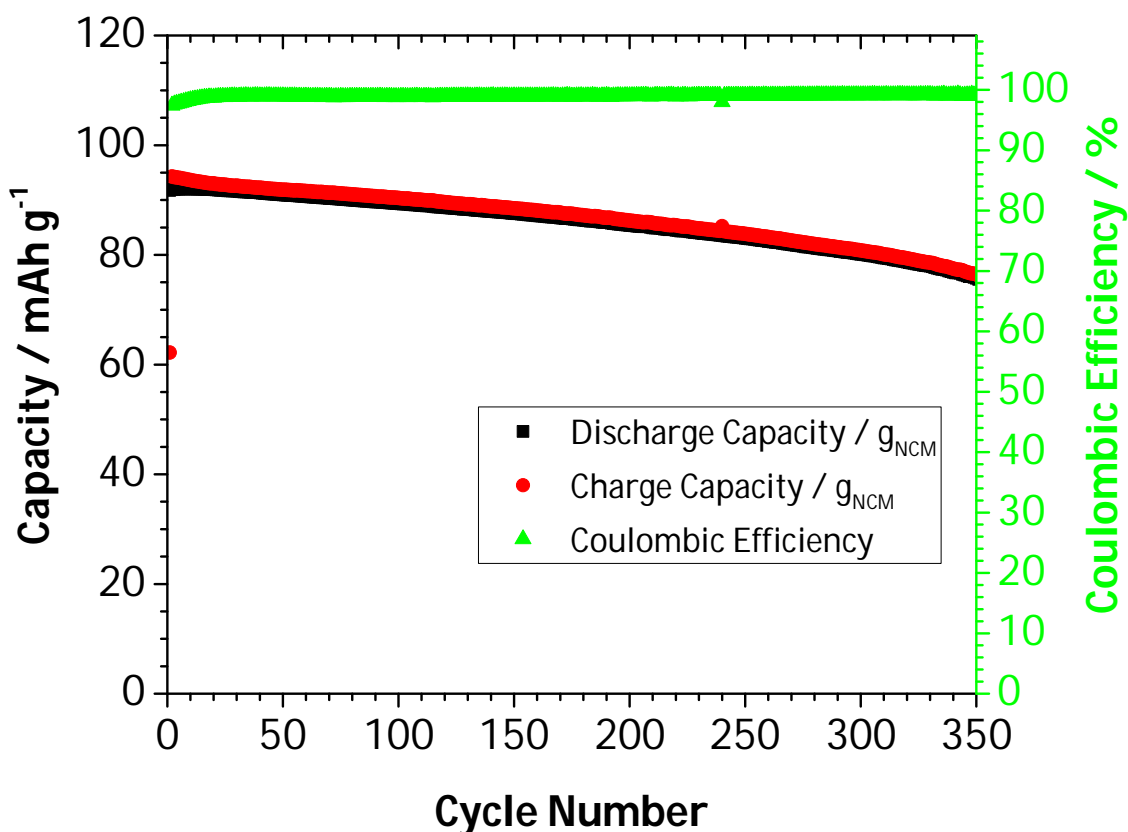


Figure 53: Capacity and coulombic efficiency vs. cycle number for a metallic sodium/NaNCM two-electrode full cell with 1.0 M NaBF₄/tetraglyme as the electrolyte; cycled between 2.0 and 4.0 V at 80 mA g⁻¹.

Since the CVs for 1.0 M NaBF₄/tetraglyme showed that it should be stable at potentials of up to 4.5 V vs. Na/Na⁺, it is to be assumed that a side reaction was occurring within these NaNCM full cells, which was responsible for the comparably low CE. In figures 54 and 55, the voltage profiles of the cells discussed above are shown. During the first cycle discharge, the voltage profile of the 1.0 M NaPF₆/PC cell was distinctively different from that of the following cycles, especially so in the voltage region between 3.7 V and 2.9 V. This indicates that side reactions were taking place that might have influenced the stability of the cathode for the rest of the test. For the following cycles up to the 301st, the discharge profiles did not change significantly. For the charge steps, the profile shifted to higher capacities between the 11th and 51st cycle and remained mostly the same during the rest of the test. For the 1.0 M NaBF₄/tetraglyme cell, the discharge profile had a very similar shape to that of the other cell, with the same plateau regions.

The only major difference was observed during the first discharge which, in this case, had the same shape as in the other cycles. For the rest of the test, charge and discharge profiles continually shifted to lower capacities over the whole voltage range. Arguably, the cause of the difference in capacity retention and coulombic efficiency for these tests is rooted in the reactions taking place during the first cycle as that was the only major difference observed between the two cells. This might indicate that either NaPF₆ or PC or a combination thereof creates a more stable SEI in regard to the cathode when compared to NaBF₄/tetraglyme.

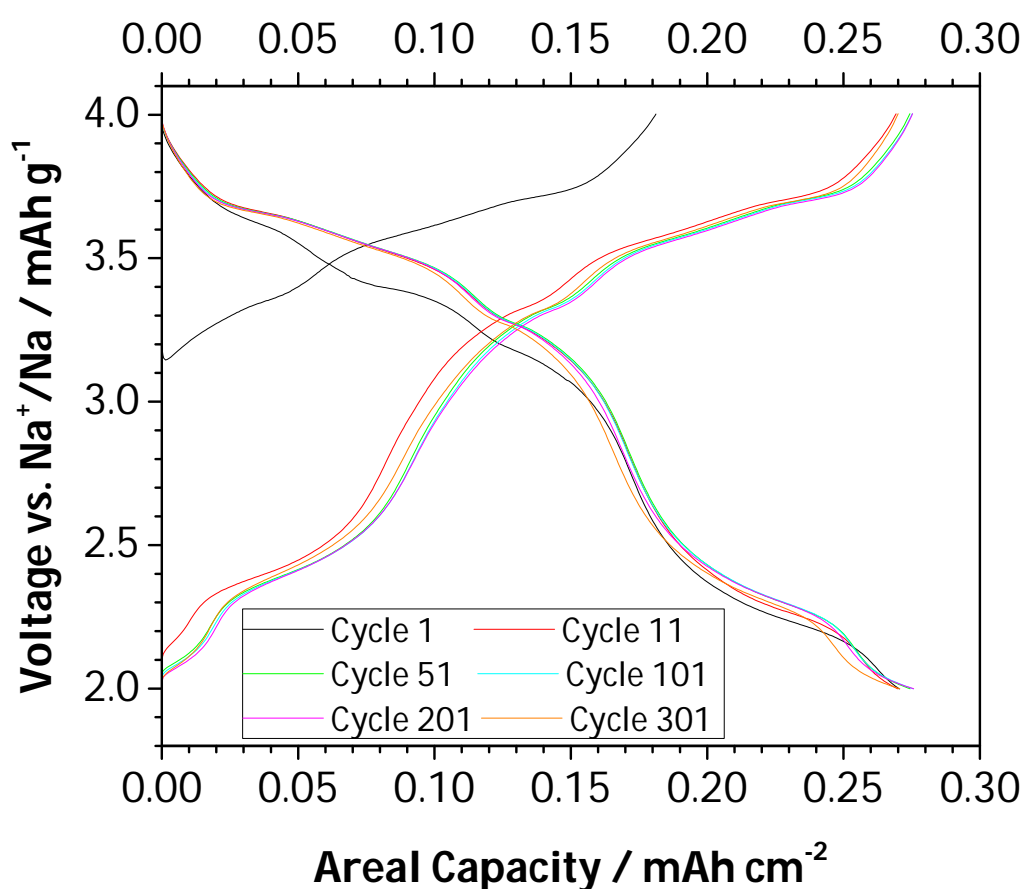


Figure 54: Voltage vs. areal capacity of a metallic sodium/NaNCM two-electrode full cell with 1.0 M NaPF₆/PC as the electrolyte; current: 80 mA g⁻¹.

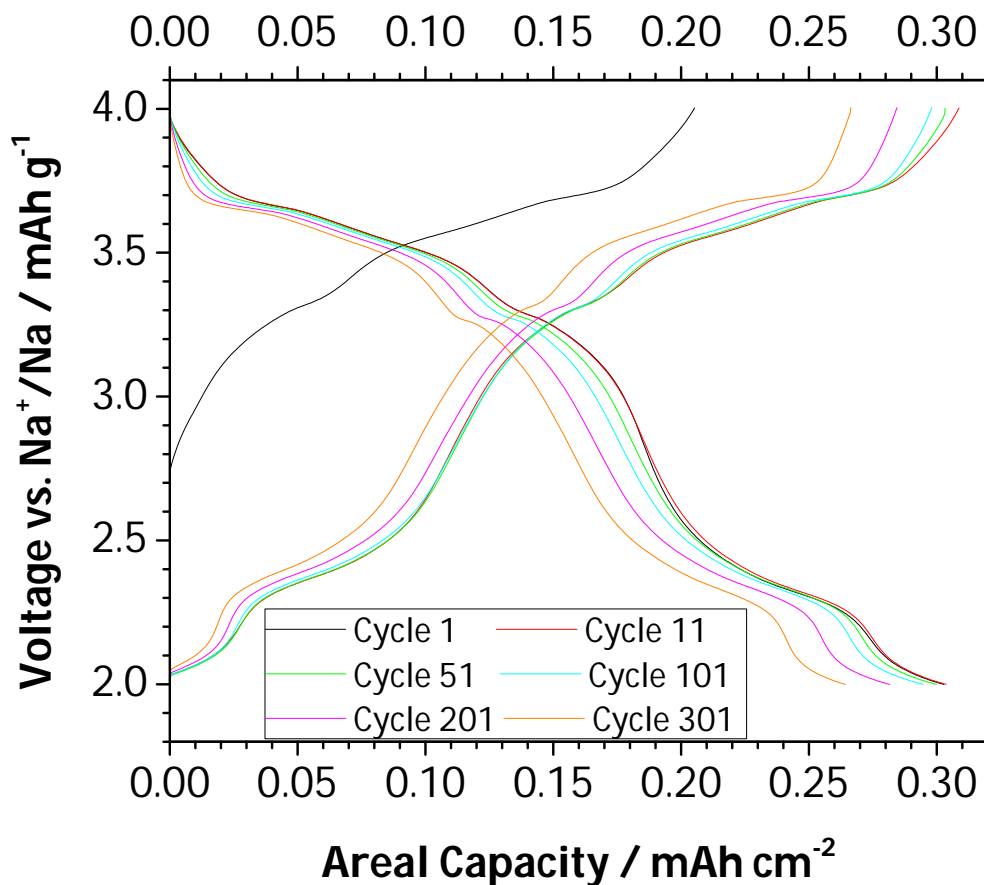


Figure 55: Voltage vs. areal capacity of a metallic sodium/NaNCM two-electrode full cell with 1.0 M NaBF₄/tetraglyme as the electrolyte; current: 80 mA g⁻¹.

4.6.2 NaBF₄/ NaPF₆/tetraglyme

Since it was possible that NaPF₆ was responsible for forming a more stable SEI between the NaNCM cathode and the electrolyte, a new electrolyte was formulated and tested. This electrolyte employed tetraglyme as the solvent but contained NaBF₄ as well as NaPF₆ at a concentration of 0.5 M each. In figure 56, the specific capacities and respective CEs for such a cell are shown. The cell exhibited a completely different behavior than those with the previous two electrolytes. While the initial discharge capacity was the same at about 90 mAh cm⁻², the coulombic efficiency was a lot lower at only about 96% and degraded even further during the first 130 cycles before increasing again as the capacity dropped. This resulted in capacity loss which meant that after 350 cycles only about 30 mAh cm⁻² or about 33% of the initial specific discharge capacity

was left. Since the performance of these cells was worse than that of the cells containing no NaPF_6 , it is safe to assume that NaPF_6 is not solely responsible for the good performance of the NaPF_6/PC electrolyte combination.

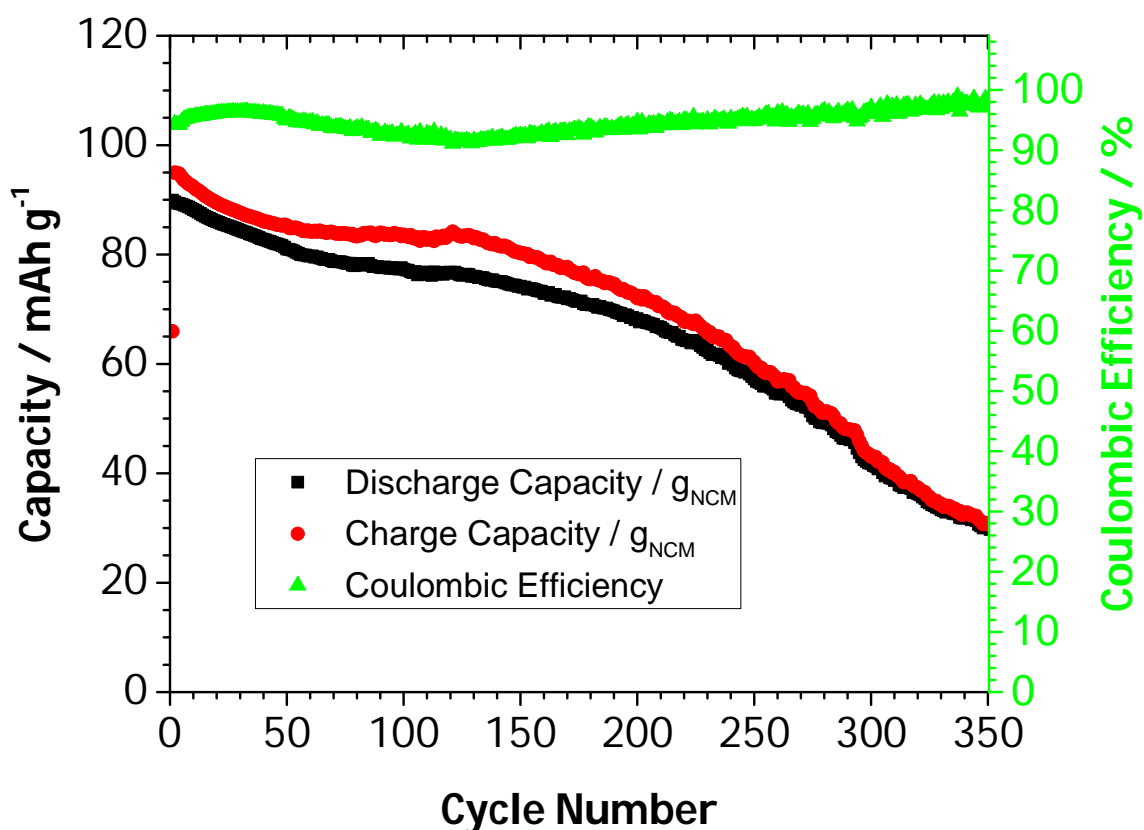


Figure 56: Capacity and coulombic efficiency vs. cycle number for a metallic sodium/ NaNCM two-electrode full cell with $0.5 \text{ M NaBF}_4/0.5 \text{ M NaPF}_6/\text{tetraglyme}$ as the electrolyte; cycled between 2.0 and 4.0 V at 80 mA g^{-1} .

In conclusion, while cells containing $\text{NaBF}_4/\text{tetraglyme}$ as the electrolyte could not be cycled at the same efficiency as those with NaPF_6/PC , they could be cycled for a few hundred cycles without cell failure and exhibited comparable specific capacities. This means that principally, an application of $\text{NaBF}_4/\text{tetraglyme}$ as a Na -metal/ NaNCM battery electrolyte should be possible, even though the cathode would have to be optimized for this system to be viable.

4.7 Alkalimetal/Sulfur Cells

Since a high capacity anode such as sodium metal could only be used to its full potential in conjunction with a high capacity cathode, full cells combining these two electrodes with different electrolytes were tested. Because the RT-Li-S system is well known, the cathodes for the Na-S tests were developed initially for this system and were then tested with sodium metal anodes afterward.

4.7.1 Lithium Sulfur Cells

In the framework of a bachelor's thesis, high-sulfur-load cathodes for Li-S cells were developed in a water-slurry-based process as described in ch. 3.2.6. [61] In this work, we present only the most promising results achieved through this approach. The cathodes that showed the highest specific capacities at sulfur loadings above $4.0 \text{ mg}_S \text{ cm}^{-2}$ contained 60 wt% sulfur as well as 10 wt% *Targray* PSBR 100 binder (dry weight SBR) and 30 wt% of a carbon mixture. This mixture was comprised of equal parts of Porocarb HG3, Porocarb HD3, and Ketjenblack EC-600JD carbons. In figure 57, the produced cathode film is shown. While the cathode had an overall uniform appearance, a network of cracks was present throughout the surface. It was discovered that these cracks had an overall beneficial influence on cathode performance since they allowed for better electrolyte penetration.



Figure 57: Top-down view of a sulfur cathode produced by water-slurry method; network of surface cracks. [61]

Close up examination of the cathodes was performed by SEM. Figures 58 and 59 show a top-down and a cross-section view of a sulfur cathode, respectively. It was observed that the aforementioned cracks were present throughout the cathode and partly penetrated it all the way down to the current collector. Sulfur was distributed evenly throughout the cathode in the form of particles no more than 50 μm in diameter.

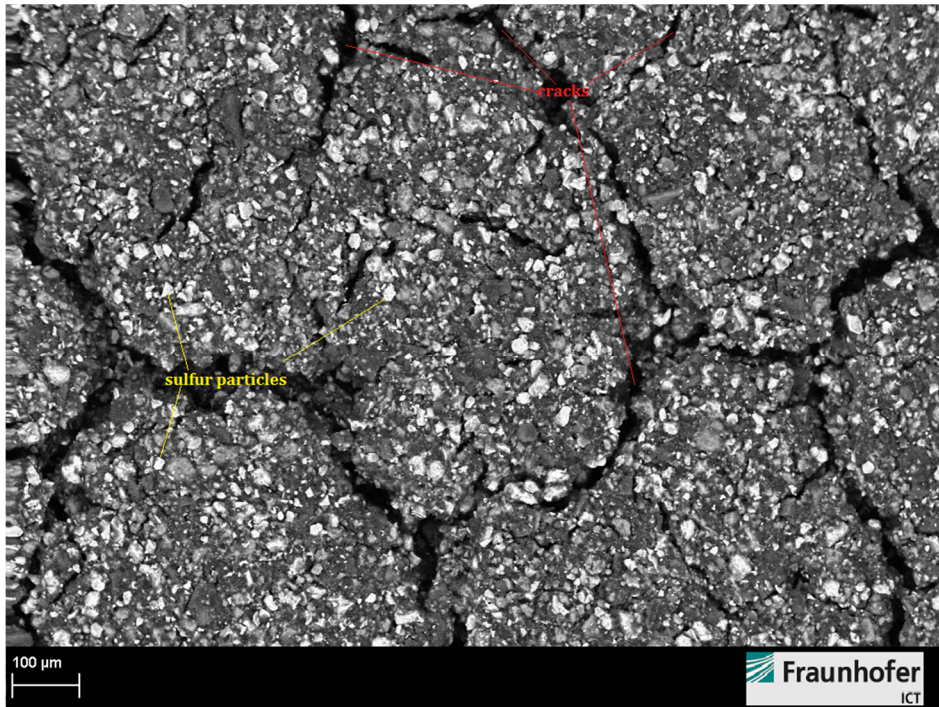


Figure 58: SEM image of the surface of a sulfur cathode produced by water-slurry method. [61]

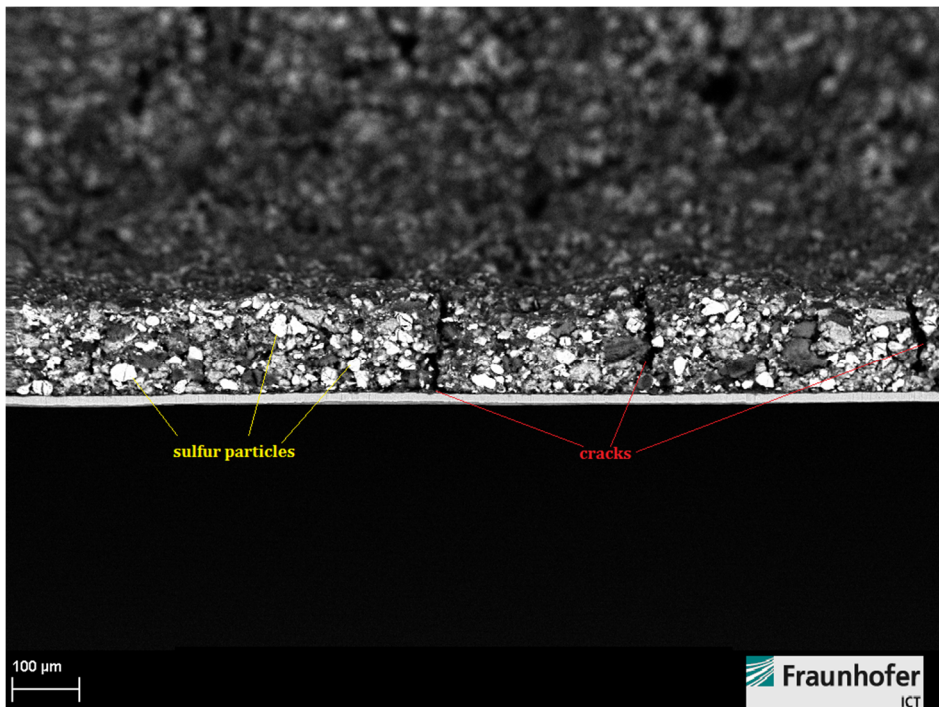


Figure 59: SEM image of a cross-section of a sulfur cathode produced by water-slurry method. [61]

Galvanostatic cycling tests for these cathodes were performed with two-electrode Li-S cells containing a lithium metal anode and an 40 μ l of an electrolyte with the following composition:



The cathodes exhibited maximum specific capacities between 930 and 960 mAh g⁻¹ in the first cycle. In figure 60, a cycling profile for a cell containing such a cathode is shown. During this cycling test, the applied current was increased after 10, 30, and 50 cycles before being reset to the initial current after 70 cycles. This was done to test the response of the cell to high current densities which are favorable for quick charging times and might be necessary for a high energy density system. It was observed that the specific capacity drops significantly after the first few cycles to about 620 mAh g⁻¹ for the lowest current density. It drops even further each time the current is increased, which is to be expected, especially so for a thick cathode with such a high sulfur loading. The minimal discharge capacity recorded in this test was 240 mAh g⁻¹ at a current density of 3.82 mA cm⁻². After the current was decreased again the capacities almost returned to their initial levels before the current increase. However, the coulombic efficiency was significantly reduced. This indicates that while the high current only had a minor impact on the overall available capacity, changes in the cathode took place which resulted in greater overpotentials during charging. Overall, the cathodes performed comparatively well when their high sulfur loads are considered.

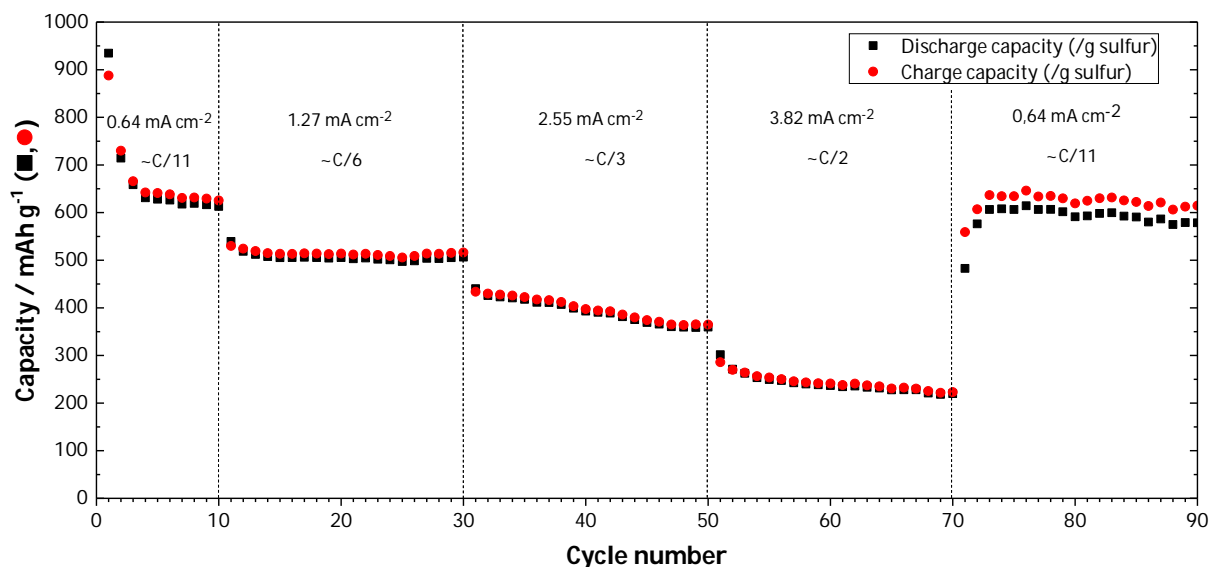


Figure 60: Capacity vs. cycle number for a Li-S two-electrode cell cycled between 1.8 and 2.6 V at various current densities; C-rates are given as fractions of theoretical maximum capacity. [61]

4.7.2 Sodium Sulfur Cells

The sulfur cathodes which had shown the best electrochemical results for the Li-S system were also tested in combination with a sodium metal anode and sodium-ion based electrolytes. For these tests, the voltage range was lowered in order to adjust for the potential difference between lithium and sodium. Furthermore, only one current density was used for each test. Two electrolytes were selected for examination. The electrolyte volume was 85 μl .

1.0 M NaTf/tetraglyme

This electrolyte was selected because it had been shown to perform well in Na-S cells by Ryu et al., enabling specific capacities of more than 500 mAh g⁻¹_{Sulfur}. [44] Furthermore, this electrolyte had shown a high CE and good stability for many cycles during the sodium metal plating and stripping tests. It was decided to apply the same test parameters for these cells as had been reported by Ryu et al., which meant a potential range from 1.2 to 2.3 V and a constant current density of 0.144 mA cm⁻².

Even though the applied current was very weak when compared to the theoretical capacity of the cathode, the cells only exhibited extremely low capacities which corresponded to a sulfur utilization of less than 4%. This indicates that the cathodes were incompatible with sodium ion intercalation, the electrolyte or a combination thereof. There are multiple possible reasons for this incompatibility, one of which is the difference between sodium and lithium ions as well as their respective sulfide species in general. The structure of the cathode may not be optimal for permeation by and storage of sodium polysulfide species. Furthermore, the electrolyte may not be suited to solvating these species which would make access to the lower layers of sulfur in the cathode impossible. However, this last explanation is unlikely, since the electrolyte is reported to be applicable for Na-S cells in literature. It has to be mentioned though, that the cathodes used for these tests had exceptionally high sulfur loads of up to 5.0 mg_Scm⁻². The sulfur loads for the cathodes used in the reference were not specified but were most likely a lot lower than that. In 2014, Hagen et al. reported that for Li-S research, the general trend is to use low areal load cathodes in order to boost sulfur utilization. [28] Thus it is possible that the electrode was simply too thick in this scenario and that a thinner electrode with a smaller sulfur load would result in a much-improved performance. Lastly, the fabrication method for the cathodes has to be taken into account. As the cathodes were cast from a water-based slurry, moisture retention in the cathode structure was almost unavoidable. Since sodium has a higher chemical reactivity with water than lithium, small quantities of moisture in the cathode may impact a Na-S cell much more than a similar Li-S cell. [30]

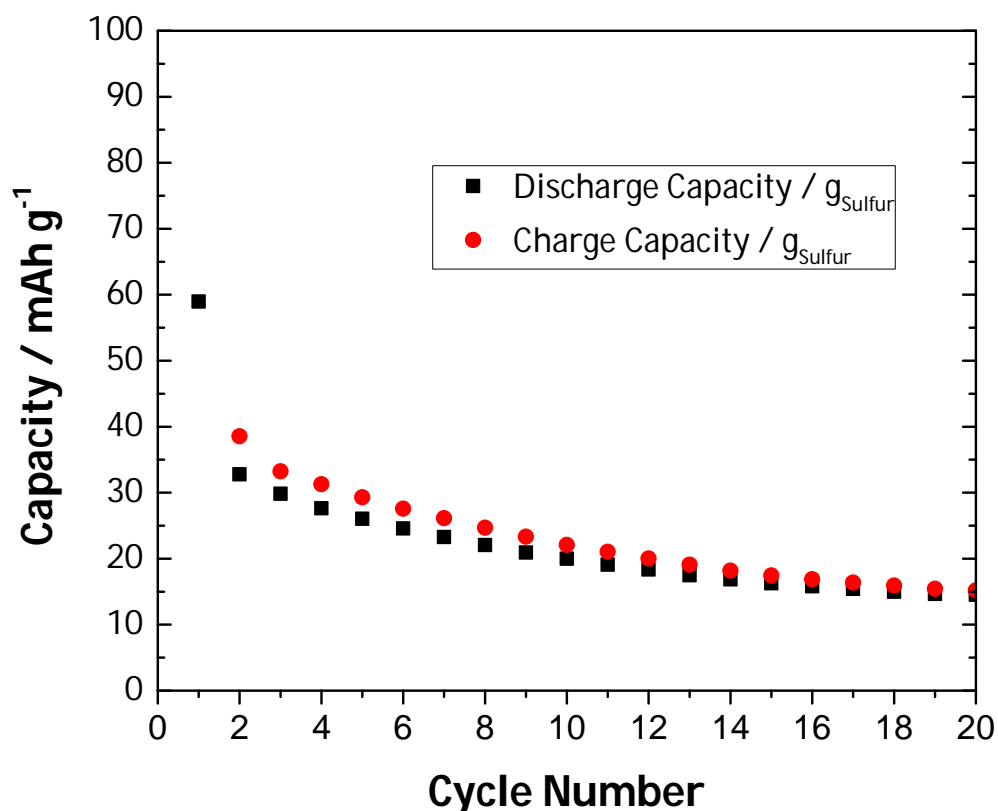


Figure 61: Capacity vs. cycle number for a Na-S two-electrode cell with 1.0 M NaTf/tetraglyme as the electrolyte, cycled between 1.2 and 2.3 V at 0.144 mA cm^{-2} .

In figure 62, the voltage profile for the cell discussed above is shown. It was observed that, while a plateau region was visible during the discharge step of the first cycle at 1.67 V, it only accounted for a low amount of capacity. Furthermore, this plateau disappeared almost completely during the following cycles. While this discharge plateau has been reported in literature, it was a lot shorter than what was previously found for Na-S cells with this electrolyte. [44]

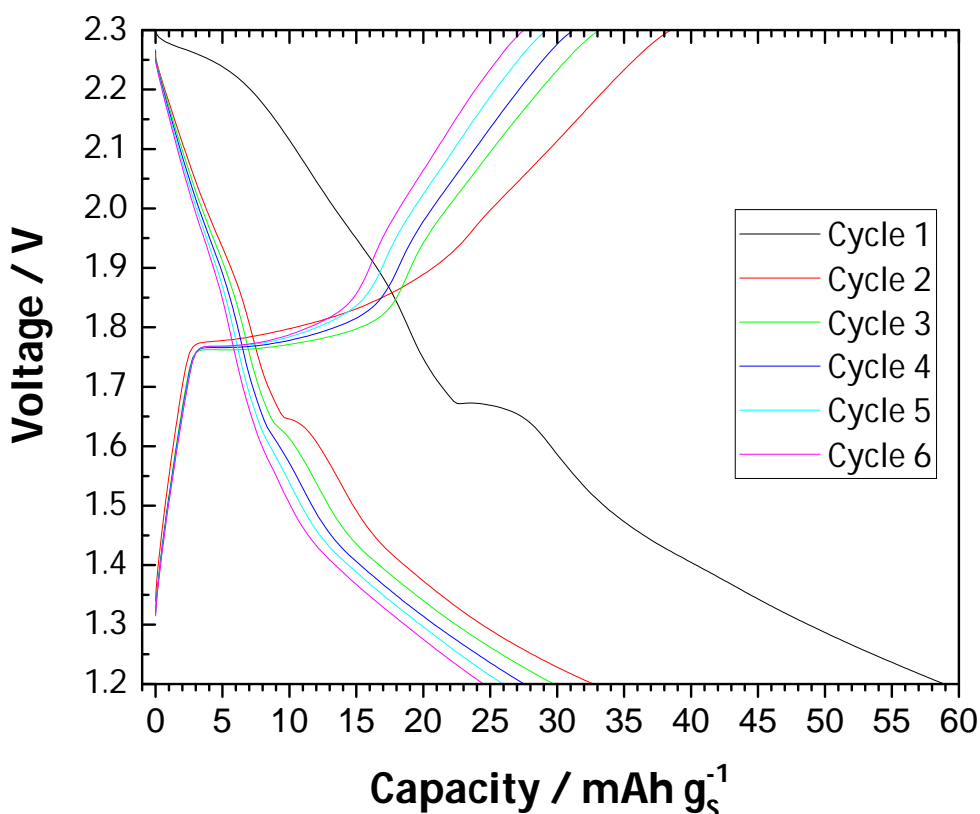


Figure 62: Charge and discharge curves for the first 6 cycles of a Na-S two-electrode cell with 1.0 M NaTf/tetraglyme as the electrolyte, cycled between 1.2 and 2.3 V at 0.144 mA cm⁻².

1.0 M NaBF₄/tetraglyme

As this is the electrolyte that had shown the best performance so far and had been studied the most in this work, it was chosen for testing in Na-S cells. The discharge and charge cutoff potentials were set to 1.2 V and 2.3 V, respectively. While these cells performed better than those with 1.0 M NaTf/tetraglyme, the obtained capacities were still very low. The highest capacity reached was 383 mAh g⁻¹ during the first cycle for a cell cycled at a low current density of 0.144 mA cm⁻². Unfortunately, the cell exhibited a short circuit during the charge step of the first cycle and failed. The discharge curve of the first cycle of this cell is shown in comparison to the voltage profile of a theoretical, ideal Li-S cell in figure 63. While the overall shape with two plateau regions and a sloping region in between is similar, the size of the respective regions differs

significantly. This is especially true for the second plateau region at 1.67 V, which is much shorter in relation to the rest of the curve than in the Li-S system.

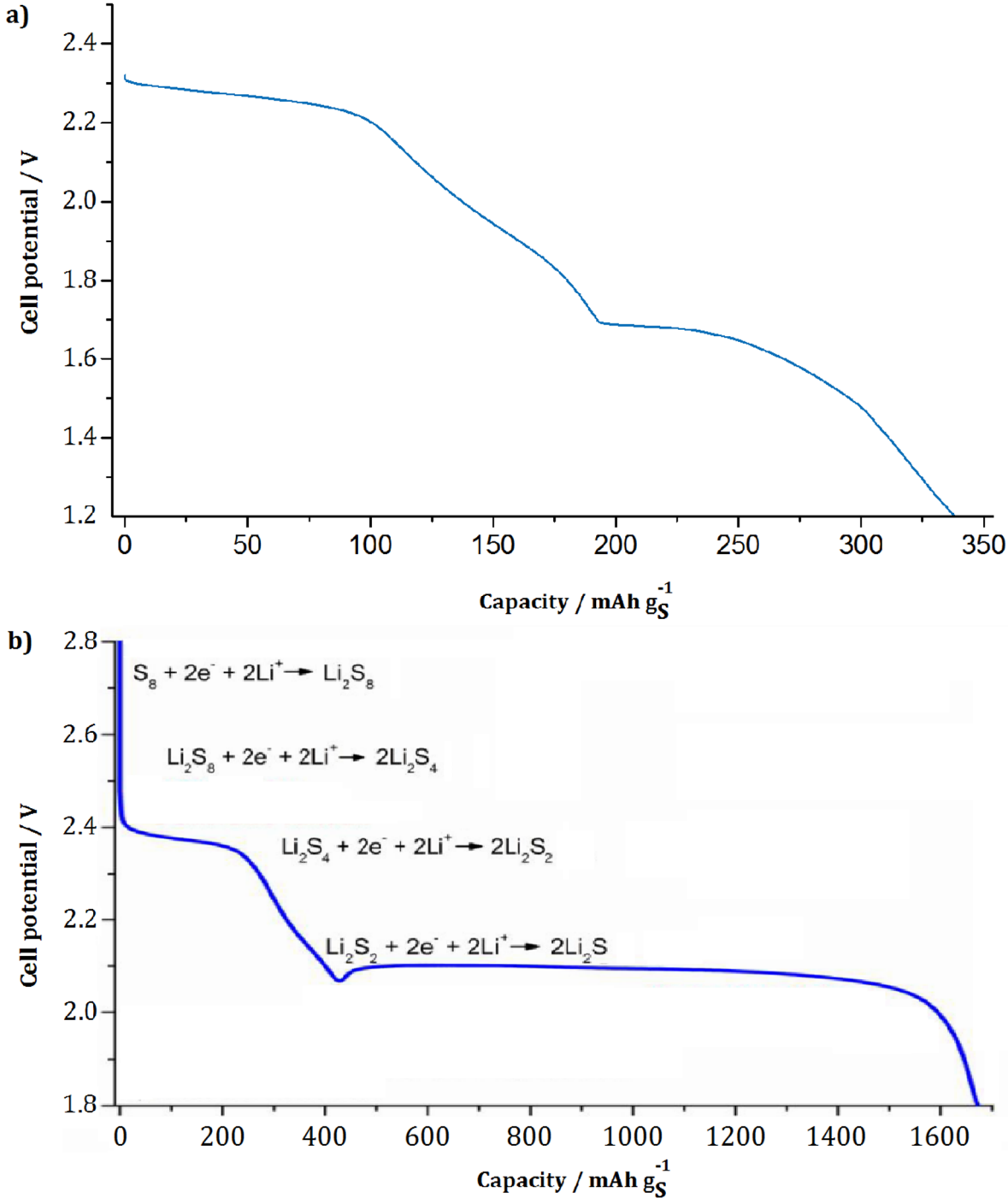


Figure 63: Cell potential vs. capacity for a) the first discharge step of a Na-S two-electrode cell cycled between 1.2 and 2.3 V at 0.144 mA cm^{-2} and b) a theoretical, ideal Li-S cell with reaction mechanisms, reproduced and modified from Affinito et al. [78]

Adelhelm et al. have proposed a series of reactions with corresponding theoretical cell potentials for an ideal discharge process of the Na-S system: [30]



The plateau at 2.2 V – 2.3 V observed in the test cells does not correspond to any of these steps which means that a different reaction must have taken place. Since Na_2S_5 is a thermodynamically stable compound, the formation of Na_2S_5 and a subsequent conversion to Na_2S_4 would be a possible explanation: [79]



However, while similar concepts have been proposed before, these reactions have not been proven to be correct so far. [80] The relative shortness of the plateau region observed at 1.67 V indicates that the conversion from Na_2S_2 to Na_2S might be incomplete in the test cells. These are the least soluble compounds in organic solvents, which means that the reaction described in equation 6 probably takes place as a solid state conversion. Thus, cathode structure and thickness might seriously impede this already disadvantaged process. Incidentally, full conversion to Li_2S is also one of the greatest challenges of Li-S cells due to the low conductivity of Li_2S . [30]

For this electrolyte, tests at a higher current density of 0.5 mA cm^{-2} were also performed. This would correspond to a charge and discharge rate of about 1/17 of the theoretical maximum capacity of the cathode per hour (C/17). With an achieved maximum specific capacity of 219 mAh g^{-1} in the first cycle, the cells had less initial capacity than those which ran at a lower current. However, the cells could at least be cycled for a few cycles without failure. While this result was significantly better than what was observed in the other Na-S tests in this work, it still corresponded only to a sulfur utilization of about

13%. Furthermore, the capacity diminished rapidly after the first cycle and dropped below 10 mAh g^{-1} within 10 cycles.

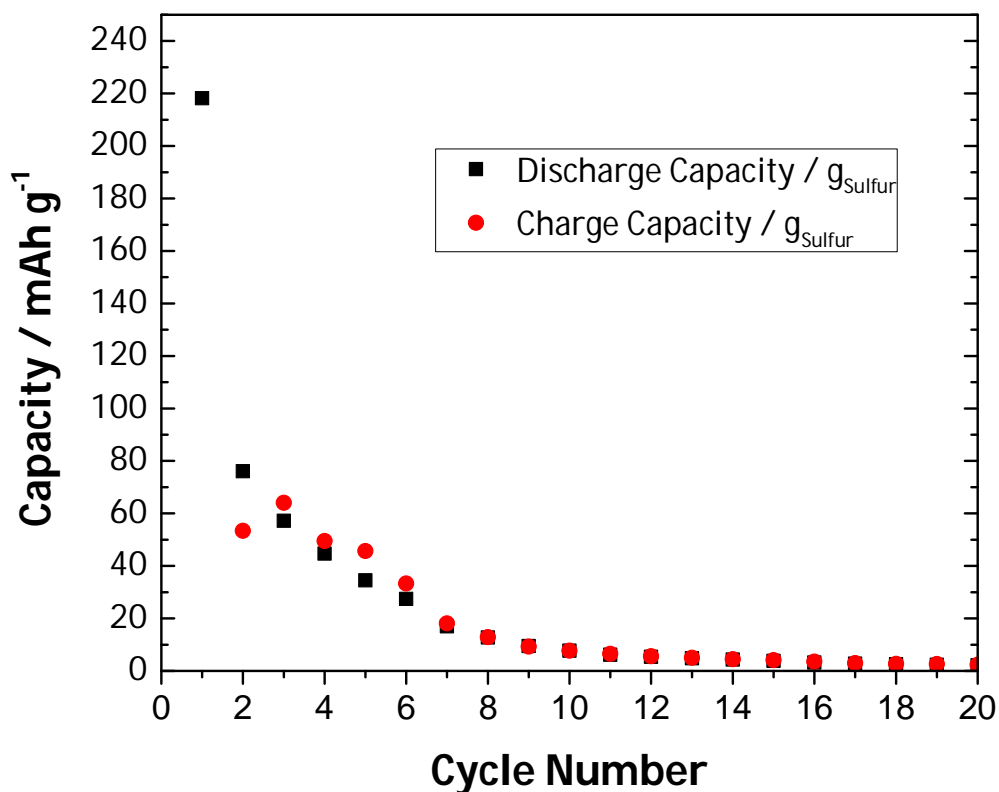


Figure 64: Capacity vs. cycle number of a Na-S two-electrode cell with $1.0 \text{ M NaBF}_4/\text{tetraglyme}$ as the electrolyte, cycled between 1.2 and 2.3 V at 0.5 mA cm^{-2} .

In figure 65, the first-cycle discharge curves for two of the Na-S cells cycled at different currents are shown. The shape of the two curves differed significantly in that the 0.5 mA cm^{-2} curve only had one plateau region compared to the two plateau regions observed for the lower current cell. However, this single plateau region at $2.2 \text{ V} - 2.3 \text{ V}$ was longer in the high-current cell. The absence of the second plateau at 1.67 V suggests that the conversion from Na_2S_2 to Na_2S , which is responsible for a major part of the theoretical capacity of the system, does not actually occur in this cell. This is possibly due to the higher current and the high thickness of the cathode preventing the solid state conversion process.

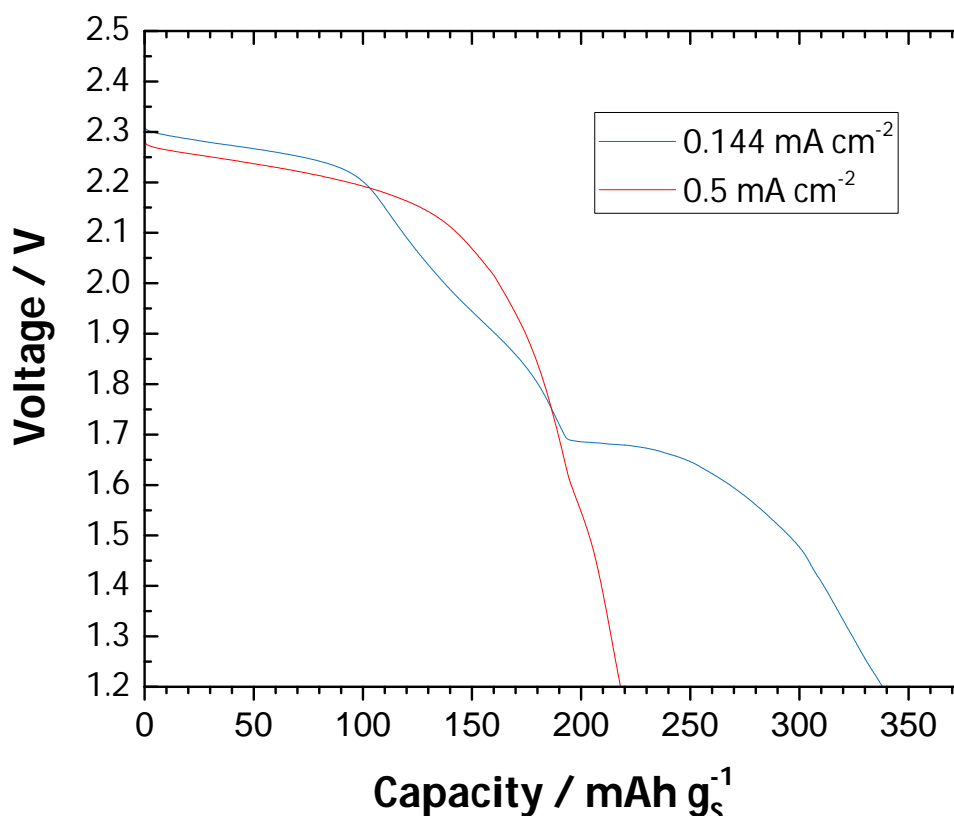


Figure 65: First-cycle discharge curves of two Na-S two-electrode cells with 1.0M NaBF₄/tetraglyme as the electrolyte, cycled in the potential range of 1.2-2.3 V at 0.144 mA cm⁻² and 0.5 mA cm⁻², respectively.

In conclusion, while it was possible to create high-sulfur-load, high-sulfur-content cathodes that performed well in Li-S cells, a combination of these cathodes with Na metal and different electrolytes failed to give comparable results. Na-S cells could be cycled a few times but exhibited low capacities and high degradation. This was most probably due to the comparatively high thickness of the cathodes as well as residual moisture from the water-slurry preparation method. Another possible factor is the high electrolyte content of the cells studied in this work, which would lead to irreversible capacity loss through dissolution of active material. For future research, the author proposes testing cells with thinner cathodes produced by a dry process.

5 Conclusion and Outlook

This thesis dealt with the study of liquid electrolytes for sodium metal anodes. The main focus was examining the plating and stripping behavior of Na metal out of a wide variety of electrolyte formulations as well as their characterization. A few of these electrolytes were chosen for a more in-depth evaluation. A second focus was put on evaluating if the most promising electrolytes identified in this study were suitable for building Na metal/cathode full cells and how they compared to electrolytes more commonly used in for cathode tests.

For the first part of the work, suitable solvents and conducting salts were selected and combined to form electrolytes. These formulations were implemented in test cells where the coulombic efficiency for sodium metal deposition and subsequent stripping could be determined via galvanostatic cycling. During these tests, it was found that in general, the best performing electrolytes were ether-based while carbonate-based electrolytes had rather low CEs. However, it was possible to improve carbonate-based electrolyte performance by adding FEC. The electrolyte with the highest CE (>99.9%) over hundreds of cycles was 1.0 M NaBF₄/tetraglyme. It was also found that this solvent/conductive salt combination exhibited very low plating and stripping potentials, which indicated the formation of a stable and thin SEI. Thus, a lot of focus was put on the study of this particular formulation for the rest of the work. Another electrolyte that performed exceptionally well was 1.0 NaTf/tetraglyme. Electrolytes that are often used in Na-ion cells in literature (e.g., 1.0 M NaPF₆/PC, 1.0 M NaClO₄/EC/DEC) exhibited comparatively low CEs and high polarization during galvanostatic cycling.

For two of the electrolytes (1.0 M NaBF₄/tetraglyme, 1.0 M NaPF₆/PC), the coulombic efficiency for plating and stripping directly onto and off of already present sodium metal was tested via an additional galvanostatic cycling procedure. The results mirrored those observed for the same processes on stainless steel.

A few electrolytes were chosen for determination of their suitable voltage range via cyclic voltammetry. It was found that while most formulations were stable in the tested voltage range of 0.01 V to 4.5 V, mixtures containing NaFSI showed high oxidation and reduction currents. NaTf containing electrolytes also exhibited elevated oxidation

currents above 4.0 V but the effects were less severe than for NaFSI. The differences between the CVs of the rest of the tested electrolytes were minor except for potentials below 1.0 V where SEI formation was occurring. Here, 1.0 M NaBF₄/tetraglyme showed exceptionally low currents and little change in the shape of the CV between cycles whereas PC based electrolytes had more pronounced SEI-formation peaks which diminished with each cycle. This, once again, was indicative of the formation of a thin and stable SEI in 1.0 M NaBF₄/tetraglyme. The addition of FEC to 1.0 M NaPF₆/PC resulted in a broad reductive peak during the first cycle but otherwise did not change the shape of the CV significantly. This indicates that FEC influences and boosts SEI formation at the beginning of cycling, which explains the improved CEs of FEC-containing carbonate-based electrolytes observed during galvanostatic cycling.

For the same selection of electrolytes, ionic conductivities were determined via EIS. In general, tetraglyme-based electrolytes exhibited lower conductivities than their PC-based counterparts. It was noted that the formulations that had shown the highest sodium plating and stripping efficiencies also had the lowest conductivities. While it is possible that a low conductivity might lead to a more evenly distributed current density and thus less dendrite formation during electrodeposition, more testing would need to be done in order to confirm a correlation. In any case, it is important to note that low electrolyte conductivity is disadvantageous for battery cell application for a number of reasons (e.g., power density).

In order to examine the surface morphology of deposited sodium metal, samples from cells with 3 different electrolytes (1.0 M NaClO₄/EC/DEC, 1.0 M NaPF₆/PC, 1.0 M NaBF₄/tetraglyme) were studied via SEM. While the carbonate-based deposits showed dendritic growth in various degrees and forms, the tetraglyme electrolyte created an extremely smooth surface. Similar results were found for sodium metal on the counter electrode where stripping had last taken place and dendrites were found on the PC sample. For electrodeposition on copper foil, the findings mirrored those of stainless steel substrates.

Since cells with 1.0 M NaBF₄/tetraglyme had shown the most promising results during CE tests and SEM deposit examination, it was attempted to study the SEI that this electrolyte forms during sodium metal electrodeposition. A potential scan from OCV to 0.1 V was performed with such a cell in order to induce SEI formation on a stainless steel

substrate. XPS spectra of the sample surface were taken while sputtering was employed to create a depth profile. It was observed that the SEI was comparatively thin and was made of organic compounds such as sodium alkoxides and inorganic compounds such as Na_2O and NaF . These inorganic compounds were more prevalent in the lower SEI layers while the surface was mostly made of organics. Studies of such interphases in lithium systems in the past have shown that this configuration is typical of a stable SEI. [71,75]

As a proof of concept, Na metal/NaNCM full cells were built with 1.0 M NaBF_4 /tetraglyme as the electrolyte. When compared to similar cells with a more commonly used formulation such as 1.0 M NaPF_6 /PC, they exhibited comparable specific capacities but worse CEs. Nevertheless, they could be cycled stably for more than 350 cycles while only losing about 17% cathode capacity. While this is not an optimal result, it indicates that a NaNCM cell with a comparatively stable sodium anode might be possible if the cathode were to be modified for better compatibility with the electrolyte. Furthermore, it was proven that NaPF_6 was not solely responsible for the high CE observed in cells with the PC electrolyte. This was done by adding the salt to NaBF_4 /tetraglyme and building comparable cells which performed more poorly than those with the other two formulations.

In order to maximize the potential of a sodium metal anode, sulfur cathodes were developed and implemented in Na-S cells. While Li-S cells with the same cathodes produced promising results, the same was not true for Na-S tests. While two different electrolytes were employed (1.0 M NaTf /tetraglyme and 1.0 M NaBF_4 /tetraglyme), none of the cells reached a specific discharge capacity above 383 mAh g^{-1} or about 23% sulfur utilization. Furthermore, the capacity faded significantly during the first cycles and cells failed frequently. A study of the voltage profiles of these cells suggested that most of the capacity was lost because of incomplete transition from sodium polysulfides to Na_2S . While there is a wide range of different possible causes for the observed poor performance, it is probable that the main reasons were extremely high sulfur load and residual moisture of the cathodes, which stemmed from the production process. In future studies, it could be beneficial to do tests with low-load cathodes created by a dry process.

In summary, while it was possible to find extremely high-CE electrolytes for sodium electrodeposition with a stable SEI, full cell tests with different cathodes showed

suboptimal results. In order to create viable liquid electrolyte room temperature full cells with Na metal anodes, it would be necessary to either create cathodes more suitable for the identified electrolytes or to further modify the electrolyte composition. Another angle of approach could be the implementation of an artificial SEI on the anode, for example in the form of a thin ion-conductive polymer layer that prevents direct contact between electrolyte and sodium metal.

Bibliography

- [1] C. Glaize, S. Genies, *Lithium batteries and other electrochemical storage systems*, ISTE, London (2013)
- [2] K. Xu, *Nonaqueous Liquid Electrolytes for Lithium-Based Rechargeable Batteries*, Chem. Rev. 104 (2004) 4303–4418
- [3] B. Scrosati, K.M. Abraham, W.A. van Schalkwijk, J. Hassoun (Eds.), *Lithium batteries: Advanced technologies and applications*, Wiley, Hoboken, NJ (2013)
- [4] J.M. Tarascon, M. Armand, *Issues and challenges facing rechargeable lithium batteries*, Nature 414 (2001) 359–367
- [5] C.H. Hamann, W. Vielstich, *Elektrochemie*, 4., vollständig überarbeitete und aktualisierte Auflage, Wiley-VCH-Verlag GmbH & Co. KGaA, Weinheim (2005)
- [6] D.H. Doughty, E.P. Roth, *A General Discussion of Li Ion Battery Safety*, Interface magazine 21 (2012) 37–44
- [7] X. Yuan, H. Liu, J. Zhang (Eds.), *Lithium-ion batteries: Advanced materials and technologies*, CRC Press, Boca Raton, Fla. (2012)
- [8] H.H. Binder, *Lexikon der chemischen Elemente: Das Periodensystem in Fakten, Zahlen und Daten ; mit vielen tabellarischen Zusammenstellungen*, Hirzel, Stuttgart u.a. (1999)
- [9] C. Wadia, P. Albertus, V. Srinivasan, *Resource constraints on the battery energy storage potential for grid and transportation applications*, Journal of Power Sources 196 (2011) 1593–1598
- [10] J. Sangster, *C-Na (Carbon-Sodium) System*, J Phs Eqil and Diff 28 (2007) 571–579
- [11] V. Palomares, P. Serras, I. Villaluenga, K.B. Hueso, J. Carretero-Gonzalez, T. Rojo, *Na-ion batteries, recent advances and present challenges to become low cost energy storage systems*, Energy Environ. Sci. 5 (2012) 5884
- [12] V. Simone, A. Boulineau, A. de Geyer, D. Rouchon, L. Simonin, S. Martinet, *Hard carbon derived from cellulose as anode for sodium ion batteries*, Journal of Energy Chemistry 25 (2016) 761–768
- [13] Q. Hu, A. Caputo, D.R. Sadoway, *Rechargeable lithium battery for wide temperature operation*, 2013
- [14] J. Hassoun, B. Scrosati, *A high-performance polymer tin sulfur lithium ion battery*, Angewandte Chemie (International ed. in English) 49 (2010) 2371–2374

- [15] Y. Yang, M.T. McDowell, A. Jackson, J.J. Cha, S.S. Hong, Y. Cui, *New nanostructured Li₂S/silicon rechargeable battery with high specific energy*, *Nano letters* 10 (2010) 1486–1491
- [16] S.M. Market, *Lithium Carbonate News and Price Analysis - Shanghai Metals Market*, <http://original.metal.com/metals/productinfo/201102250059>, accessed 30 October 2017
- [17] *Sodium Carbonate, Sodium Carbonate Suppliers and Manufacturers at Alibaba.com*, <https://www.alibaba.com/showroom/sodium-carbonate.html>, accessed 30 October 2017
- [18] H. Okamoto, *Alloy phase diagrams* (2016)
- [19] A. Mauger, H. Xie, C. M. Julien, *Composite anodes for lithium-ion batteries*, *AIMS Materials Science* 3 (2016) 1054–1106
- [20] J.-I. Yamaki, S.-I. Tobishima, in: J.O. Besenhard (Ed.), *Handbook of Battery Materials*, Wiley-VCH Verlag GmbH, Weinheim, Germany, 2010, 339–357
- [21] J. Steiger, D. Kramer, R. Mönig, *Microscopic observations of the formation, growth and shrinkage of lithium moss during electrodeposition and dissolution*, *Electrochimica Acta* 136 (2014) 529–536
- [22] N. Yabuuchi, M. Kajiyama, J. Iwatate, H. Nishikawa, S. Hitomi, R. Okuyama, R. Usui, Y. Yamada, S. Komaba, *P2-type Na_xFe_{1/2}Mn_{1/2}O₂ made from earth-abundant elements for rechargeable Na batteries*, *Nature materials* 11 (2012) 512–517
- [23] D. Kim, E. Lee, M. Slater, W. Lu, S. Rood, C.S. Johnson, *Layered Na[Ni_{1/3}Fe_{1/3}Mn_{1/3}]O₂ cathodes for Na-ion battery application*, *Electrochemistry Communications* 18 (2012) 66–69
- [24] M. Sathiya, K. Hemalatha, K. Ramesha, J.-M. Tarascon, A.S. Prakash, *Synthesis, Structure, and Electrochemical Properties of the Layered Sodium Insertion Cathode Material*, *Chem. Mater.* 24 (2012) 1846–1853
- [25] D. Kim, S.-H. Kang, M. Slater, S. Rood, J.T. Vaughey, N. Karan, M. Balasubramanian, C.S. Johnson, *Enabling Sodium Batteries Using Lithium-Substituted Sodium Layered Transition Metal Oxide Cathodes*, *Adv. Energy Mater.* 1 (2011) 333–336
- [26] D. Buchholz, L.G. Chagas, M. Winter, S. Passerini, *P2-type layered Na_{0.45}Ni_{0.22}Co_{0.11}Mn_{0.66}O₂ as intercalation host material for lithium and sodium batteries*, *Electrochimica Acta* 110 (2013) 208–213
- [27] D. Buchholz, A. Moretti, R. Kloepsch, S. Nowak, V. Siozios, M. Winter, S. Passerini, *Toward Na-ion Batteries*, *Chem. Mater.* 25 (2013) 142–148

- [28] M. Hagen, P. Fanz, J. Tübke, *Cell energy density and electrolyte/sulfur ratio in Li-S cells*, Journal of Power Sources 264 (2014) 30–34
- [29] U.S. Geological Survey, *Mineral Commodity Summaries* (2013)
- [30] P. Adelhelm, P. Hartmann, C.L. Bender, M. Busche, C. Eufinger, J. Janek, *From lithium to sodium: cell chemistry of room temperature sodium-air and sodium-sulfur batteries*, Beilstein journal of nanotechnology 6 (2015) 1016–1055
- [31] X. Ji, K.T. Lee, L.F. Nazar, *A highly ordered nanostructured carbon-sulphur cathode for lithium-sulphur batteries*, Nature materials 8 (2009) 500–506
- [32] S.-E. Cheon, S.-S. Choi, J.-S. Han, Y.-S. Choi, B.-H. Jung, H.S. Lim, *Capacity Fading Mechanisms on Cycling a High-Capacity Secondary Sulfur Cathode*, J. Electrochem. Soc. 151 (2004) A2067
- [33] F. Wu, S.X. Wu, R.J. Chen, S. Chen, G.Q. Wang, *Electrochemical performance of sulfur composite cathode materials for rechargeable lithium batteries*, Chinese Chemical Letters 20 (2009) 1255–1258
- [34] S.S. Zhang, *Liquid electrolyte lithium/sulfur battery*, Journal of Power Sources 231 (2013) 153–162
- [35] N.-I. Kim, C.-B. Lee, J.-M. Seo, W.-J. Lee, Y.-B. Roh, *Correlation between positive-electrode morphology and sulfur utilization in lithium-sulfur battery*, Journal of Power Sources 132 (2004) 209–212
- [36] Y.-J. Choi, K.-W. Kim, H.-J. Ahn, J.-H. Ahn, *Improvement of cycle property of sulfur electrode for lithium/sulfur battery*, Journal of Alloys and Compounds 449 (2008) 313–316
- [37] Y. Jung, S. Kim, *New approaches to improve cycle life characteristics of lithium-sulfur cells*, Electrochemistry Communications 9 (2007) 249–254
- [38] X.-B. Cheng, J.-Q. Huang, H.-J. Peng, J.-Q. Nie, X.-Y. Liu, Q. Zhang, F. Wei, *Polysulfide shuttle control*, Journal of Power Sources 253 (2014) 263–268
- [39] M.-K. Song, Y. Zhang, E.J. Cairns, *A long-life, high-rate lithium/sulfur cell: a multifaceted approach to enhancing cell performance*, Nano letters 13 (2013) 5891–5899
- [40] Z. Wei Seh, W. Li, J.J. Cha, G. Zheng, Y. Yang, M.T. McDowell, P.-C. Hsu, Y. Cui, *Sulphur-TiO₂ yolk-shell nanoarchitecture with internal void space for long-cycle lithium-sulphur batteries*, Nature communications 4 (2013) 1331
- [41] M. Hagen, S. Dörfler, P. Fanz, T. Berger, R. Speck, J. Tübke, H. Althues, M.J. Hoffmann, C. Scherr, S. Kaskel, *Development and costs calculation of lithium-sulfur*

- cells with high sulfur load and binder free electrodes*, Journal of Power Sources 224 (2013) 260–268
- [42] J. Wang, J. Yang, Y. Nuli, R. Holze, *Room temperature Na/S batteries with sulfur composite cathode materials*, Electrochemistry Communications 9 (2007) 31–34
- [43] S. Xin, Y.-X. Yin, Y.-G. Guo, L.-J. Wan, *A high-energy room-temperature sodium-sulfur battery*, Advanced materials (Deerfield Beach, Fla.) 26 (2014) 1261–1265
- [44] H. Ryu, T. Kim, K. Kim, J.-H. Ahn, T. Nam, G. Wang, H.-J. Ahn, *Discharge reaction mechanism of room-temperature sodium–sulfur battery with tetra ethylene glycol dimethyl ether liquid electrolyte*, Journal of Power Sources 196 (2011) 5186–5190
- [45] I. Bauer, M. Kohl, H. Althues, S. Kaskel, *Shuttle suppression in room temperature sodium-sulfur batteries using ion selective polymer membranes*, Chemical communications (Cambridge, England) 50 (2014) 3208–3210
- [46] S. Wenzel, H. Metelmann, C. Reiß, A.K. Dürr, J. Janek, P. Adelhelm, *Thermodynamics and cell chemistry of room temperature sodium/sulfur cells with liquid and liquid/solid electrolyte*, Journal of Power Sources 243 (2013) 758–765
- [47] K. Xu, *Electrolytes and interphases in Li-ion batteries and beyond*, Chemical reviews 114 (2014) 11503–11618
- [48] A. Ponrouch, E. Marchante, M. Courty, J.-M. Tarascon, M.R. Palacín, *In search of an optimized electrolyte for Na-ion batteries*, Energy Environ. Sci. 5 (2012) 8572
- [49] A. Ponrouch, D. Monti, A. Boschini, B. Steen, P. Johansson, M.R. Palacín, *Non-aqueous electrolytes for sodium-ion batteries*, J. Mater. Chem. A 3 (2015) 22–42
- [50] J. Barthel, H.J. Gores, in: J.O. Besenhard (Ed.), *Handbook of battery materials*, Wiley-VCH, Weinheim, New York, 2010, 457–497
- [51] M. Hagen, G. Feisthammel, P. Fanz, H.T. Grossmann, S. Dorfler, J. Tubke, M.J. Hoffmann, D. Borner, M. Joos, H. Althues, S. Kaskel, *Sulfur Cathodes with Carbon Current Collector for Li-S cells*, Journal of the Electrochemical Society 160 (2013) A996-A1002
- [52] W. Wang, G.-c. Li, Q. Wang, G.-r. Li, S.-h. Ye, X.-p. Gao, *Sulfur-Polypyrrole/Graphene Multi-Composites as Cathode for Lithium-Sulfur Battery*, Journal of the Electrochemical Society 160 (2013) A805-A810
- [53] Y. Diao, K. Xie, S. Xiong, X. Hong, *Analysis of Polysulfide Dissolved in Electrolyte in Discharge-Charge Process of Li-S Battery*, J. Electrochem. Soc. 159 (2012) A421

- [54] K. Fridman, R. Sharabi, R. Elazari, G. Gershinsky, E. Markevich, G. Salitra, D. Aurbach, A. Garsuch, J. Lampert, *A new advanced lithium ion battery*, *Electrochemistry Communications* 33 (2013) 31–34
- [55] H. Nakai, T. Kubota, A. Kita, A. Kawashima, *Investigation of the Solid Electrolyte Interphase Formed by Fluoroethylene Carbonate on Si Electrodes*, *J. Electrochem. Soc.* 158 (2011) A798
- [56] K.H. Seng, L. Li, D.-P. Chen, Z.X. Chen, X.-L. Wang, H.K. Liu, Z.P. Guo, *The effects of FEC (fluoroethylene carbonate) electrolyte additive on the lithium storage properties of NiO (nickel oxide) nanocuboids*, *Energy* 58 (2013) 707–713
- [57] S. Komaba, T. Ishikawa, N. Yabuuchi, W. Murata, A. Ito, Y. Ohsawa, *Fluorinated ethylene carbonate as electrolyte additive for rechargeable Na batteries*, *ACS applied materials & interfaces* 3 (2011) 4165–4168
- [58] *Grade GF/A Fine Retention Filter | GE Healthcare Life Sciences*, http://www.gelifesciences.com/webapp/wcs/stores/servlet/catalog/en/GELifeSciences/products/AlternativeProductStructure_16176/28418308, accessed 15 October 2017
- [59] *Innovative Battery Separator Technology | Celgard*, <https://www.celgard.com/battery-innovation/>, accessed 15 October 2017
- [60] *Cellulose Separators | NIPPON KODOSHI CORPORATION*, http://www.kodoshi.co.jp/english/product/battery_separators.html, accessed 15 October 2017
- [61] O. Witzgall, *Herstellung und Optimierung von wässrigen Lithium-Schwefelkathoden für Hochenergiebatterien* (2016)
- [62] *Anode Binders for Li-ion Batteries: PVDF and SBR Materials | Targray*, <https://www.targray.com/li-ion-battery/anode-materials/binders>, accessed 15 October 2017
- [63] *Superconductive Carbon Blacks | AkzoNobel*, <https://polymerchemistry.akzonobel.com/products/polymer-additives/conductive-blacks/>, accessed 15 October 2017
- [64] *Porocarb Carbons | Heraeus*, https://www.heraeus.com/en/hpt/products_solutions_renewables/porocarb/home_porocarb/porocarb-home.aspx, accessed 15 October 2017

- [65] Fluorosurfactant FC-4430 | 3M, https://www.3m.com/3M/en_US/company-us/all-3m-products/~/3M-Fluorosurfactant-FC-4430?N=5002385+3292678640&rt=rud, accessed 21 October 2017
- [66] D. Aurbach, *The Correlation Between Surface Chemistry, Surface Morphology, and Cycling Efficiency of Lithium Electrodes in a Few Polar Aprotic Systems*, J. Electrochem. Soc. 136 (1989) 3198
- [67] J. Xia, J.R. Dahn, *Improving sulfolane-based electrolyte for high voltage Li-ion cells with electrolyte additives*, Journal of Power Sources 324 (2016) 704–711
- [68] S.S. Zhang, *A review on electrolyte additives for lithium-ion batteries*, Journal of Power Sources 162 (2006) 1379–1394
- [69] L.G. Chagas, D. Buchholz, C. Vaalma, L. Wu, S. Passerini, *P-type $\text{Na}_x\text{Ni}_{0.22}\text{Co}_{0.11}\text{Mn}_{0.66}\text{O}_2$ materials*, J. Mater. Chem. A 2 (2014) 20263–20270
- [70] S. Komaba, W. Murata, T. Ishikawa, N. Yabuuchi, T. Ozeki, T. Nakayama, A. Ogata, K. Gotoh, K. Fujiwara, *Electrochemical Na Insertion and Solid Electrolyte Interphase for Hard-Carbon Electrodes and Application to Na-Ion Batteries*, Adv. Funct. Mater. 21 (2011) 3859–3867
- [71] P. Verma, P. Maire, P. Novák, *A review of the features and analyses of the solid electrolyte interphase in Li-ion batteries*, Electrochimica Acta 55 (2010) 6332–6341
- [72] M.D. Tikekar, S. Choudhury, Z. Tu, L.A. Archer, *Design principles for electrolytes and interfaces for stable lithium-metal batteries*, Nat. Energy 1 (2016) 16114
- [73] W. Xu, J. Wang, F. Ding, X. Chen, E. Nasybulin, Y. Zhang, J.-G. Zhang, *Lithium metal anodes for rechargeable batteries*, Energy Environ. Sci. 7 (2014) 513–537
- [74] L. Gireaud, S. Grugeon, S. Laruelle, B. Yrieix, J.-M. Tarascon, *Lithium metal stripping/plating mechanisms studies*, Electrochemistry Communications 8 (2006) 1639–1649
- [75] G.G. Eshetu, T. Diemant, S. Grugeon, R.J. Behm, S. Laruelle, M. Armand, S. Passerini, *In-Depth Interfacial Chemistry and Reactivity Focused Investigation of Lithium-Imide- and Lithium-Imidazole-Based Electrolytes*, ACS applied materials & interfaces 8 (2016) 16087–16100
- [76] NIST X-ray Photoelectron Spectroscopy (XPS) Database, Version 3.5, <https://srdata.nist.gov/xps/Default.aspx>, accessed 6 October 2017
- [77] XPS Interpretation of Sodium, <https://xpssimplified.com/elements/sodium.php>, accessed 7 October 2017

- [78] J. Affinito, *Symposium on scalable energy beyond Li-Ion: Material Perspectives- Developing Li-S Chemistry for high energy rechargeable batteries*, Oak Ridge National Laboratory (2010)
- [79] J. Sangster, A.D. Pelton, *The Na-S (Sodium-Sulfur) system*, JPE 18 (1997) 89–96
- [80] C.-W. Park, H.-S. Ryu, K.-W. Kim, J.-H. Ahn, J.-Y. Lee, H.-J. Ahn, *Discharge properties of all-solid sodium–sulfur battery using poly (ethylene oxide) electrolyte*, Journal of Power Sources 165 (2007) 450–454